



## **A Novel Site-Selective Bioconjugation Strategy for the Synthesis of Energy Harvesting Protein-Conjugates**

**Jansen, Charlotte Uldahl**

*Publication date:*  
2022

*Document Version*  
Publisher's PDF, also known as Version of record

[Link back to DTU Orbit](#)

*Citation (APA):*  
Jansen, C. U. (2022). *A Novel Site-Selective Bioconjugation Strategy for the Synthesis of Energy Harvesting Protein-Conjugates*. DTU Chemistry.

---

### **General rights**

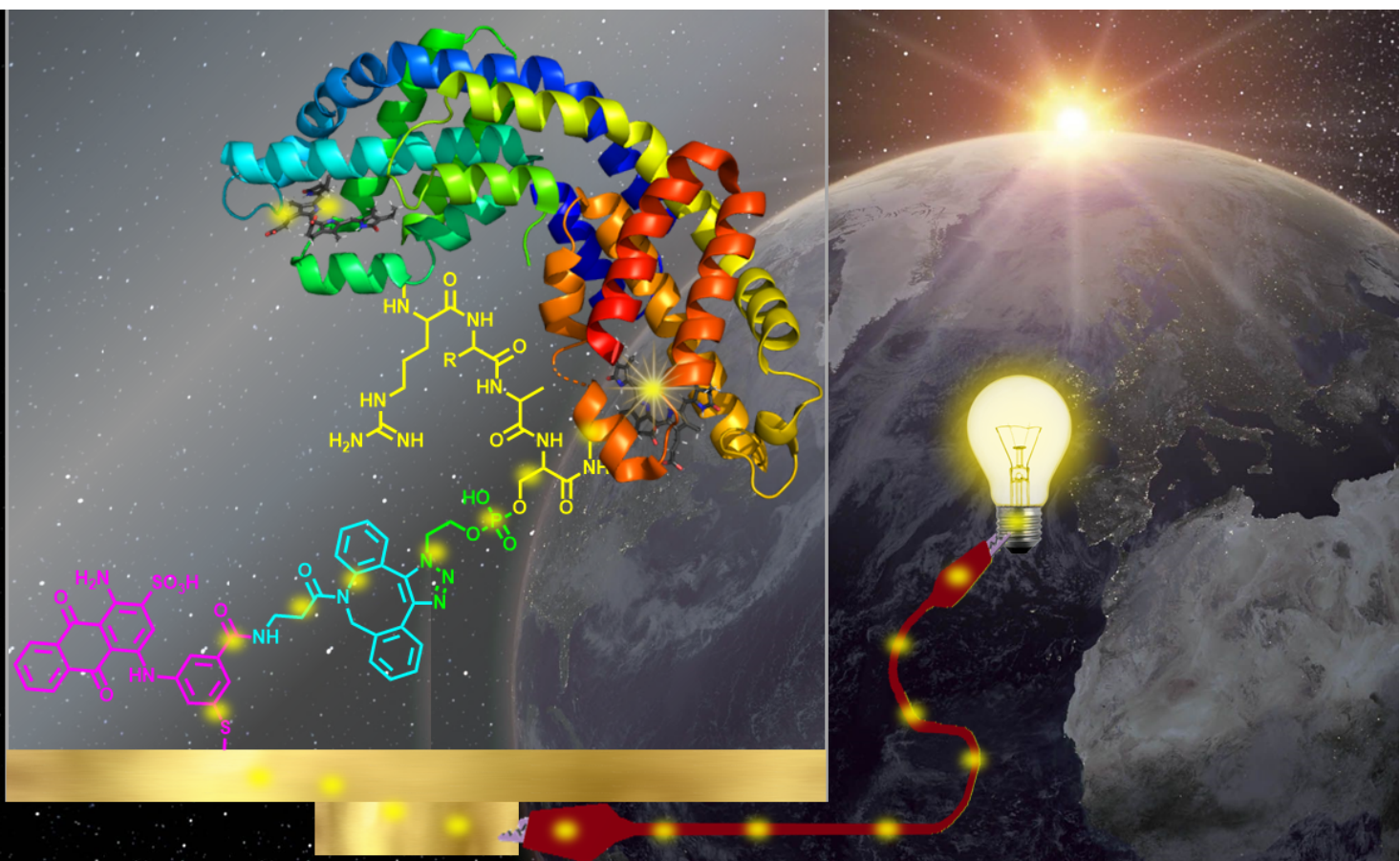
Copyright and moral rights for the publications made accessible in the public portal are retained by the authors and/or other copyright owners and it is a condition of accessing publications that users recognise and abide by the legal requirements associated with these rights.

- Users may download and print one copy of any publication from the public portal for the purpose of private study or research.
- You may not further distribute the material or use it for any profit-making activity or commercial gain
- You may freely distribute the URL identifying the publication in the public portal

If you believe that this document breaches copyright please contact us providing details, and we will remove access to the work immediately and investigate your claim.

Charlotte Uldahl Jansen, PhD Thesis

# A Novel Site-Selective Bioconjugation Strategy for the Synthesis of Energy Harvesting Protein-Conjugates



**Principal Supervisor:** Associate Professor Katrine M. Qvortrup

**Co-supervisor:** Professor Jens Øllgaard Duus

Technical University of Denmark

Kongens Lyngby February 2022



## Quotes from lab

*You are not the brightest spot on the TLC plate*

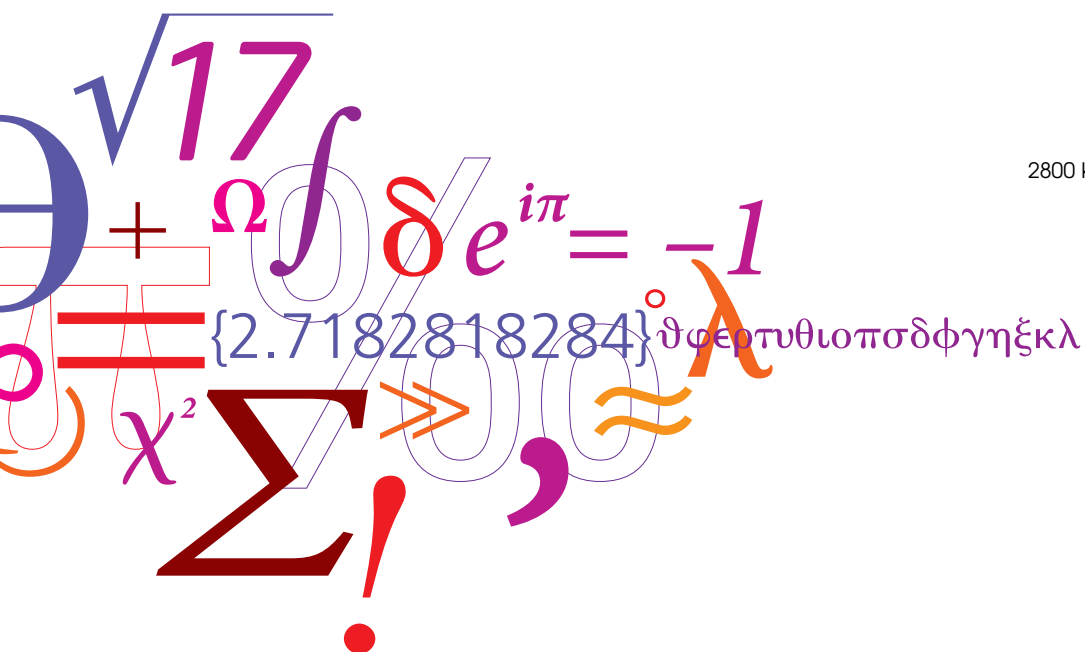
- June 2020

*Good advice comes from painful experience*

- February 2021

DTU Chemistry  
Department of Chemistry  
Technical University of Denmark

Kemitorvet  
Building 207  
2800 Kongens Lyngby, Denmark  
Phone +45 4525 2419



# Preface

---

The work presented in this thesis was conducted during my PhD studies at the Department of Chemistry, Technical University of Denmark (DTU) from Marts 2019 to February 2022, under the supervision of Associate Professor Katrine Qvortrup. This PhD project was founded by The Carlsberg Foundation. Due to the global pandemic (covid-19) my originally plan regarding external stay was cancelled, but fortunately Researcher Xinxin Xiao and Professor Jens Ulstrup, from the NanoChemistry department, gave me the opportunity to work with them in their electrochemistry group, hereby giving me experience with an exciting change of research environment. The stay at DTU NanoChemistry was proceeded with practical guidance from PhD Xiaomei Yan and Researcher Xinxin Xiao.

This thesis investigates the development of energy harvesting conjugates, which are divided into two parts. The first part focuses on developing novel strategies for site-selective bioconjugation, while the second part investigates the development of an improved anthraquinone-based bridging molecule to provide good electron transfer between protein and electrode.

Simultaneously with my PhD studies I have been involved in other exiting projects that is not included in my dissertation. These projects include photoinduced indigo formation for a greener production of denim-clothes, total synthesis of the natural compound Exochelin 772SM for cancer treatment, and the development of a novel biofilm dispersal drug for treatment of resistant infections.

Kongens Lyngby, February 28, 2022



---

Charlotte Uldahl Jansen



# Abstract

---

Site-selective bioconjugation is a powerful technique that is important for production of well-defined conjugates, which is needed in many research fields, including biology, pharmacology and electro chemistry. It is, however, challenging to achieve good site-selectivity due to the high number of each amino acid in a protein of interest. There are around 300 amino acids in a protein, and with only 21 available amino acids to choose from, there will unavoidably be unselectivity. Another strategy involves the recombinant installation of unnatural amino acids. However, this is time consuming and often give low yields. In addition, the installation of an unnatural amino acid can alter the function of a protein. In this thesis is presented two novel strategies to achieve site-selective bioconjugation on a protein containing only natural amino acids. Both strategies utilize the site-specificity achieved by the phosphorylating enzyme PKA. In one strategy, an azido handle is site-selectively installed by utilizing an azide-functionalized ATP-analogues as PKA substrate. The other strategy makes use of the natural enzyme substrate ATP followed by a selective pyrophosphorylation reaction to install the azido functionality.

Connecting proteins to electrodes is important for varies applications, with energy harvesting being one important field. However, the effect of the resulting conjugate is highly dependent on the protein having the right orientation on the electrode, as well as a good bridging molecule to ensure efficient electron transfer. In this thesis, an anthraquinone-based bridge molecule is investigated, which contains a thiol handle for electrode binding and a handle allowing future conjugation to the protein.

These are the themes of this PhD thesis.





# Resume

---

Positions-selektiv biokonjugation er et vigtigt værktøj med mange anvendelsesmuligheder inden for både det medicinske-, biologiske og elektrokemiske felt. Udfordringerne i at opnå en god positions-selektiv biokonjugation beror på at antallet af kopier af en given aminosyre i et protein er stor. Der er kun 21 aminosyrer at vælge i mellem og et protein indeholder ca. 300 aminosyrer, derfor vil der uundgåeligt være uselektivitet. Man kan inkorporere unaturlige aminosyre med en unik funktionalitet ved rekombinant syntese, men inkorporering af unaturlige aminosyrer er ofte en tidskrævende proces og giver lave udbytter. Desuden vil det potentielt ændre proteinets egenskaber. I denne PhD afhandling bliver der præsenteret to strategier der tillader positions-selektiv biokonjugation på proteiner der kun indeholder naturlige aminosyrer. Metoderne opnår positions-selektivitet ved at udnytte en phosphorylerings reaktion fra enzymet PKA. Den første strategi gør brug af et unaturligt azido-funktionaliseret PKA phosphorylerings substrat, mens den anden metode bruger det naturlige enzym substrat (ATP), hvilket efterfølges af en pyrophosphorylerings reaktion til at installere azido gruppen for videre funktionalisering.

Brugen af protein-elektrode konjugation har bred anvendelse, hvoraf en af de vigtige er energi høstning. For at opnå effektive konjugater er det yderst vigtigt at proteinets orientering på elektroden er specifik og ligeledes er det afgørende at den molekylære-bro der forbinder protein og elektrode giver effektiv elektron-transport. I denne PhD afhandling undersøges en anthraquinon-baseret molekylær-bro, som har både en thiol-funktionalitet der kan binde til elektroden, såvel som et håndtag der tillader kovalent konjugation til proteinet.

Dette er temaerne præsenteret i denne PhD afhandling.



# Acknowledgements

---

First and foremost, my deepest gratitude to my **supervisor**; Katrine Qvortrup. Thank you for the trust and the opportunity you gave me three years ago. Thank you for countless rewarding discussions often leading to a thousand new ideas. Thank you for your mentorship and guidance since starting my master thesis, I look forward to more years with great chemistry and new projects.

## **The Group:**

Katja Egeskov Grier and Amalie Nørskov, my fellow PhD's and friends, thank you for three great PhD-years, good discussions and excellent company through good and bad. For your inexhaustible effort to teach me sarcasm, your endurance is inspiring. Thank you for always offering your help when I needed proof-reading of an email, and for the, by now, litres of coffee (and gin-and-tonics). For great company and rewarding discussions that both led to exciting new pathways but also sometimes went a little off-course, thank you to both current and former members of the KQ-group; Weiguang Yin, Stavroula Louka, Christina Sophie Haxvig, Anders Højgaard Hansen, Jesper Uhd, Karoline Hauberg Rasmussen and Ida Aaberg Lillethorup. To all the students who has passed through the group, thank you for truly testing my knowledge and teaching skills.

## **Collaborators:**

Jens Øllgaard Duus, thank you for making the arrangement of my external stay possible, even though covid-19 had other plans, I am very grateful for what could have been. To the NanoChemistry group: first for our collaboration in the first years of my PhD, but even more for accepting me into your lab when my external stay got cancelled. I am truly grateful for your hospitality and mentorship in a field that was very new to me. Thank you Xiaomei Yan and Xinxin Xiao, Jens Ulstrup, David Tanner and Jingdong Zhang. To the National Biologics Facility at DTU Bioengineering: thank you, Sanne Schoffelen, Bjørn Gunnar Voldborg, Sara Petersen Bjørn and Folmer Fredslund, for designing, expressing and purifying the recombinant protein that will be used in a future site-selective bioconjugation paper.



**Technical staff** – for keeping the department afloat:

Dearest Anne Hector, thank you for always taking care of us (both as students and as teachers) whenever we were the least in doubt. No problem was too small for you, and we could always count on you. Great thanks to Johanne Marie Nielsen, Ea Judith Larsen and Lisbeth Riber for great morning-talks when the hallways were still empty, 'office-chair'-race and elevator-pauses. You are always ready to provide a laugh. To our lab-technicians, Phillip Charlie Johansen and Brian Dideriksen, for not only solving the problems you had expertise in, but also for solving the various creative problems that have occurred over the years. To the NMR-team for their expertise and guidance when my knowledge proved too short; Charlotte Held Godtfredsen, Kasper Enemark-Rasmussen and Sebastian Meier. The IT-team, Burak Yildiz, Daniel Due and Bo Sørensen for fixing all the problems my computer could possibly think of. Especially the one time my lunch attacked my computer. Engineer and service staff, Lars Bruhn, Andreas Graff Pedersen, John Nissen, Ishaq Khaliqdad and Stephan Jean Jeannenot Galsøe, for daily help and assistance with repair of equipment and finding needed items. Administrative personal, Mette Hansen, Josefine Lønholdt, Jette Berg Nestén, Monica Esterajher Søndergaard, Mette Møller and Kristine Albrektsen, for helping me with all the things I know nothing about. To David Frej Nielsen, Regitze Børsen Hansen and Marie Kofoed for helping with ordering chemicals and what-else we could possibly need in the laboratory. Thank you.

**Family and Friends:**

To my dearest ever-supporting and "trying to understand what I am saying" family and friends, I can never thank you enough. A quick sincere apology to my parents, I might have lied for the past few years – I went to work at 5 in the morning... not 6. Thank you for all your love. A great thanks to my little sister for preparing food for me for the last three years, my little brother for making sure I get some fun breaks every now and then, and my best friend for being there and just making sure I am staying sane – thank you! To all the friends who has offered their help for proofreading my thesis for spelling and grammar mistakes due to my dyslexia – I am very grateful and blessed to have such good people in my life. Thank you.

Last but not least to the **Carlsberg Foundation** who saw the potential in this project and choose to found it – thank you for the opportunity (and cheers!).

# List of Abbreviations

---

This list of abbreviations is assembled alphabetically according to the abbreviation.

A	surface area
AA	amino acid
Abl	tyrosine-kinase
ABTS	2,2'-azino-bis(3-ethylbenzothiazoline-6-sulfonic acid
Ac	acetyl
ACN	acetonitrile
ADC	antibody-drug-conjugate
ADP	adenosine 5'-diphosphate
Ala	alanine
AP	allophycocyanin
AQ	anthraquinone
Arg	arginine
Asp	aspartic acid
ATP	adenosine 5'-triphosphate
BME	meaptoethanol
Boc	tert-Butyloxycarbonyl
C $\alpha$	catalytic alpha unit
CDI	1,1'-carbonyldiimidazole
cdk2	kinase cyclin E1
CE	counter electrode
CK2	casein kinase II

---

COSY	correlation spectroscopy
CV	cyclic voltammetry
Cy	cyclohexyl
D	diffusion coefficient
dba	dibenzylideneacetone
DBCO	dibenzocyclooctyne
DCM	dichloromethane
$\Delta E_p$	peak separation
$\Delta j$	electrocatalytic current
DET	direct electron transfer
DIC	N,N -diisopropylcarbodiimide
DIPEA	N,N-diisopropylethylamine
DMA	dimethylacetamide
DMF	dimethylformamide
DMSO	dimethyl sulfoxide
$e^-$	electron
E. coli	Escherichia coli
EDC	1-ethyl-3-(3-dimethylaminopropyl)carbodiimide
EDG	electron donating group
eq.	equivalent(s)
Et	ethyl
EWG	electron withdrawing group
FAD	flavin adenine dinucleotide
FDH	fructose dehydrogenase
FeMeOH	ferrocene-MeOH
FGE	formylglycine-generating enzyme
Fmoc	fluorenylmethyloxycarbonyl
GCE	glassy carbon electrodes
Gly	glycine
His	histidine
HOMO	highest occupied molecular orbital
HPLC	high pressure liquid chromatography

---

Im	imidazole
ImB	imidazole buffer
$I_p$	peak current
j	current density
$k_s$	electron transfer rate constant
LCMS	liquid chromatography - mass spectrometry
Leu	leucine
LplA	lipoic acid ligase
LUMO	lowest unoccupied molecular orbital
MCB	McIlvaine buffer
Me	methyl
MET	mediated electron transfer
MOPS	3-(N-morpholino)propanesulfonic acid
MW	microwave
NEM	N-ethylmorpholine
NHS	N-hydroxysuccinimide
NMR	nuclear magnetic resonance
NPG	nanoporous gold electrode
$\nu$	scan rate
Oxyma	ethyl cyanohydroxyiminoacetate
PB	phosphate buffer
PC	phycoerythrin
PCET	proton-coupled electron transfer
PDB	protein data bank
PE	phycoerythrin
PKA	protein kinase A
PyBOP	benzotriazol-1-yl-oxytripyrrolidinophosphonium hexafluorophosphate
<i>quant.</i>	quantitative
RE	reference electrode
RF	reverse phase
rpm	rounds-per-minute



rt	room temperature
SAM	self-assessment monolayer
sat.	saturated
Ser	serine
SPPS	solid-phase peptide synthesis
SPAAC	copper-free strain-promoted azide–alkyne cycloaddition
sub	substituents
tBu	tert-butyl
TCFH	chloro-N,N,N ,N -tetramethylformamidinium hexafluorophosphate
TEAB	triethylamine carbonate buffer
TFA	trifluoroacetic acid
Thr	threonine
TIPS	triisopropyl silane
TLC	thin layer chromatography
TMS	trimethylsilyl
Tyr	tyrosine
UV	ultra violet
WE	working electrode
$\chi_{DET}$	DET-capable fraction
Å	Ångström

# Contents

---

<b>Preface</b>	<b>i</b>
<b>Abstract</b>	<b>iii</b>
<b>Resume</b>	<b>v</b>
<b>Acknowledgements</b>	<b>vii</b>
<b>List of Abbreviations</b>	<b>ix</b>
<b>Contents</b>	<b>xiii</b>
<b>1 Energy Harvesting Conjugates</b>	<b>1</b>
1.1 Inspiration from Nature . . . . .	1
1.2 Proteins-Modified Electrodes . . . . .	2
1.3 Energy Harvesting Conjugates . . . . .	3
1.3.1 The Need for Site-selective Bioconjugation Strategy . . . . .	3
<b>2 Site-Selective Bioconjugation</b>	<b>7</b>
2.1 Bioconjugation . . . . .	7
2.2 Site-Selective Bioconjugation . . . . .	8
2.2.1 Chemically Enhancement . . . . .	9
2.2.2 Enzyme Reignition Sequence . . . . .	9
<b>3 Bioconjugation with Kinase</b>	<b>11</b>
3.1 Scope . . . . .	11
3.2 Phosphorylation . . . . .	12
3.2.1 Specificity of the Enzyme . . . . .	13
3.3 Strategy 1 . . . . .	16
3.3.1 Design of Analogue . . . . .	16
3.3.2 Synthetic Procedure . . . . .	18

3.3.3	Phosphorylation with ATPC . . . . .	19
3.3.4	Phosphorylation with ATPO . . . . .	20
3.4	Strategy 2 . . . . .	21
3.4.1	Investigation of Phosphorimidazolid (13) Water Stability . . . . .	22
3.4.2	Investigation of Reaction Components . . . . .	24
3.4.3	Investigation of the Two-Step-One-Pot Reaction . . . . .	25
3.4.4	Investigating Peptide Concentration . . . . .	27
3.4.5	Investigation of Reaction Solvents . . . . .	28
3.5	Recombinant Protein . . . . .	30
<b>4</b>	<b>Experimental Section Part I</b>	<b>31</b>
4.1	Synthesis of Compounds . . . . .	31
4.2	Methods . . . . .	34
4.3	Peptide Synthesis . . . . .	34
<b>5</b>	<b>Electroactive Molecules</b>	<b>39</b>
5.1	Synthetic Strategy . . . . .	41
5.1.1	Commercially Available Anthraquinone . . . . .	43
5.1.2	Ullmann Condensation . . . . .	45
5.2	Electrochemical Study in Solution . . . . .	50
5.2.1	Experimental Set-up . . . . .	50
5.2.2	Recording CVs or Measuring CVs . . . . .	51
5.2.3	Data Processing . . . . .	51
5.3	Electrochemical Study of AQOMe (28) . . . . .	57
5.3.1	Synthesis of AQOMe Derivatives . . . . .	57
5.3.2	Electrochemical Study of AQOMe Derivatives in Solution . . . . .	59
5.4	Addition of the Protein Handle . . . . .	60
5.5	Summary . . . . .	61
<b>6</b>	<b>Anthraquinone as an Electron Bridge for Enzyme</b>	<b>63</b>
6.1	Design and Synthesis of Anthraquinones . . . . .	65
6.2	Electrochemical Study as Monolayer . . . . .	66
6.2.1	Laccase . . . . .	67
6.2.2	Fructose dehydrogenase . . . . .	68
6.2.3	Comparison with Mecaptoethanol . . . . .	71
6.3	Future Work . . . . .	72

---

<b>7</b>	<b>Experimental Section Part II</b>	<b>75</b>
7.1	Synthesis of Compounds in Chapter 5 . . . . .	75
7.2	Synthesis of Compounds in Chapter 6 . . . . .	85
7.3	Electrochemical Preparation . . . . .	88
7.3.1	Preparation of Electrodes . . . . .	88
7.3.2	Preparation of Solutions . . . . .	90
<b>8</b>	<b>Conclusion</b>	<b>91</b>
<b>A</b>	<b>General Methodologies</b>	<b>93</b>
<b>B</b>	<b>Additional HPLC-Spectras</b>	<b>95</b>
<b>C</b>	<b>List of Publications</b>	<b>99</b>
	<b>Bibliography</b>	<b>101</b>





# CHAPTER 1

# Energy Harvesting Conjugates

---

One of the major crises in modern times is the burden of the society's high energy demand on the environment and overall health of the planet, primarily due to the use of fossil fuels. To overcome this, sustainable, environmentally friendly and green energy sources have become an essential part of the solution. The Sun is the largest accessible energy source[1] on Earth and is of great potential for a development of both sustainable and environmentally friendly energy-harvesting technologies[2, 3]. Solar harvesting complexes utilizing organic molecules[4–6], aqueous solvents[6, 7] and proteins[8] are of interest in this PhD thesis.

## 1.1 Inspiration from Nature

Plants and some bacteria (cyanobacterial[9, 10] and red alga[11, 12]) harvest energy from the Sun using photosynthetic proteins. Phycobilisome[13–16] (see figure 1.1 with inspiration from Singh et al.[15], PDB: 6kgx[11]) is one of the largest antenna proteins found in cyanobacterial[9] and red alga[11, 12]. The structure of the phycobilisome from the red alga *Porphyridium purpureum*[11], and its many subunits (phycoerythrin (PE), phycocyanin (PC), allophycocyanin (AP) and linker proteins), can be seen on figure 1.1. The PEs absorb light at 480–570 nm and PCs absorb light at 550–650 nm[14]. Afterwards the excited electron is travelling[17] through the protein complex to the core (AP), where a photooxidation can occur, resulting in donation of electrons[18] from the protein to an electron acceptor.

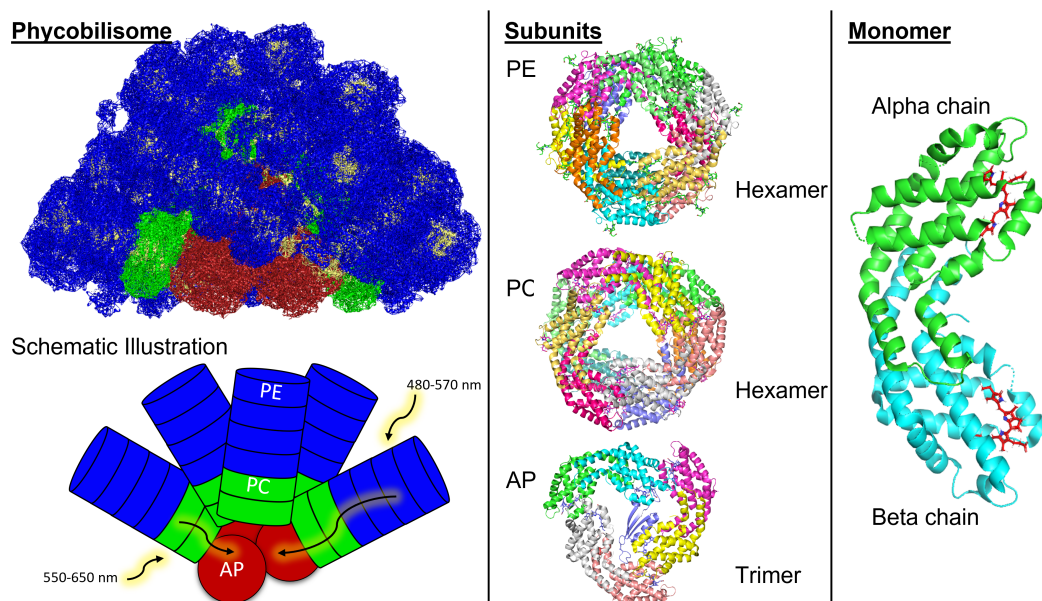


**Figure 1.1:** Illustration of Phycobilisome and its subunits. PDBs: Phycobilisome (6KGX), PE (5B13) outer end of antenna rod (blue in schematic illustration), PC (4L1E) end close to the middle of the antenna rod (green in schematic illustration), AP (1B33) the middle of the antenna (dark red in schematic illustration) and monomer (5TJF). Linker proteins (located multiple places, yellow in schematic illustration).

## 1.2 Proteins-Modified Electrodes

Protein-modified electrodes is a renowned phenomenon[3, 19–24] that makes it possible to efficiently exchange electrons between proteins and electrodes, which has been used in a broad range of applications, incl. glucose biosensors[25, 26] for diabetics, cancer diagnostics (detection)[24, 27, 28] with antibodies, bilirubin detection[29, 30], biofuels[31–34] and environmental monitoring[35], but also for mechanistic understanding of enzymes[20].

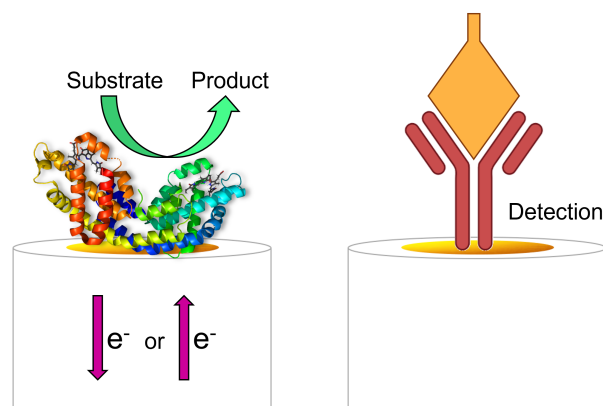


**Figure 1.2:** Schematic illustration of protein-modified electrodes

## 1.3 Energy Harvesting Conjugates

Liu et al.[36] published in 2018 a study of energy harvesting conjugates consisting of a protein conjugated to quantum dots. More specifically, they conjugated the photoreaction centre from the bacteria *Rhodobacter sphaeroides* to water-soluble cadmium telluride quantum dots through a His-tag linker. In a minireview from 2019 by Howe and colleagues[37], the development of biophotovoltaic systems using microorganisms is discussed. One of their conclusions is that a good electrical wiring connecting the electron donor and the anode is important to obtain good electron transfer.

### 1.3.1 The Need for Site-selective Bioconjugation Strategy

Based on the above referenced literature, it is evident that the orientation[21, 31, 38, 39] of the protein is of high importance when developing energy harvesting conjugates. Yates et al.[21] presents in a review the different attempts of anchoring the proteins to an electrode; illustrations from this review is collected in figure 1.3 (modified). The protein conjugation techniques discussed include the formation of peptide bonds through NHS/EDC chemistry (figure 1.3A), non-covalent binding in hydrophobic pockets (figure 1.3B) and various chemistries through installation of a biorthogonal handle (figure 1.3C) or unnatural amino acid (figure 1.3D) via genetic manipulation, as well as conjugation through imine formation (figure 1.3E) and cysteine-maleimide (figure 1.3F) chemistry.

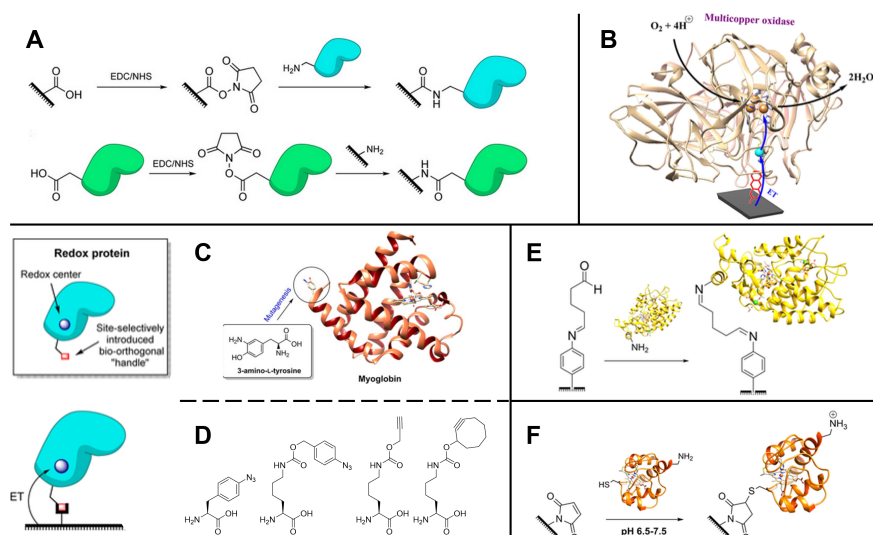


**Figure 1.3:** Illustrations from Yates et al.[21], A) NHS/EDC coupling, B) non-covalent hydrophobic pocket, C) biorthogonal handle, D) unnatural amino acid E) imine formation F) cysteine-maleimide chemistry.

The use of natural amino acids in recombinant production of proteins are highly desirable due the higher yield and more reliable methods. However, when the conjugation methods allowing attachment of a prope to proteins rely on only natural amino acids low selectivity are often observed as there are many copies of each amino acid moiety in the protein, which will lead to a heterogeneous mixture of proteins functionalized in different positions.

Therefore, when designing solar harvesting protein-based conjugates two major elements are crucial to investigate; how to orient the protein in the optimal position and how to the design the anchoring linker to achieve efficient electron transfer, see figure 1.4. This thesis is divided into two parts, one for each element. **Part I** first introduces the concept 'site-selective bioconjugation', its importance and challenges. In the second chapter of **Part I**, the investigation of new kinase-mediated bioconjugation methods is presented. **Part II** is centred around the organic bridge, focusing on the synthesis and electrochemical studies both in solution (chapter one) and anchored to an electrode (chapter two). The electrochemical studies were conducted in collaboration with PhD Xiaomei Yan and Researcher Xinxin Xiao during the 'change of research environment'.

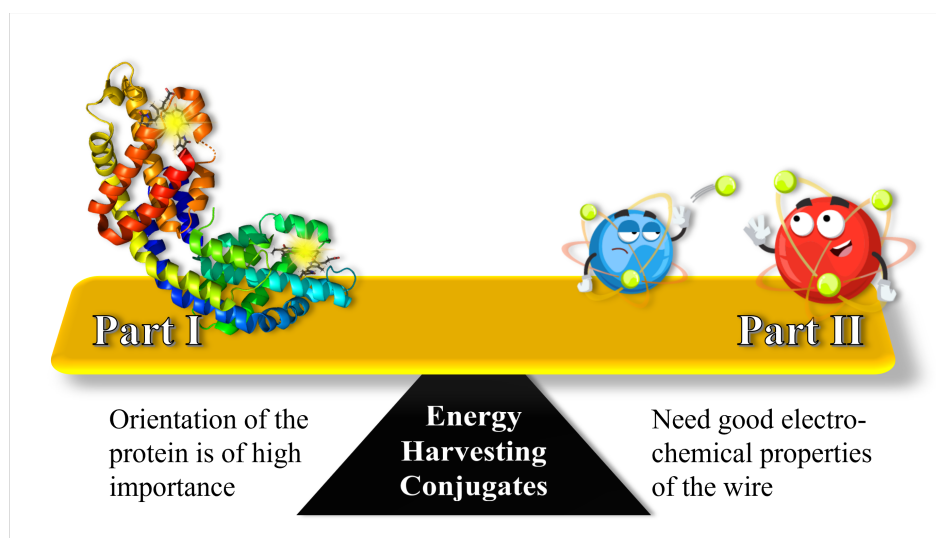
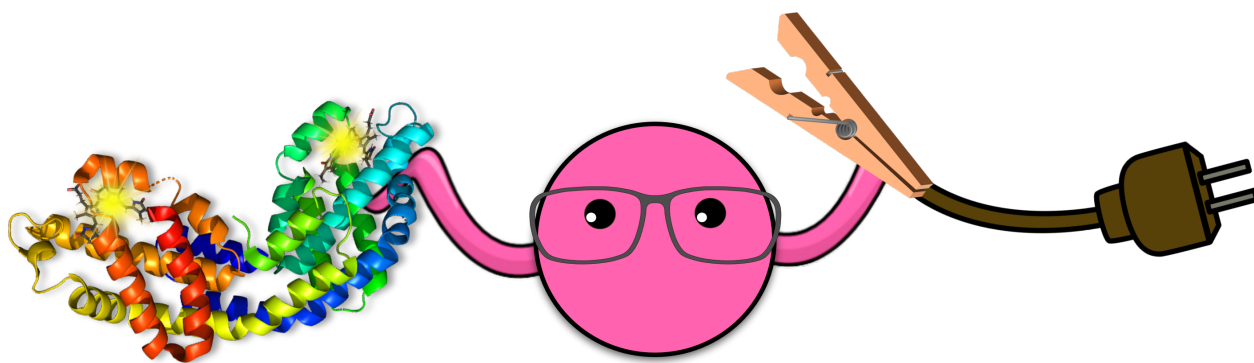


**Figure 1.4:** Thesis Build-up. Illustration protein PDB 5TJF and redox illustration from [www.toppr.com](http://www.toppr.com).

# PART I

## Bioconjugation





## CHAPTER 2

# Site-Selective Bioconjugation

---

This chapter will introduce the concept bioconjugation, and more importantly site-selective bioconjugation.

### 2.1 Bioconjugation

Bioconjugation in its simplest form is the coupling to a macro-biomolecule to a small molecular component[40] through a covalent bond. A highly researched field of bioconjugation involve the coupling of an antibody and a small-molecule drug to form a so-called antibody-drug-conjugate (ADC)[41]. A major challenge for bioconjugation[42] is to achieve chemoselectivity and regioselectivity of the conjugation reaction, as a protein consists of several of the same amino acid (AA) and even different AAs with similar side-chain reactivity. This often leads to a heterogeneous mixture of different bioconjugates[43], where the small molecular component is located in different positions on the proteins as well as bioconjugates with different numbers of the small molecular component attached to each biomolecule. The resulting bioconjugated species may have different properties as well as stability. For better control of the bioconjugation reaction, methods have been developed that allow recombinant installation of an unnatural AA[44], e.g., an azido, allowing chemoselective chemistry only on this position. While this method allows high control the number and position of conjugation sites, a major drawback is the need for recombinant installation of an unnatural AAs, which seriously complicates the protein production, resulting in low yields of the desired protein. In addition, installation of an unnatural AA[45] may often affect the stability and/or reactivity and solubility of the resulting biomolecule.

Many conjugation techniques have been applied for various types of applications. Figure



2.1 illustrates the most used conjugation techniques[46] with natural AAs and examples of their applications, which include the improvement of properties of therapeutic proteins[40, 47–49] e.g., half-life[47, 49, 50] as well as bioconjugates for targeted delivery (ADCs[41, 47, 51, 52], peptide-drug-conjugates[49, 50], imaging[53, 54]) and biosensors[55–57].

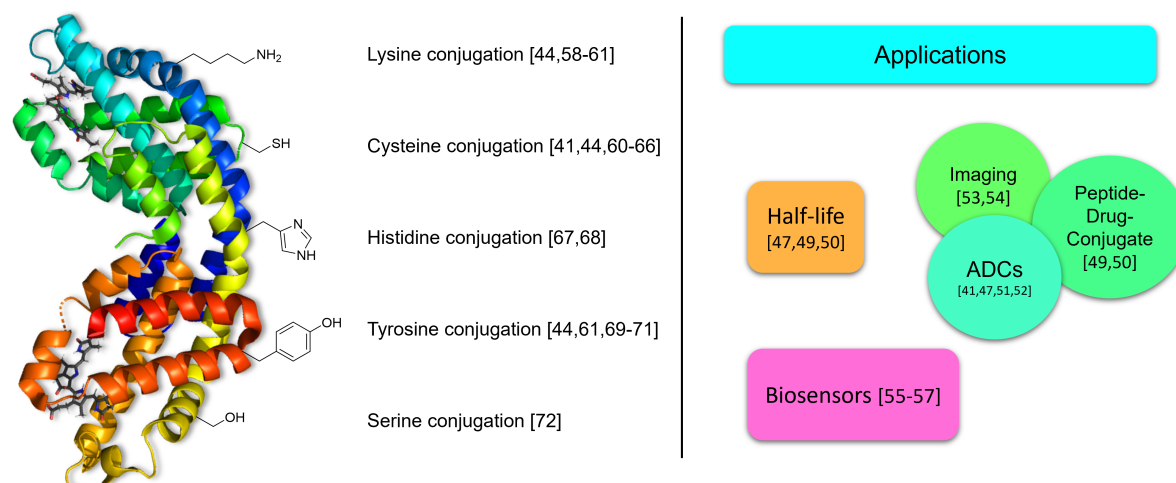


**Figure 2.1:** Conjugation techniques with natural AAs and examples of their applications: lysine[44, 58–61], Cysteine[41, 44, 60–66], Histidine[67, 68], Tyrosine[44, 61, 69–71], Serine[72], half-life[47, 49, 50], ADCs[41, 47, 51, 52], peptide-drug-conjugates[49, 50], imaging[53, 54]) and biosensors[55–57].

For further reading see review by Hoyt et al.[73] and the above-mentioned references. As the position, on the biomolecule, of the conjugation and the number of molecules attached to each biomolecule can be of critical importance, it is of high interest to develop controlled, site-selective bioconjugation strategies[43, 73–75].

## 2.2 Site-Selective Bioconjugation

To achieve site-selective bioconjugation, different methods could be employed[76] (as described above and in section 1.3.1); however, in this project, focus was given to methods using only natural AAs as this will simplify the protein expression[43] and produce the desired protein in higher yields. Strategies have been developed that allow selective conjugation to either only the N-terminal[44, 61, 77] or the C-terminal[61, 78] of the protein. While these strategies allow attachment of only one small molecule to the protein of interest, the application is limited as they only allow conjugation at highly fixed positions. Another interesting example of a site-selective bioconjugation strategy was achieved by Chen et al.[79], utilizing a kinetically controlled approach to conjugate to one lysine that is more nucleophilic than the other lysine residues present in the protein.

### 2.2.1 Chemically Enhancement

Another strategy is to enhance chemical reactivity of one specific AA in an area of interest on the protein, by installing specific AAs in the surrounding environment of that specific AA. Inspired by nature and how enzymes work, one such strategy could involve a sequence mimicking the catalytic triad[80] of hydrolytic enzymes, for example the Asp-His-Ser sequence[81] seen in serine proteases[80], as investigated by Miller et al.[82]. Other techniques include a certain sequence to obtain chemoselectivity, e.g. the dibenzocyclooctyne (DBCO) tag (L**C**YPWVY) invented by Pentelue and colleges[83] (see figure 2.2a), or the N-terminal His-tag (G**H**HHHHH) in the group of Jensen[84] (see figure 2.2b).

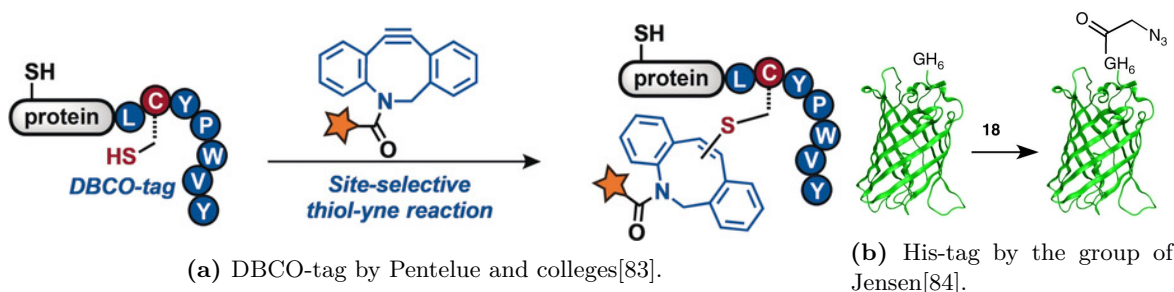


**Figure 2.2:** Site-selective strategies utilizing chemically enhanced sequences.

### 2.2.2 Enzyme Reognition Sequence

Another strategy allowing protein conjugation uses enzymes and installation of their specific substrates sequence inserted in the protein of interest, which allows a highly selective installation of a given tag at only that position. The utilization of both terminal and internal tags[43] have been demonstrated using this concept. Some examples of internal tags investigated are the formylglycine-generating enzyme (FGE) and its motif L**C**TPSR where the cysteine gets oxidized to the aldehyde, which can afterwards be further selectively modified[85]. Another example is the lipoic acid ligase (LplA) that selectively modify the lysine in GFEID**K**VWYDLDA with a lipoic acid[86], which has been utilized to install an azido-handle with a modified substrate[87].

Inspired by the enzyme strategy in this thesis will investigate the use of a phosphorylating enzyme as a novel method to achieve site-selective bioconjugation.



## CHAPTER 3

# Bioconjugation with Kinase

---

Enzymes are known to be effective and dependable with high specificity for their substrate and the reaction they catalyze. These abilities have been efficiently used in industrial production for years, examples include the food industry (cheese production and general preservation) and the textile industry (manufacturing and washing powder)[88].

Kinases is a family of phosphorylation enzymes which transfer a phosphor group from the high energy molecule adenosine 5 -triphosphate (ATP) to either a serine (Ser), a threonine (Thr), or a tyrosine (Tyr)[89–91], where each specific kinase-subtype phosphorylates the relevant amino acid sitting located in a very specific sequence. Recombinantly incorporation of this specific sequence of natural amino acids at desired position(s) of the target biomolecule, can allow for selective modification of the protein of interest without introducing any unnatural amino acids.

### 3.1 Scope

This chapter investigates two strategies to achieve site-selective bioconjugation, see figure 3.1, where **Strategy 1** applies an ATP analogue containing an azido handle for further conjugation and **Strategy 2** applies the natural ATP followed by a pyrophosphorylation reaction with a phosphate reagent containing an azido handle. Both strategies are of high interest as the first allows for quick installation of a simple azido handle, whereas the other will allow for installation of a more complex and bulkier handle.

When designing a bioconjugation method using enzymes there is a certain desired standard for the enzyme, this includes that it should be highly active, robust, and have high substrate specificity. Therefore, the protein kinase A (PKA) catalytic subunit alpha was chosen, which is described to have high activity (<8.000.000 U/mg)[92]. It is recombinantly expressed in *E. coli*, with the preferred substrate sequence LRRASLG, in which the serine gets phosphorylated.

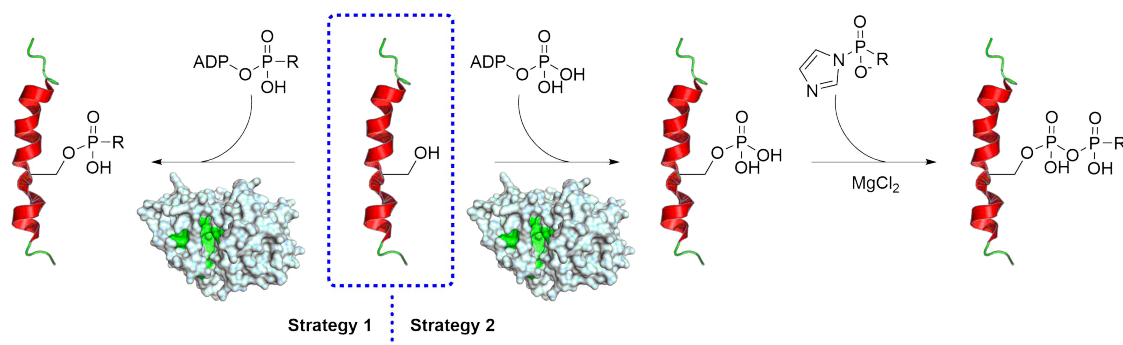


**Figure 3.1:** Site-selective bioconjugation strategies investigated in this thesis. In illustration enzyme PDB 3KKV and peptide PDB 2ME3.

## 3.2 Phosphorylation

The phosphorylation assay was performed as described by Roskoski[93] with few modifications, where the specific concentrations used can be seen in table 3.1. Milli-Q water was used as solvent for the stock solutions of the peptide, ATP and  $\text{MgCl}_2$ . The 3-(N-morpholino)propanesulfonic acid (MOPS) buffer was made with MOPS and milli-Q water, and afterwards adjusted to pH 7.0 with 10 M NaOH. Lastly the enzyme bought was 0.16 mg enzyme/mL in a 50 mM MOPS solution buffered at pH 7.0.

**Table 3.1:** Calculation table for phosphorylation assay.

Component	Stock Concentration		Added	Final Concentration	
<b>Peptide</b>	12.5	mM	20 $\mu\text{L}$	2	mM
<b>ATP</b>	62.5	mM	4 $\mu\text{L}$	2	mM
<b><math>\text{MgCl}_2</math></b>	250	mM	2 $\mu\text{L}$	10	mM
<b>MOPS (pH 7)</b>	104.17	mM	20 $\mu\text{L}$	50	mM
<b>Enzyme</b>	0.16	$\mu\text{g}/\mu\text{L}$	4 $\mu\text{L}$	0.0128	$\mu\text{g}/\mu\text{L}$
Final Volume			50 $\mu\text{L}$		

All the peptides used was synthesized using solid-phase peptide synthesis (SPPS) and the UV-active p-nitro cinnamic acid (**1**, **UV**) was added in the N-terminal to enhance the UV absorbance of the peptide, helping analysis. See chapter 4 for synthetic procedure. The sequences synthesized are UV-FLRRASLG- $\text{NH}_2$  (SerUV, **2**), for phosphorylation, and UV-FLRRAS( $\text{PO}_3\text{H}_2$ )LG- $\text{NH}_2$  (SerPUV, **3**), for control. All can be seen in figure 3.2. The assay was performed at  $37^\circ\text{C}$ , shaking at 1200 rounds-per-minuet (rpm) for 2 hours, which gave full conversion to the phosphorylated peptide as determined by HPLC, see spectrum in figure 3.3.

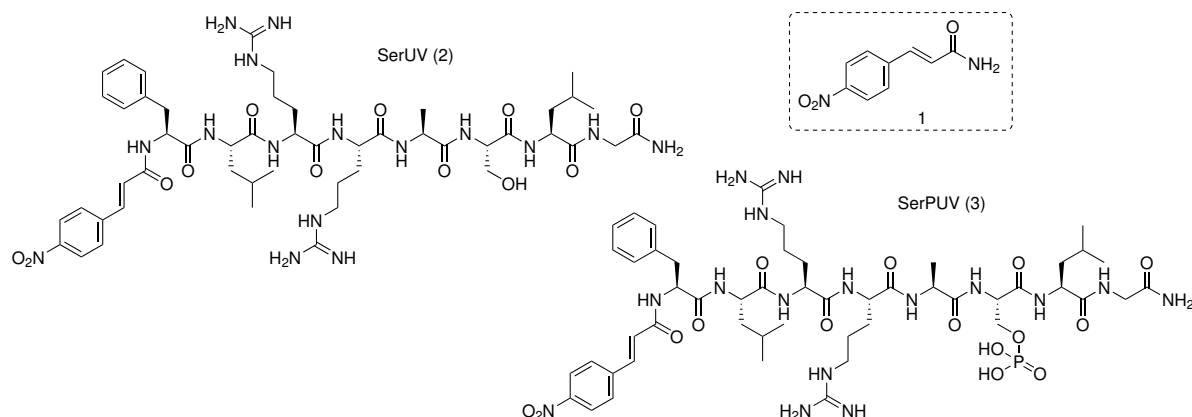


**Figure 3.2:** p-nitro cinnamic acid (1), SerUV (2) and SerPUV (3).

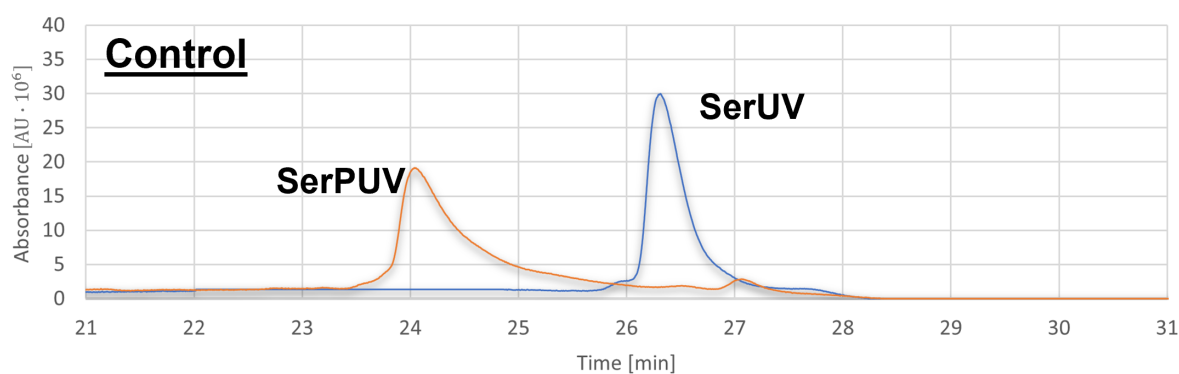


**Figure 3.3:** Combined HPLC spectrums of SerUV (2) and SerPUV (3). The data has been manipulated for display, see raw spectra in appendix B.

### 3.2.1 Specificity of the Enzyme

The substrate specificity of the enzyme was previously investigated by Walsh et al.[94] They found that the smallest motif was Arg-Arg-X-Ser-Z, and by testing one amino acid at a time, they identified Leu-Arg-Arg-Ala-Ser-Leu-Gly to result in highest phosphorylation. This depicts that the X and Z should be hydrophobic sidechains, X relatively small whereas Y can be bulkier.

To ensure the specificity of the enzyme follows these guidelines, a series of peptides was synthesized with variations as marked with red in table 3.2. V1 and V2 make small variation to the X position, whereas V3 and V4 vary the Z position. Lastly V5 and V6 substitute one Arg at a time to investigate whether both Arg amino acids are important. The peptides are listed in table 3.2 alongside with the results from the enzyme assay.

Conversion (%-phosphorylation) was calculated by the integrated area under the peaks as;

**Table 3.2:** Peptide sequences used for testing enzyme specificity and the %-phosphorylation observed by HPLC.

ID	Peptide Sequence*								Conversion
Motif			R	R	X	S	Z		
Identified		L	R	R	A	S	L	G	
SerUV (2)	F	L	R	R	A	S	L	G	100%
V1	F	L	R	R	G	S	L	G	87%
V2	F	L	R	R	V	S	L	G	0%
V3	F	L	R	R	A	S	V	G	53%
V4	F	L	R	R	A	S	I	G	46%
V5	F	L	R	A	A	S	L	G	93%
V6	F	L	A	R	A	S	L	G	0%

\* One letter code

$$\%_{conversion} = \frac{area_{product}}{area_{product} + area_{reactant}} \cdot 100 \quad (3.1)$$

It was found that X insertion of the smaller glycine instead of alanine (V1) was allowed but the larger valine (V2) completely quenched the phosphorylation. If the position Y was exchanged for either a smaller (valine, V3) or larger (isoleucine V4) side chain a decrease in phosphorylation was observed, but not complete loss of recognition from the enzyme. Interestingly it was found that the arginine furthest from the serine (V6) was of high importance, but the other arginine (one closer to the serine, V5) was of no importance, when incubated for 2 hours. To test if V5 was equally as good as the double arginine a mix of SerUV and V5 (one equivalent each) was incubated as described above with approximately one equivalent of ATP. The results showed that all SerUV had been phosphorylated and only some of V5, indicating that there was a preference for phosphorylation of the double arginine analogues (SerUV) compared to the analogues containing only one arginine residue (V5), see figure 3.4.

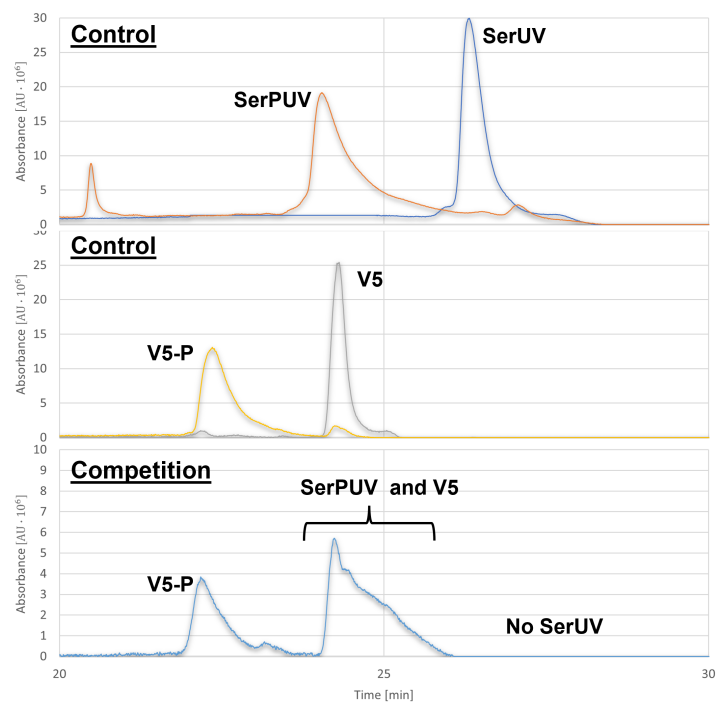


**Figure 3.4:** HPLC results from the competition between SerUV and V5 for investigating phosphorylation specificity.



### 3.3 Strategy 1

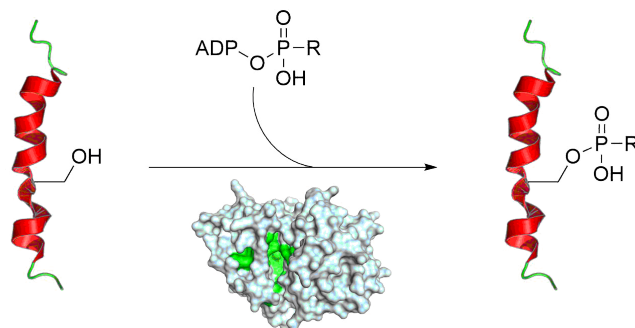


**Figure 3.5:** Schematic illustration of strategy 1: phosphorylation with an ATP analogue to install handle.

ATP analogues have previously been utilized to study the enzymatic pathways and functions of kinases[95–97]. Suwal et al.[98] investigated the ‘co-substrate’<sup>1</sup>-tolerance of three different kinases (PKA, CK2 and Abl) with a structural scope of ATP analogues. They observed that it is not allowed to have large groups close to the  $\gamma$ -phosphate, however, with an alkyl/ethoxy chain installed as spacer even large groups were accepted by the enzymes. Another study by Suwal et al.[99] showed how this approach with ATP-azido analogues could be used to cross-link enzyme and substrate to identify substrates for a specific kinase. Some of the most studied kinases, include PKA, CK2 and Abl[98–101]. The majority of the ATP analogues in literature are phosphoramidates[98–104], see also figure 3.6, but also phosphoesters[103–105], phosphorothioesters[104, 106, 107] and phosphonates[108] have been reported. Phosphoramidate analogues were however, shown to be unstable under acidic conditions[108].

When designing ATP analogues, it is important to consider enzymatic acceptance, co-substrate stability and product stability.

#### 3.3.1 Design of Analogue

It is important to find a good balance between high stability of the final conjugate and good reactivity and enzyme recognition of the ATP analogue. The phosphates will be discussed according to the  $\alpha$ ,  $\beta$  and  $\gamma$  nomenclature as indicated in figure 3.7, where the  $\gamma$ P is the one being transferred by the enzyme to the specific serine residue. It is predicted that binding of the  $\gamma$ P to a carbon will change the overall electronegative properties of the linkage between  $\gamma$ P and  $\beta$ P (marked in red on figure 3.7). This modification is expected to make the bond more stable and less prone to unspecific hydrolysis in the final conjugation[108, 109]. This may however

<sup>1</sup>Co-substrate refers to ATP or ATP-analogue.

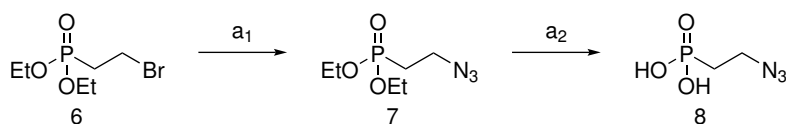


To investigate the potential of strategy 1 in site-specific bioconjugation, two almost-identical analogues were designed which contained either a  $\gamma$ P-CR bond-type or a  $\gamma$ P-OR bond-type. These were designed to investigate the balance between product-stability and enzyme recognition versus reactivity. The  $\gamma$ P-CR analogue is expected to provide high stability of the final conjugate towards acidic and basic conditions, while the  $\gamma$ P-OR analogue is expected to have a better enzyme recognition and a better catalytic turnover.

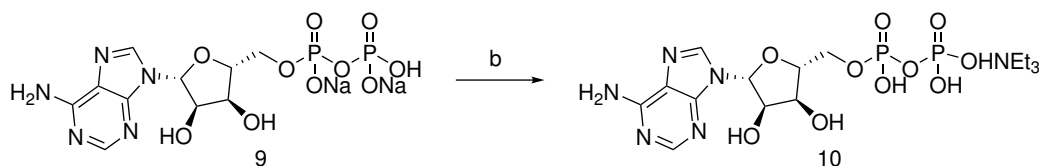
### 3.3.2 Synthetic Procedure

The synthetic strategy of the targeted  $\gamma$ P-CR (ATPC, **4**) can be seen in figure 3.8. The synthesis can be divided into three parts **a**) phosphor reagent[110, 111], **b**) activation of ADP[112] and **c**) 1,1'-carbonyldiimidazole (CDI) mediated coupling[112] to give the ATP analogue. The  $\gamma$ P-OR variant (ATPO, **5**) of that analogue was commercially available[113, 114]. Synthetic details can be found in the experimental section (chapter 4).

#### a) Phosphor Reagent



#### b) ADP Activation



#### c) CDI-mediated Coupling

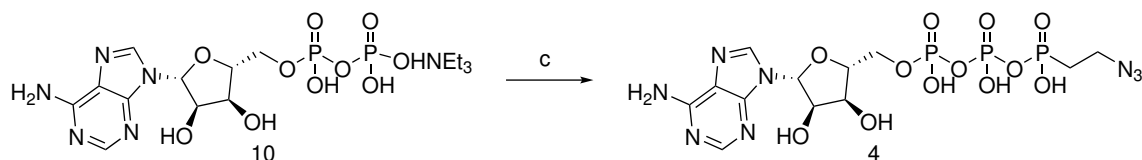


**Figure 3.8:** Synthetic strategy for the ATP analogue: ATPC (**4**). a<sub>1</sub>) NaN<sub>3</sub>, milli-Q, MW, 100°C, 30 min. a<sub>2</sub>) TMSBr, dry ACN, 0°C → rt, overnight. b) NEt<sub>3</sub>, H<sub>2</sub>O:EtOH, pH = 7. c) CDI, dry DMF, rt, overnight then MeOH, NEt<sub>3</sub>, **8**.

### 3.3.3 Phosphorylation with ATPC

ATPC (4) was tested under the same conditions as described above (section 3.2) for ATP, however, no phosphorylation was observed. It was expected, due to the electronic effect previously mentioned, that the analogue would have a slower reaction rate. Therefore, it was also tried with 24 hours incubation time, however, neither this showed any phosphorylation. Higher ATPC concentration was likewise tried and did not provide any phosphorylation, as seen from figure 3.9.

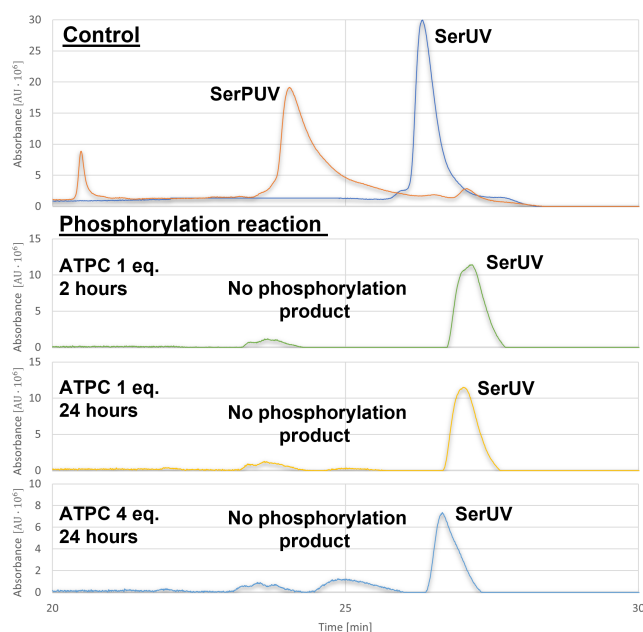


**Figure 3.9:** HPLC results from the phosphorylation assay with the ATP analogue: ATPC (4).

It is relevant to test if the analogue had an inhibitory effect on the enzyme, or if it was lack of recognition and/or low reactivity that caused the results. Therefore, two experiments were set up to see whether the PKA enzyme could still phosphorylate with ATP in the presence of ATPC. In the first test 4 eq. of ATPC was added along with 1 eq. of ATP and the reaction incubated for 24 hours. In the other test the enzyme and peptide were first incubated with 4 eq. ATPC for 12 hours, before 1 eq. of ATP was added, and then incubated for 12 more hours. The results, see figure 3.10, showed that the enzyme is still active after exposure to ATPC, however, there is no sign of competition neither reaction with the ATPC analogue.

It is known that enzymes are highly specific when it comes to substrates, and it was evident that the chosen enzyme does not tolerate the ATP analogue with a phosphonate functionality at the  $\gamma$ -P. The kinase used is a human recombinant PKA  $C\alpha$ . This specific PKA is described as a highly active subunit, unfortunately for this strategy it does not recognize the analogue as a co-substrate. The results indicate PKA cannot catalyze phosphorylation with ATPC as

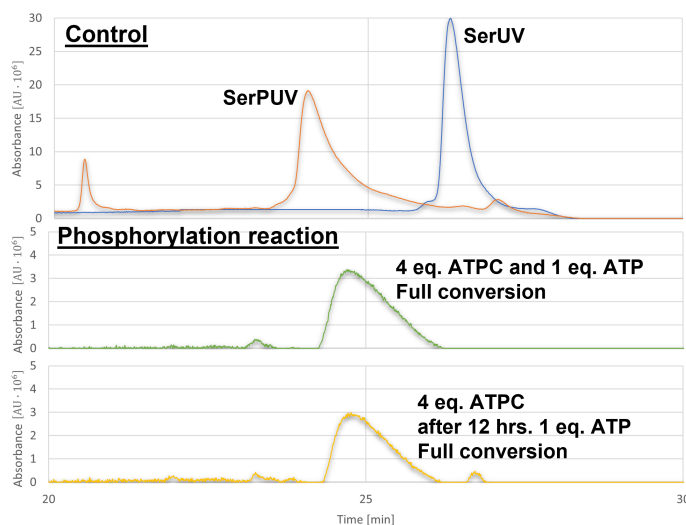


**Figure 3.10:** HPLC results from the control assays to ensure ATPC (**4**) is not inhibiting the enzyme.

co-substrate, probably because of the high stability of the P-C bond. Therefore, focus was given to the ATPO analogue (**5**).

### 3.3.4 Phosphorylation with ATPO

A 10 mM solution ( $\text{H}_2\text{O}$ , pH 7.5) of the ATPO analogue was used in the experiments under similar conditions as describe above. Unfortunately, no successful phosphorylation with ATPO could be achieved.

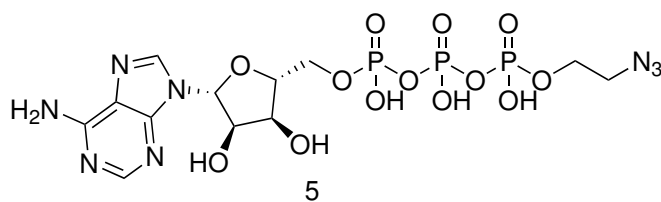


**Figure 3.11:** ATPO analogue (**5**).

Lee et al.[115] used this exact analogue in a study of the kinase pathway and substrate specificity using protein kinase cyclin E1 (cdk2) along with a known substrate,  $\text{p27}^{\text{kip1}}$ . It might very well be that the initially chosen kinase-type was not the optimal for using ATP-analogues. Therefore, it would be feasible for future work to set up a screen with different kinases against both analogues (ATPC (**4**) and ATPO (**5**)) and see which enzymes tolerates which type of analogue. However, this was not reached in this PhD project due to time limitations.

## 3.4 Strategy 2

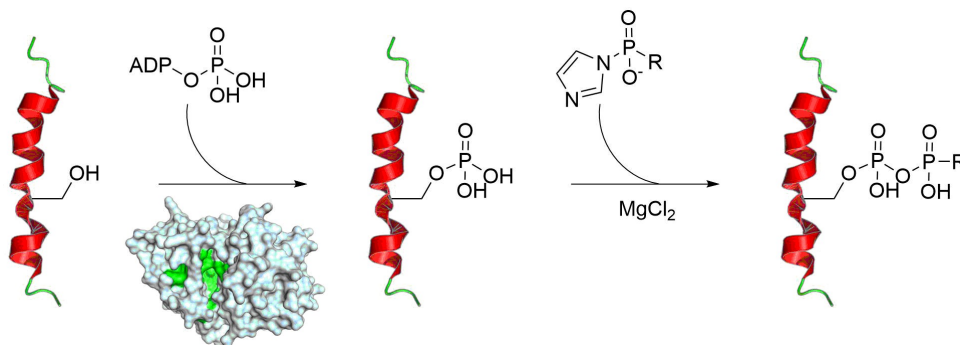


**Figure 3.12:** Schematic illustration of strategy 2: phosphorylation with ATP followed by a pyrophosphorylation to install a handle.

In 2013 Fiedler and coworkers[116] published some pioneering work describing a chemical method for pyrophosphorylation of phosphorylated proteins utilizing phosphorimidazolides[116–118]. Stability studies of the pyrophosphorylated serine showed that the compounds were stable in the pH range of 4.5 to 9.3[119], and therefore are stable under biological relevant conditions. Higher pH caused  $\beta$ -elimination while lower pH resulted in hydrolysis[119].

Learning from Friedler's work, it is hypothesized that a site-selective enzymatic phosphorylation followed by a pyrophosphorylation with an azido-functionalized phosphorimidazolidine derivative, could allow site-selective installation of an azido handle, for further functionalization with standard azide-alkyne cycloaddition chemistry (see section 5.4). For synthesis of the required azido-functionalized phosphorimidazolidine derivative, the procedure presented by Fielder and coworkers[118] was not applicable due to the presence of the azido group. The procedure presented by Friedler uses triphenyl phosphine, which would convert the azido to an amine via the Staudinger reduction. Therefore, the triethylammonium specie (**11**)[110–112] was reacted with imidazole and CDI[120], to get the desired azido-functionalized phosphorimidazolidine (**12**), which was then precipitated as the lithium salt (**13**) using lithium perchlorate, see figure 3.13.

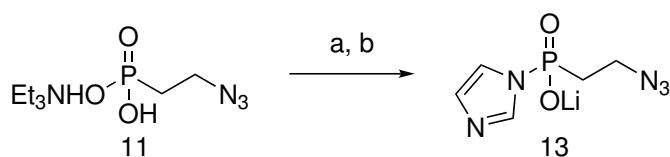


**Figure 3.13:** Synthetic strategy for the phosphorimidazolidine (**13**) used in pyrophosphorylation. a) CDI, NEt<sub>3</sub>, dry DMF, rt, 3 hours. b) LiClO<sub>4</sub>, dry acetone.

The pyrophosphorylation step was tested on the phosphorylated model peptide SerPUV (**3**), see synthesis in experimental section chapter 4. In the paper by Fielder and colleagues the pyrophosphorylation proceeded in DMA in the presence of an excess of  $\text{ZnCl}_2$  at  $45^\circ\text{C}$  for 90 min. Reacting the azido-functionalized phosphorimidazolide (**13**) under the same conditions, resulted in less than 21% conversion, see figure 3.14 green. Rewardingly, changing the solvent to DMF resulted in full conversion, see figure 3.14 orange.

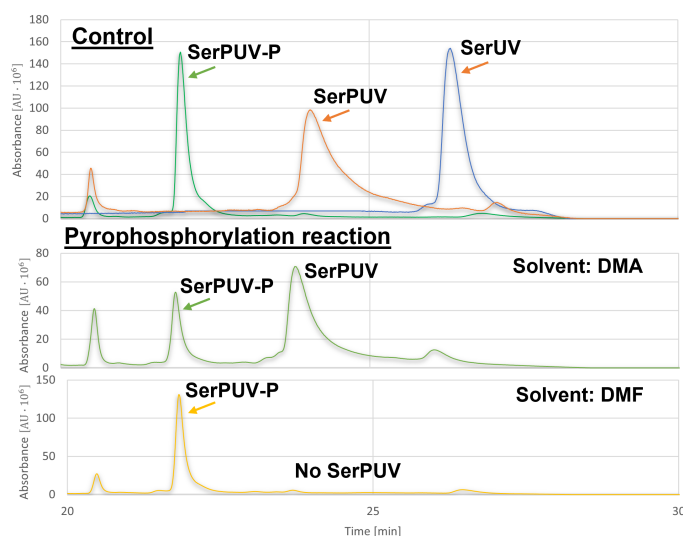


**Figure 3.14:** HPLC results from the pyrophosphorylation reaction run in either DMA or DMF.

### 3.4.1 Investigation of Phosphorimidazolide (**13**) Water Stability

With relevant phosphorylation and pyrophosphorylation conditions in hand, a series of test reactions were initiated to determine whether the pyrophosphorylation could run in an aqueous environment, which would allow the enzymatic phosphorylation and chemical pyrophosphorylation steps to be run in a two-step-one-pot reaction.

An important factor for the pyrophosphorylation to work in an aqueous environment, is that the phosphorimidazolide (**13**) is stable in water. Therefore, the stability was investigated by NMR in three different solvent combinations; DMF- $\text{d}_7$  (3.16A), 50/50 DMF- $\text{d}_7/\text{D}_2\text{O}$  (3.16B) and  $\text{D}_2\text{O}$  (3.16C). The results for the  $^{31}\text{P}$ -NMR at different time-points is shown at figure 3.16. The top line is from the phosphor reagent (**8**), in  $\text{D}_2\text{O}$ .

The water tolerance studies showed that the phosphorimidazolide (**13**) was stable under the aqueous conditions and no hydrolysis was observed at room temperature. As an additional test, the NMR-samples were heated to  $45^\circ\text{C}$  and run at different time-points, figure 3.17, again without any hydrolysis.

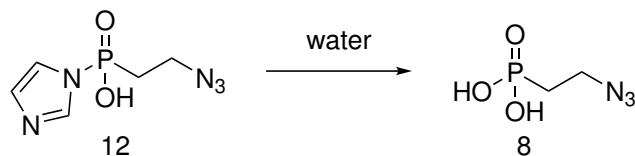


**Figure 3.15:** Hydrolysis of **12** to **8**, used for  $^{31}\text{P}$ -NMR study of **12**s water stability.

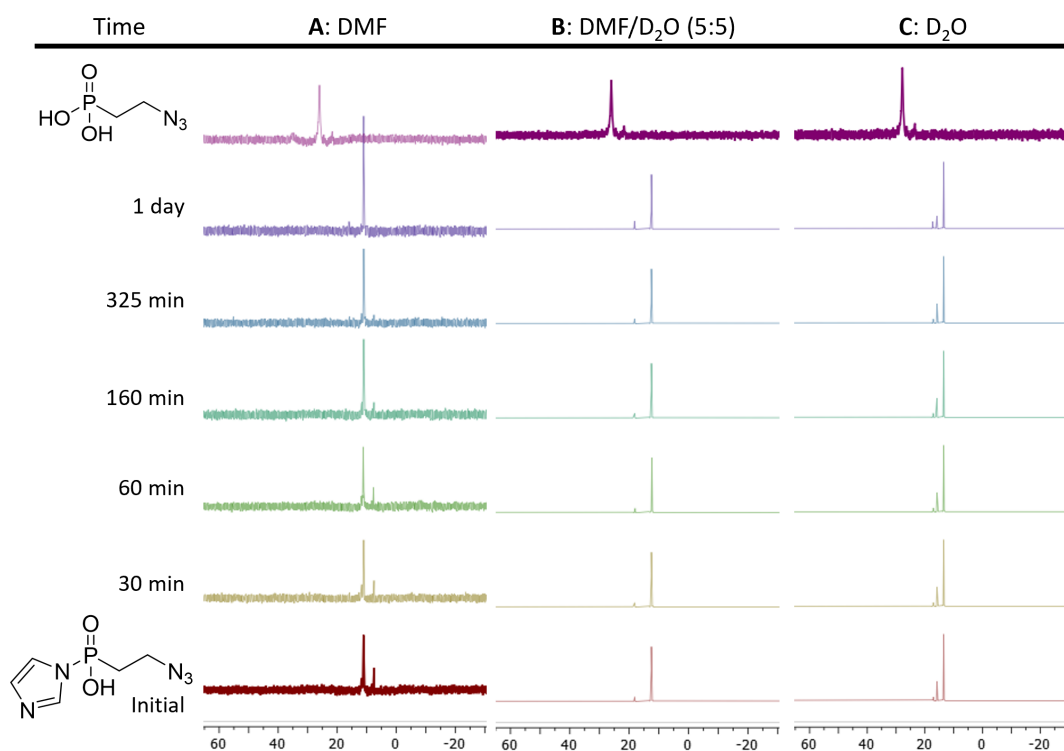


**Figure 3.16:** Results for  $^{31}\text{P}$ -NMR water stability study of **12** at room temperature, in DMF-d<sub>7</sub> (A), 50/50 DMF-d<sub>7</sub>:D<sub>2</sub>O (B), D<sub>2</sub>O (C). At the top is shown the  $^{31}\text{P}$ -NMR of **8**.

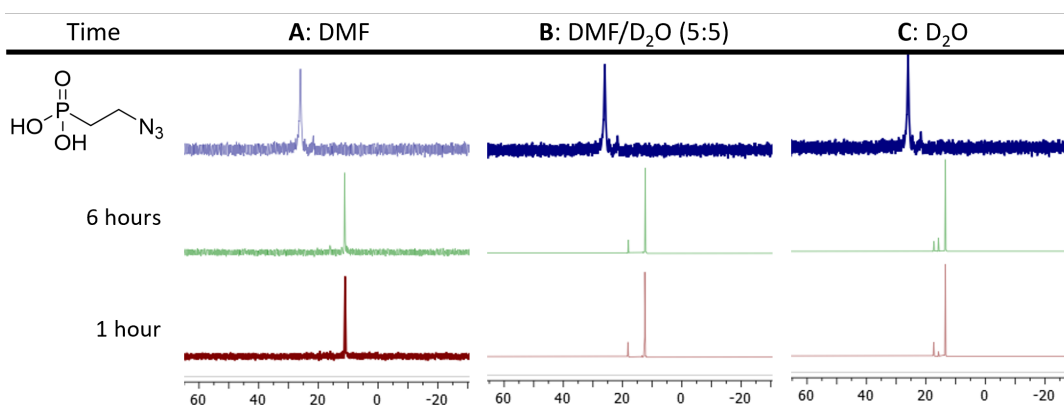


**Figure 3.17:** Continued  $^{31}\text{P}$ -NMR study of water stability, here the results after heating the samples to 45°C.



Initially, the tolerance of water in the pyrophosphorylation step was tested by a series of reactions with varying amounts of water (5%, 10% and 20%). Rewardingly, the results, see figure 3.18, showed that water was indeed tolerated.

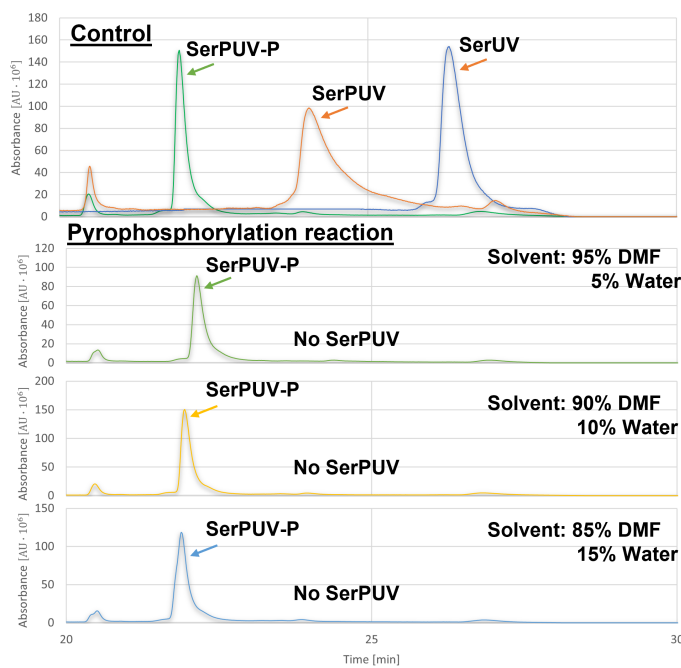


**Figure 3.18:** HPLC results from the pyrophosphorylation assay containing 5%, 10% or 20% water.

### 3.4.2 Investigation of Reaction Components

Besides the phosphorylated peptide and the kinase, the phosphorylation solution also contains excess ATP and  $\text{MgCl}_2$ , and is run in a MOPS buffer at pH 7.0, while the pyrophosphorylation step uses  $\text{ZnCl}_2$  for coordination of the peptide-phosphor and the phosphorimidazolide. It was investigated if  $\text{MgCl}_2$  could likewise coordinate the two phosphor-components for the pyrophosphorylation reaction, see figure 3.19.

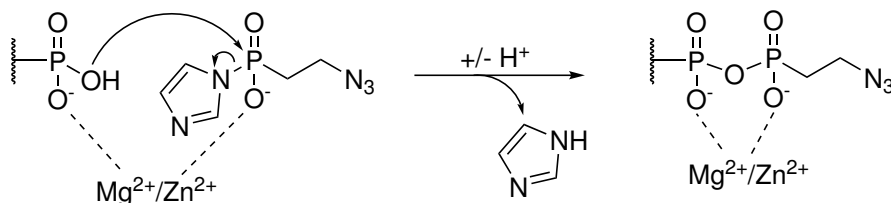


**Figure 3.19:** The function of  $\text{Zn}^{2+}/\text{Mg}^{2+}$  during the pyrophosphorylation.

Rewardingly, full conversion in DMF was achieved with both  $\text{ZnCl}_2$  and  $\text{MgCl}_2$ , see spectra

in appendix B figure B.4. Therefore, all the pyrophosphorylation experiments were run with  $\text{MgCl}_2$  instead of  $\text{ZnCl}_2$ , as this will be beneficial for investigation of a potential two-step-one-pot reaction.

### 3.4.3 Investigation of the Two-Step-One-Pot Reaction

For initial investigation of the two-step-one-pot reaction, four phosphorylation assays were started and after 2 hours a solution of the alkyl-azido phosphorimidazolide (**13**, 3 eq.) in dry DMF (ending with 20% water) was added while varying the amount of  $\text{MgCl}_2$  in the solutions. As there is already an excess of  $\text{MgCl}_2$  present in the reaction mixture, the added phosphorimidazolide solution contained 0 eq., 2 eq. or 6 eq. of  $\text{MgCl}_2$ . The pyrophosphorylation reactions were allowed to shake at  $45^\circ\text{C}$  for 24 hours and mixtures analysed by HPLC, figure 3.20. The very low concentrations of the samples made analysis difficult but focusing on the area of interest (20-30 min), it is seen the addition of extra  $\text{MgCl}_2$  is important, as product is mainly seen in reactions where both 2 and 6 eq. of extra  $\text{MgCl}_2$  were added. Unfortunately, it was difficult to make any clear conclusion due to the very dilute samples, but although product was formed, there was still unreacted peptide present in the reactions.

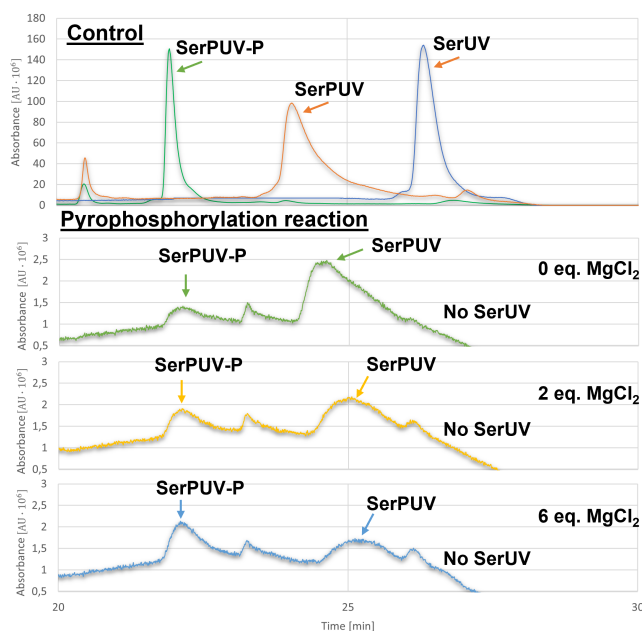


**Figure 3.20:** HPLC results from the assay with phosphorylation followed by the pyrophosphorylation in a two-step-one-pot reaction, adding either 0 eq., 2 eq. or 6 eq. of  $\text{MgCl}_2$  for the pyrophosphorylation step.

To solve the concentration-issue, it was chosen, going forward, to add a minimal amount of DMF resulting in a 66% water in the pyrophosphorylation. It was next investigated if

addition of the phosphorimidazolid (**13**, total 6 eq.) and  $\text{MgCl}_2$  (total 16 eq.) in portions over time, could push the reaction towards further product formation. The addition followed the scheme seen on table 3.3, where the solution containing the phosphorimidazolid derivative and  $\text{MgCl}_2$  was added in one (25  $\mu\text{L}$ ), two (2x 12.5  $\mu\text{L}$ ) or five (5x 5  $\mu\text{L}$ ) portions over 4 hours. Unfortunately, this did not improve the conversion of the pyrophosphorylation reaction.

**Table 3.3:** Scheme for addition of **13** and  $\text{MgCl}_2$  during a pyrophosphorylation assay.

Sample	Hour 0	Hour 1	Hour 2	Hour 3	Hour 4
1	25 $\mu\text{L}$ $\text{MgCl}_2$				
	25 $\mu\text{L}$ <b>13</b>				
2	25 $\mu\text{L}$ $\text{MgCl}_2$				
	12.5 $\mu\text{L}$ <b>13</b>		12.5 $\mu\text{L}$ <b>13</b>		
3	12.5 $\mu\text{L}$ $\text{MgCl}_2$				
	12.5 $\mu\text{L}$ <b>13</b>		12.5 $\mu\text{L}$ <b>13</b>		
4	25 $\mu\text{L}$ $\text{MgCl}_2$				
	5 $\mu\text{L}$ <b>13</b>	5 $\mu\text{L}$ <b>13</b>	5 $\mu\text{L}$ <b>13</b>	5 $\mu\text{L}$ <b>13</b>	5 $\mu\text{L}$ <b>13</b>
5	12.5 $\mu\text{L}$ $\text{MgCl}_2$		12.5 $\mu\text{L}$ $\text{MgCl}_2$		
	5 $\mu\text{L}$ <b>13</b>	5 $\mu\text{L}$ <b>13</b>	5 $\mu\text{L}$ <b>13</b>	5 $\mu\text{L}$ <b>13</b>	5 $\mu\text{L}$ <b>13</b>
6	5 $\mu\text{L}$ $\text{MgCl}_2$	5 $\mu\text{L}$ $\text{MgCl}_2$	5 $\mu\text{L}$ $\text{MgCl}_2$	5 $\mu\text{L}$ $\text{MgCl}_2$	5 $\mu\text{L}$ $\text{MgCl}_2$
	5 $\mu\text{L}$ <b>13</b>	5 $\mu\text{L}$ <b>13</b>	5 $\mu\text{L}$ <b>13</b>	5 $\mu\text{L}$ <b>13</b>	5 $\mu\text{L}$ <b>13</b>

It was speculated whether the MOPS buffer had a negative effect on the pyrophosphorylation reaction. Fielder and coworkers[119, 121, 122] found that the pyrophosphorylated-peptides were unstable in sulphonic acid-types buffer, suggesting that the reaction may be reversible in the MOPS buffer. Fielder et al.[116] demonstrate that the pyrophosphorylation reaction can proceed in an imidazole buffer (ImB) at pH 7.2 in 85% yield. To further test the medium for the pyrophosphorylation reaction, three aqueous solvents were compared; 50 mM MOPS pH 7.0, 50 mM ImB pH 7.1 and milli-Q, the HPLC results is shown in figure 3.21.

It was found that the pyrophosphorylation proceeded best with the peptide in milli-Q water (48%), compared to the 50 mM imidazole buffer (45%) and the 50 mM MOPS buffer (39%). Therefore, it was tested whether the enzymatic phosphorylation reaction could run in any of these solvents. The test showed that 50 mM ImB was well tolerated but unbuffered milli-Q water was not allowed, see spectra in appendix B figure B.5. Unfortunately, when running the pyrophosphorylation reaction in concentrations similar to the enzymatic phosphorylation, no reaction was observed. Changing the concentration of the phosphorimidazolid and  $\text{MgCl}_2$  did not change the outcome significantly; tried eq. **13**/eq  $\text{MgCl}_2$ ; 6/12, 9/24, and 12/32 added in 20  $\mu\text{L}$  DMF to the peptide (SerPUV (**3**), 2 mM) in either 50  $\mu\text{L}$  ImB (50 mM) or milli-Q.

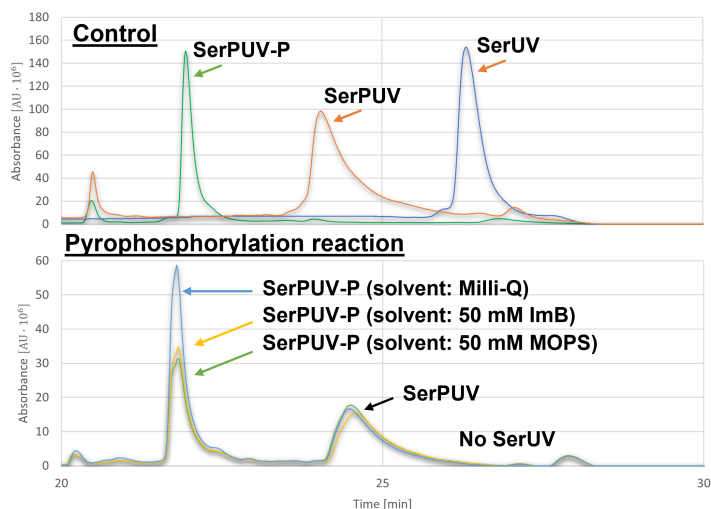


**Figure 3.21:** HPLC results from the pyrophosphorylation assay in different solvent systems; 50 mM MOPS (green), 50 mM ImB (orange) and milli-Q (blue).

### 3.4.4 Investigating Peptide Concentration

Looking at the peptide concentration difference for the phosphorylation and the pyrophosphorylation, it was clear that the concentration of the phosphorylation was almost 9 times lower than the reported[116] concentration for pyrophosphorylation reactions (12.5 mM versus 1.4 mM). Therefore, changing the concentration of the enzymatic phosphorylation reactions were instead investigated. Enzymatic phosphorylation at 16.8 mM in 50  $\mu$ L was tested, which would allow pyrophosphorylation to proceed at 12.5 mM after addition of the solution containing the phosphorimidazolid reagent (**13**) and  $\text{MgCl}_2$  (final volume = 60  $\mu$ L). Two reactions were tested with the standard 2 hours incubation and 24 hours incubation, respectively. Results showed that the phosphorylation reaction did not proceed at these high concentrations.

Therefore, reactions running at concentration in-between the optimal *phosphorylation-reaction* and *pyrophosphorylation-reaction* concentrations were tested, see table 3.4. It was found that the pyrophosphorylation would work to some degree at all the tested concentrations, however, the conversion was still not satisfying, see figure 3.22.

**Table 3.4:** The concentrations reported for the pyrophosphorylation reaction[116] (left) and the phosphorylation reaction[93] (right), and the "in-between" concentration-range investigated.

Pyrophosphorylation concentrations		Investigated reaction concentrations			Phosphorylation concentrations	
$C_{\text{peptide}}$	12.5 mM	9.73 mM	6.95 mM	4.18 mM	1.4 mM	$C_{\text{peptide}}$
$C_{13}$	75 mM	58.4 mM	41.8 mM	25.2 mM	8.6 mM	$C_{13}$

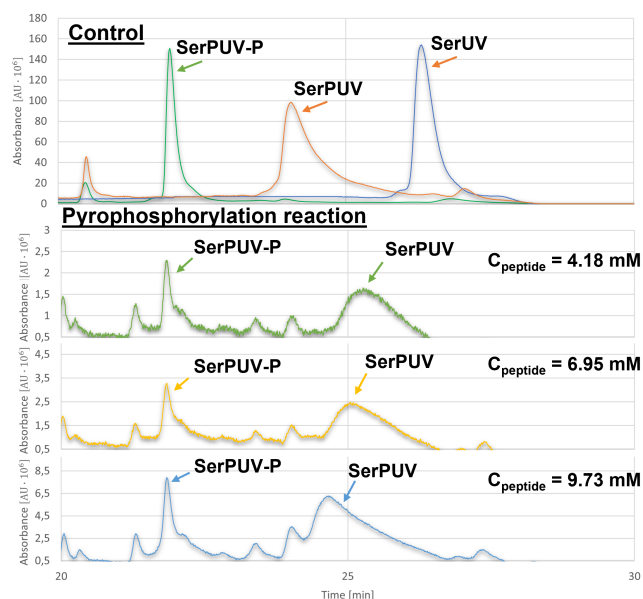


**Figure 3.22:** HPLC results from the pyrophosphorylation assay at different peptide concentrations.

As the pyrophosphorylation showed conversion at 4.18 mM, the phosphorylation was tested at 5.04 mM which after addition of pyrophosphorylation-reagents would result in the 4.18 mM. Rewardingly, the phosphorylation proceeded cleanly at this concentration, see spectra in appendix B figure B.6. Attempts to phosphorylation and pyrophosphorylation in a one-pot two-reaction fashion at this concentration was investigated. Unfortunately, without any satisfying results.

### 3.4.5 Investigation of Reaction Solvents

All previous described two-step-one-pot assays were done in a mixture of phosphorylation-buffer and DMF. However, as the phosphorimidazolid (**13**) has previously been shown stable and reactive in aqueous solvent (see section 3.4.1 and section 3.4.3 respectively), the next assay was proceeded without DMF. The phosphorylation reaction, run in ImB (50 mM), with SerUV (**2**), ATP and  $\text{MgCl}_2$ , was added the phosphorimidazolid and additional  $\text{MgCl}_2$  in milli-Q. This resulted in a significantly higher product formation, as can be seen on figure 3.23. For comparison can the pyrophosphorylation reaction where the phosphorimidazolid and additional  $\text{MgCl}_2$  was added in DMF also be seen on figure 3.23.

Unfortunately, it was not possible to drive the pyrophosphorylation to completion and addition of more of the reagents did not significantly change the outcome. To further understand the reaction, a range of reactions with different equivalents and different times of

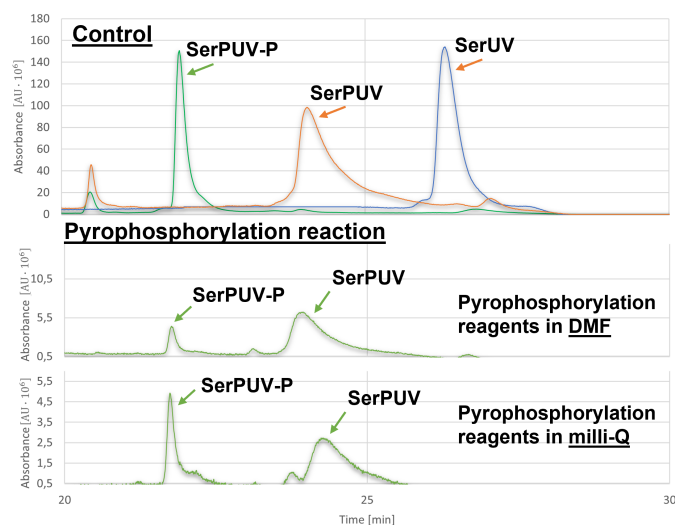


**Figure 3.23:** HPLC results from the phosphorylation reaction in 50 mM ImB followed by the pyrophosphorylation-reagents added in either DMF or milli-Q.

addition of phosphorimidazolid and  $\text{MgCl}_2$  was tested, see table 3.5. For all reactions, the phosphorylation reaction was done at 7.7 mM in 50  $\mu\text{L}$ , while the pyrophosphorylation reaction concentration was varied. See results on figure 3.24.

**Table 3.5:** Scheme for addition of pyrophosphorylation-reagents **13** and  $\text{MgCl}_2$ .

Sample	Start (hour 0)	+9 hours	+24 hours	+33 hours	+48 hours
1	Add		Stop		
2	Add	Add	Stop		
3	Add		Add		Stop
4	Add			Add	Stop
5	Add	Add	Add		Stop
6	Add		Add	Add	Stop

Add = 5  $\mu\text{L}$  of phosphorimidazolid (3 eq.) and  $\text{MgCl}_2$  (8 eq.). Stop = the reaction was stopped and analysed by HPLC.

Sample 3 looks satisfyingly better than most other attempts up till now having approx. 32% product formation. It was next investigated whether the volume of the Eppendorf reaction tubes and/or rpm would affect the reaction outcome. The results are showed that 41% conversion could be achieved with 200  $\mu\text{L}$  Eppendorf reaction tubes and 900 rpm compared to the previous 500  $\mu\text{L}$  Eppendorf reaction tubes and 1200 rpm. Due to time limitations no further studies were made in this thesis work. For future work, other aqueous buffer solutions and different concentrations should be investigated for the pyrophosphorylation reaction. It may also

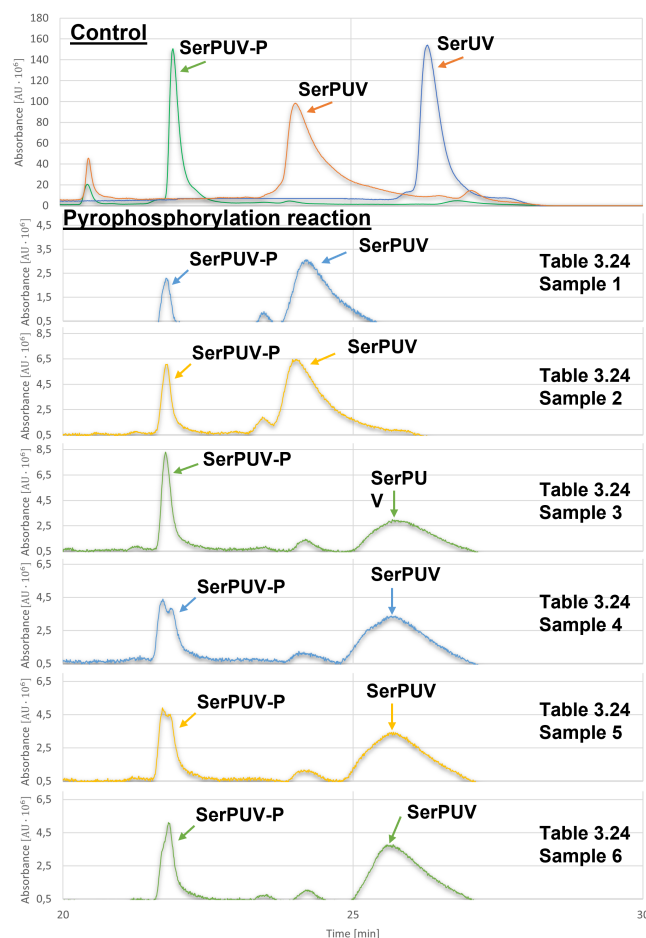


**Figure 3.24:** The HPLC results from the portionswise added pyrophosphorylation-reagents noted in table 3.5.

be relevant to investigate up-concentration and/or buffer exchange after phosphorylation before the pyrophosphorylation-reagents are added. This should include both investigation of spin filtration techniques with a relevant cut-off filter, followed by lyophilization to up-concentrate the reaction. Dialysis with a 100-500 Da membrane should likewise be investigated for a buffer exchange.

## 3.5 Recombinant Protein

For future demonstration of the novel conjugation strategies on a protein, a modified version of the SUMO protein (uniprot: Q12306) have been successfully recombinantly made in collaboration with DTU Biosustain, Bjørn G. Voldborg, Sara P. Bjørn and Folmer Fredslund. The C-terminal was modified to contain a MAAAF**LRRASL**GLVPRG sequence, where the red letters indicate the PKA phosphorylation sequence.

# CHAPTER 4

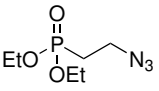
## Experimental Section Part I

---

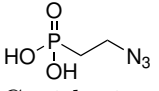
General Methodologies relevant for all experimental work can be found in appendix A.

### 4.1 Synthesis of Compounds

#### Diethyl (2-azidoethyl)phosphonate (**7**)

 Procedure[110]: Diethyl (2-bromoethyl)phosphonate (**6**, 2.3 mL, 12.65 mmol, 1 eq.) and NaN<sub>3</sub> (1.23 g, 18.98 mmol, 1.5 eq.) was dissolved in milli-Q (1.5 mL/mmol phosphonate) in a  $\mu$ wave-vial with a magnetic stir-bar. The vial was capped and heated by  $\mu$ wave for 30 minutes at 100°C and 250 W as initial power. The reaction mixture was then extracted with Et<sub>2</sub>O (4x 30 mL), which was then combined and washed with 30 mL H<sub>2</sub>O followed by 30 mL brine. Afterwards the organic phase was dried with Na<sub>2</sub>SO<sub>4</sub> and the solvent was removed *in vacuo*. The azido product (1.94g, 74%) was achieved without further purification. <sup>1</sup>H NMR (400 MHz, CDCl<sub>3</sub>) 4.19 – 4.02 (m, 4H), 3.51 (dt, J = 12.0, 7.6 Hz, 2H), 2.03 (dt, J = 18.4, 7.6 Hz, 2H), 1.31 (t, J = 7.1 Hz, 6H). <sup>13</sup>C NMR (101 MHz, CDCl<sub>3</sub>)  $\delta$  61.96 (d, J = 6.6 Hz), 45.38, 25.94 (d, J = 140.9 Hz), 16.39 (d, J = 6.1 Hz). Coupling in <sup>13</sup>C due to Carbon-Phosphorus. In accordance with [123].

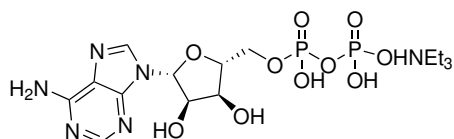
#### (2-azidoethyl)phosphonic acid (**8**)

 Procedure[111]: The azido-phosphonate (**7**, 1.9 g, 9.17 mmol, 1 eq.) was dissolved in dry ACN (4.31 mL/mmol **7**) and the solution was cooled to 0°C with vigorous stirring and nitrogen atmosphere. Trimethylbromo-silane (TMSBr, 4.8 mL, 36.68 mmol, 4 eq.) was added dropwise over 40 min. The reaction mixture was then allowed to stir at rt overnight, then the solvent was removed *in vacuo* to give a dark red/brown oil. A mixture of ACN:H<sub>2</sub>O (5:5, 1.72 mL/mmol **7**) was added, given a light green solution colour, which was stirred at rt overnight. Afterwards the mixture was evaporated to dryness *in vacuo* and a co-evaporation with toluene (3x 20 mL), gave the azido-phosphonic acid (**8**, 1.36 g,



*quant.*) as a dark red oil.  $^1\text{H}$  NMR (400 MHz,  $\text{D}_2\text{O}$ )  $\delta$  3.54 – 3.36 (m, 2H), 1.98 (d,  $J$  = 17.6 Hz, 2H).  $^{31}\text{P}$  NMR (162 MHz,  $\text{D}_2\text{O}$ )  $\delta$  26.02. HRMS (ESI)  $m/z$ :  $[\text{C}_2\text{H}_6\text{N}_3\text{O}_3\text{P} - \text{H}]^-$  Calcd 150.0074; Found 150.0557. In accordance with [111].

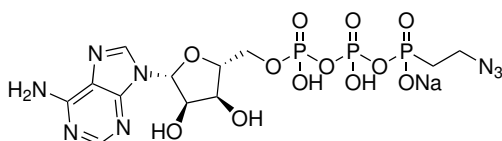
**Triethylamine ((2R,3S,4R,5R)-5-(6-amino-9H-purin-9-yl)-3,4-dihydroxytetrahydrofuran-2-yl)methyl diphosphate (10)**



Procedure: Adenosine 5'-diphosphate (ADP (**9**), 3 g, 6.37 mmol, 1 eq.) was dissolved in  $\text{H}_2\text{O}:\text{EtOH}$  (3:1, 12.2 mL/mmol), and while stirring was triethylamine ( $\text{NEt}_3$ ) added until pH 7 (1.5 mL). Then the solvent

was removed, and the activated ADP intermediate (**10**) was put under high vacuum overnight before being used without further purification in the next step.

**Sodium (((2R,3S,4R,5R)-5-(6-amino-9H-purin-9-yl)-3,4-dihydroxytetrahydrofuran-2-yl)methyl di-phosphoric) (2-azidoethyl)phosphonic anhydride (4, ATPC)**

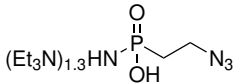


Procedure[109]: The ADP intermediate (**10**, 3.36 g, 6.37 mmol, 1 eq.) was dissolved in dry DMF (75.76 mL/mmol **10**), CDI (5.16 g, 31.79 mmol, 5 eq.) was added, and the mixture was stirred at rt overnight.

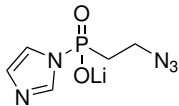
Next day methanol (4.55 mL/mmol **10**) was added, and the mixture stirred for 1 hr at rt before addition of  $\text{NEt}_3$  (0.03 eq.) and then a solution of azido-phosphonic acid (**8**, 1.25 g, 8.27 mmol, 1.3 eq.) in dry DMF (7.5 mL/mmol **10**). The reaction was allowed to stir overnight at rt, then diluted with a 5% solution of 1 M triethylamine carbonate buffer in milli-Q (TEAB, pH approx. 8-9). The diluted mixture was run through an anion exchange and all fractions containing the product, ATPC (determined by LCMS), was collected, this gave a mix of product and ADP **9**. The mix was concentrated to dryness, before being redissolved appropriately for preparative HPLC, where fractions containing only ATPC was collected. After removal of the HPLC-solvent the product was redissolved in minimal dry DMF, and then precipitated by addition of sodium perchlorate ( $\text{NaClO}_4$ , 4 eq. of crude product mass) in dry acetone (8x DMF volume)[112], centrifuged and washed with dry acetone. Finally, the sodium-salt of ATPC (**4**) was freeze dried to give 53.3 mg.  $^1\text{H}$  NMR (400 MHz,  $\text{D}_2\text{O}$ )  $\delta$  8.43 (s, 1H), 8.14 (s, 1H), 6.05 (d,  $J$  = 5.9 Hz, 1H), 4.54 – 4.43 (m, 1H), 4.33 – 4.29 (m, 1H), 4.18 – 4.13 (m, 2H), 3.49 – 3.36 (m, 3H), 2.06 – 1.93 (m, 2H), 1.88 – 1.75 (m, 1H).  $^{13}\text{C}$  NMR (101 MHz,  $\text{D}_2\text{O}$ )  $\delta$  155.56, 152.79, 149.07, 139.79, 118.56, 86.71, 83.86, 74.26, 70.32, 65.20 (d,  $J$  = 5.4 Hz), 45.95, 27.79 (d,  $J$  = 129.4 Hz).  $^{31}\text{P}$  NMR (162 MHz,  $\text{D}_2\text{O}$ )  $\delta$  13.85 (d,  $\gamma\text{P}$ ), -11.39 (d,  $\alpha\text{P}$ ), -23.07 (t,  $\beta\text{P}$ ). Coupling in  $^{13}\text{C}$  due to Carbon-Phosphor. HRMS (ESI)  $m/z$ :  $[\text{C}_{12}\text{H}_{18}\text{N}_8\text{NaO}_{12}\text{P}_3 -$

$\text{Na}]^-$  Calcd 559.0263; Found 559.0167.

### Triethylamine (2-azidoethyl)phosphonate (**11**)


 Procedure: Azido-phosphonic acid (**8**, 1.34 g, 8.87 mmol, 1 eq.) was dissolved in  $\text{H}_2\text{O}$  (4.5 mL/mmol **8**) and added  $\text{NEt}_3$  until neutral pH. Afterwards the solvent was removed, and co-evaporated with ACN, to give the activated azido-product as a light green semi-solid, which was used directly without further purification.  $^1\text{H}$  NMR (400 MHz,  $\text{D}_2\text{O}$ )  $\delta$  3.49 – 3.38 (m, 2H), 3.11 (q,  $J = 7.3$  Hz, 8H), 1.95 – 1.83 (m, 2H), 1.18 (t,  $J = 7.3$  Hz, 12H).  $^{13}\text{C}$  NMR (101 MHz,  $\text{D}_2\text{O}$ )  $\delta$  46.63, 46.07, 27.19 (d,  $J = 132.4$  Hz), 8.20.  $^{31}\text{P}$  NMR (162 MHz,  $\text{D}_2\text{O}$ )  $\delta$  21.87. Coupling in  $^{13}\text{C}$  due to Carbon-Phosphor.

### Lithium (2-azidoethyl)(1H-imidazol-1-yl)phosphinate (**13**)


 Procedure[120]: Triethylamine (2-azidoethyl)phosphonate (**11**, 506 mg, 1.98 mmol, 1 eq.) was dissolved in dry DMF (5 mL/mmol **11**), and under vigorous stirring was then added dry  $\text{NEt}_3$  (0.28 mL, 1.98 mmol, 1 eq.) and CDI (643 mg, 3.96 mmol, 2 eq.). The reaction proceeded for 3 hours at rt with continued vigorous stirring, LCMS confirmed full conversion to (2-azidoethyl)(1H-imidazol-1-yl)phosphinic acid (**12**). Lastly the phosphorimidazolide was precipitated as the lithium salt by addition of lithium perchlorate ( $\text{LiClO}_4$ , 843.5 mg, 7.93 mmol, 4 eq.) in dry acetone (8x DMF volume)[112], centrifuged and washed with dry acetone, to give the lithium phosphorimidazolide (**13**, 271.3 mg, 66%) as an off-white solid.  $^1\text{H}$  NMR (400 MHz,  $\text{D}_2\text{O}$ )  $\delta$  7.77 (s, 1H), 7.06 (s, 2H), 3.49 – 3.39 (m, 2H), 2.03 – 1.92 (m, 2H).  $^{13}\text{C}$  NMR (101 MHz,  $\text{D}_2\text{O}$ )  $\delta$  135.73, 121.42, 46.06, 28.08 (d,  $J = 136.6$  Hz).  $^{31}\text{P}$  NMR (162 MHz,  $\text{D}_2\text{O}$ )  $\delta$  13.51. Coupling in  $^{13}\text{C}$  due to Carbon-Phosphor. HRMS (ESI)  $m/z$ :  $[\text{C}_5\text{H}_7\text{LiN}_5\text{O}_2\text{P} - \text{Im}^1 - \text{Li} + \text{H}]^-$  Calcd 150.0074; Found 150.0051 (hydrolyzed).

## 4.2 Methods

### Analytical HPLC

HPLC: Waters e2695 Separations Module.

Column: EC 250/4 NUCLEOSIL 120-5 C18.

**ATP-analysis:** Solvent C - 15 mM NH<sub>4</sub>Ac in water, Solvent D - 15 mM NH<sub>4</sub>Ac in ACN/water 9:1. Gradient: 5% D, hold 8 min., gradient: 5% D to 100% D in 1 min., gradient: 100% D to 5% D in 0.5 min., hold 0.5 min. Total run time – 10 min.

**Peptide-analysis:** Solvent C - 15 mM NH<sub>4</sub>Ac in water, Solvent D - 15 mM NH<sub>4</sub>Ac in ACN/water 9:1. Gradient: 5% D hold 3 min., gradient: 5% D to 20% D in 10 min., gradient: 20% D to 70% D in 10 min., gradient: 70% D to 100% D in 5 min., hold 1.5 min., gradient: 100% D to 5% D in 0.5 min., hold 3 min. Total run time – 33 min.

### Preparative HPLC

HPLC and column type can be found in appendix A.

**Peptides:** Solvent A: 15 mM NH<sub>4</sub>Ac in water, Solvent B - 15 mM NH<sub>4</sub>Ac in ACN/water 9:1. Gradient: 95% A hold 3 min., gradient: 95% A to 80% A in 2 min., gradient: 80% A to 50% A in 2 min., gradient: 50% A hold in 2 min., gradient: 50% A to 30% A in 3 min., gradient 30% A to 0% A in 3 min., gradient: 0% A hold in 3 min., gradient: 0% A to 95% A in 0.5 min., gradient 95% A hold in 1.5 min. Total run time - 20 min.

**ATP:** Solvent A: 15 mM NH<sub>4</sub>Ac in water, Solvent B - 15 mM NH<sub>4</sub>Ac in ACN/water 9:1. Gradient: 95% A hold 5 min., gradient: 95% A to 0% A in 2 min., gradient: 0% A hold in 1 min., gradient: 0% A to 95% A in 1 min., gradient 95% A hold in 1 min. Total run time - 10 min.

## 4.3 Peptide Synthesis

Peptides were synthesised using solid phase peptide synthesis (SPPS) both automated with the Alstra from Biotage and manually using a microwave from Biotage during couplings. The SPPS strategy uses a solid support (resin) for attachment of the growing amino acid chain. This makes it possible to easily wash between couplings, without washing out the forming peptide. The overall outline for SPPS can be seen on figure 4.1, and after the linker is added to the resin the cycle begins. First is the deprotection, where this project utilised the Fmoc-approach, then addition of the first amino acid and coupling reagents, Oxyma and DIC. This gives the first completed cycle and leads back to the deprotection. When the last deprotection

has been performed the resin is cleaved from the resin by acid, this step also removes all side-chain protection groups.

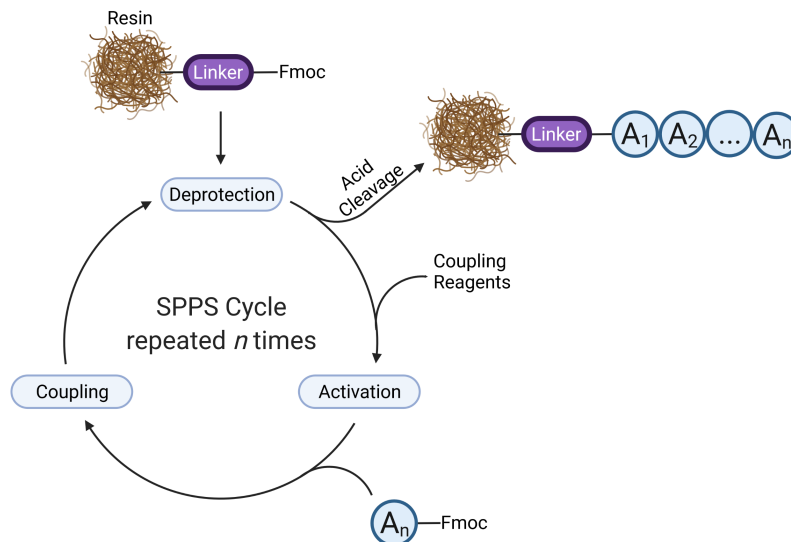


**Figure 4.1:** Schematic illustration of SPPS, made with Biorender.com.

In SPPS the resin is first swelled in DMF before addition of a Fmoc-protected linker under Oxyma/DIC coupling conditions, 75°C for 5 min under microwave influence. After removal of the Fmoc-group by 20% piperidine in DMF, the first amino acid is coupled under the same conditions as for the linker: Oxyma/DIC, 75°C, 5 min, MW. In a continuous repeat the peptide is built up from C- to N-terminal before the final deprotection. To boost the UV signal of the peptide 4-nitrocinnamic acid (**1**) was added to the N-terminal manually using Oxyma/DIC under microwave heating at 75°C for 10 min.

SerUV (**2**) and SerPUV (**3**) was synthesized on the automated SPPS Alstra from Biotage, whereas V1-6 was synthesised manually. During the manual synthesis, the resin is transferred between a syringe with permanent filter (for the deprotection and wash), to a microwave vial (for coupling).

For cleavage from the resin, as well as removal of any side chain protection groups, a TFA:H<sub>2</sub>O:TIPS (95:2.5:2.5) mixture was used. Afterwards the TFA solution containing free peptide was concentrated and added ether to precipitate the peptide. The suspension was centrifugated and decanted, this was repeated a few times, and lastly the peptide was purified by preparative HPLC.



# PART II

## Electrochemistry





## CHAPTER 5

# Electroactive Molecules

---

It was briefly mentioned in the introduction (chapter 1) that apart from the orientation of the protein, the bridge (wire) between the protein and the electrode is also of high importance to obtain efficient energy-harvesting conjugates. In the field of electrochemistry, the quinone family (e.g., benzoquinones, naphthoquinones and anthraquinones[124–127] (AQs), see figure 5.1) is of great interest due to their unique electrochemical properties rising from their very conjugated nature around the unsaturated diketones[128]. Additionally, they are attractive molecules for fabricating of electrochemical materials due their low cost[125, 129] and environmental safety[129]. These aqueous organic redox-active compounds[128] are seen in for example in biosensors[39, 130], flow batteries[126, 131, 132] (biofuel cells) and energy storage[125].

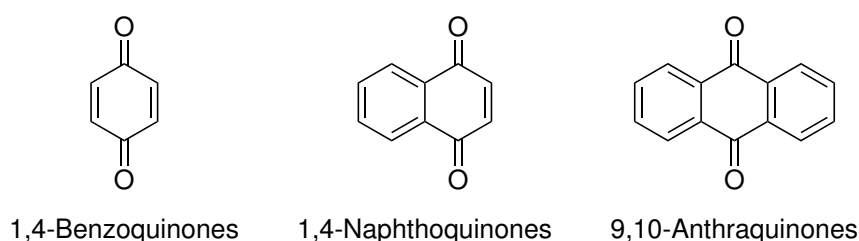


**Figure 5.1:** Quinone family.

The core can be decorated with different substituents to tune the redox properties. It has previously been shown that both the nature of the substituent and its position[124–126, 133] will greatly affect the electrochemical properties. Another important role of the substituents, when it comes to the anthraquinones, is to enhance the overall hydrophilicity[125] as the core by itself is very hydrophobic, and therefore are not be soluble in aqueous solvents.

Both experimental[126] and computational[124, 125] studies have shown that electron donating groups (EDGs) decrease the redox potential as they can donate electrons to the system, making them easier to oxidize. In contrast, electron withdrawing groups (EWGs) increase the redox potential by extending the conjugated system, making it easier to reduce. Either



property is useful[132] depending on the electrochemical system and setup.

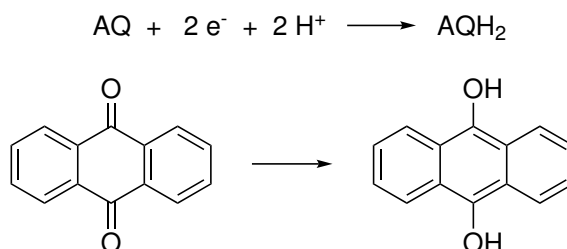


**Figure 5.2:** Anthraquinone being reduced in a 2 electron 2 proton PCET process.

Anthraquinones are reduced to the corresponding 9,10-anthracenediol in a 2 electron 2 proton PCET (proton-coupled electron transfer) process[127, 134, 135], see figure 5.2. As briefly mentioned in the introduction, chapter 1, this thesis will investigate the use of anthraquinones as bridging molecules for an electron harvesting conjugate; therefore, a high redox potential is desired. Sulphonate is an EWG widely used[128] to tune electrochemical properties as it has both a desired electronic and solubilising effect. In 2019, Gao et al.[128] published a study investigating how the position and number of sulphonate-substituents affected the electrochemical properties of anthraquinones. They found that 9,10-anthraquinone with a sulphonate in position 2 showed the best properties with regards to both reversibility and electrochemical performance.

### *Initial Design*

Certain requirements were needed when designing the anthraquinone molecule to be incorporated in the light-harvesting conjugate. To incorporate it as a covalent attached bridge between the protein and the electrode, two handles were needed as illustrated in the general schematic drawing in figure 5.3. Based on the discussing above, the R-groups were planned to be EWGs.

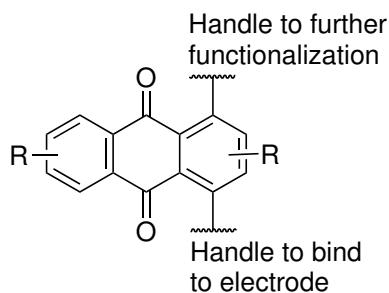


**Figure 5.3:** Schematic drawing of the AQ bridge design.

## 5.1 Synthetic Strategy

First approach to synthesise the decorated anthraquinones was through a Friedel-Crafts acylation of benzene containing the desired substituents with a relevant phthalic anhydride, followed by a dehydration and ring closure with  $\text{H}_2\text{SO}_4$  and heat as seen on figure 5.4.

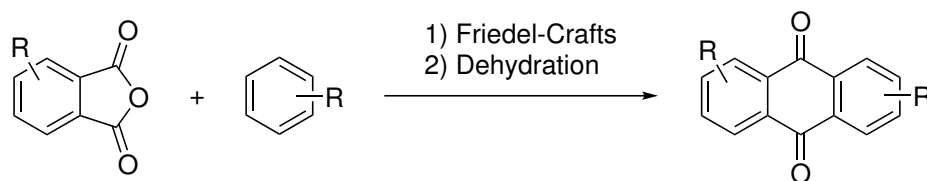
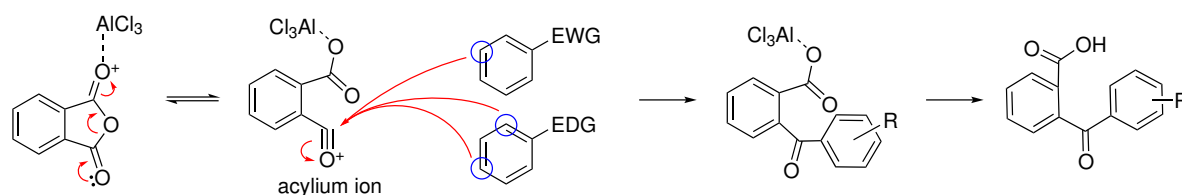


**Figure 5.4:** Friedel-Crafts strategy.

The general mechanism[136] for the Friedel-Crafts is illustrated on figure 5.5. The Lewis acid,  $\text{AlCl}_3$ , coordinate to one of the carbonyls of the phthalic anhydride, pulling the electrons from the other carbonyl to form the corresponding acylium ion, leading to ring opening. The highly electrophilic acylium ion is then attacked by the nucleophilic benzene ring, yielding the intermediate 2-benzoylbenzoic acid. Reactivity will follow the predictive rules of electrophilic aromatic substitution (ortho/para or meta directing activating vs deactivating), which should be taken into mind when designing the synthesis[137].

### Friedel-Crafts Acylation



### Dehydration

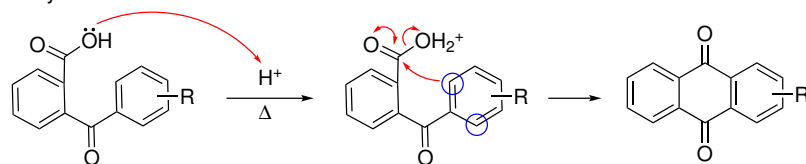


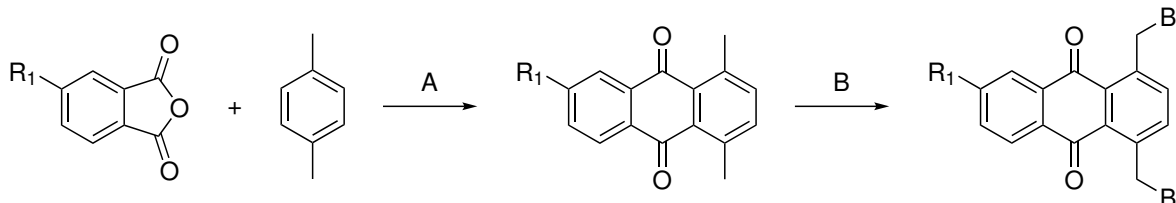
**Figure 5.5:** Friedel-Crafts mechanism.

Next step is the dehydration. Using concentrated sulphonic acid and extensive heating, the phenone will form through an intramolecular nucleophilic attack from the benzene ortho position. These positions are not highly nucleophilic as the ketone is a strong EWG; however, the energy provided by the heat and the formation of the aromatic anthraquinone system will

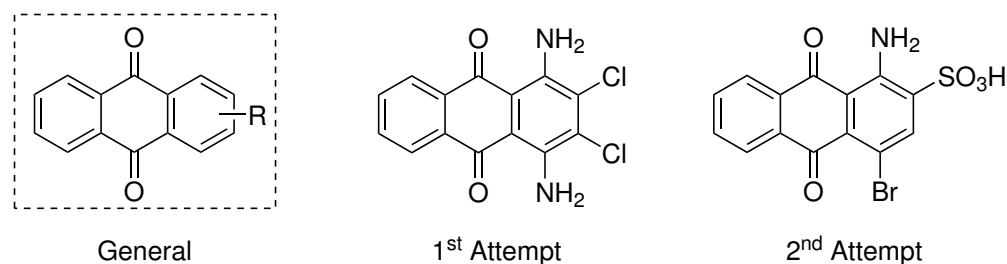
drive the reaction.

In initial attempts, xylene was reacted with either unsubstituted phthalic anhydride or 4-chlorophthalic anhydride, giving 1,4-dimethylantraquinone (**14**) or 7-Chloro-1,4-dimethylantraquinone (**15**) respectively, see table 5.1 reaction A. This would allow installation of a bromide-handle using a radical initiator[138–141], reaction B.

**Table 5.1:** Reaction conditions for anthraquinone synthesis.

		
Entry	R1	A
14	H	Two steps: AlCl <sub>3</sub> , dry DCM, 40°C, 5 hours, 92%, then H <sub>2</sub> SO <sub>4</sub> , 100°C, 1 hour, 53%
15	Cl	One pot: AlCl <sub>3</sub> , MeSO <sub>3</sub> H, 95-100°C – no product formation observed
15	Cl	Two steps: AlCl <sub>3</sub> , dry DCM, 40°C, 5 hours, 87% (2 peaks), then H <sub>2</sub> SO <sub>4</sub> , 135°C, 6 hours, 22% cannot dissolve

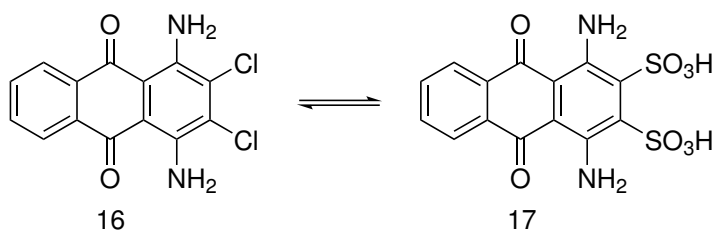
Unfortunately, the highly hydrophobic nature of the anthraquinone skeleton proved difficult to work with and the desired compounds were never confirmed by NMR analysis, while LCMS of the crude reaction mixture showed formation of a product with the desired mass. The use of benzenes functionalised with more polar groups was investigated but still gave inefficient reactions. Therefore, another strategy was designed utilizing commercially available 9,10-anthraquinones with varying functionalities, see figure 5.6.



**Figure 5.6:** Commercially available 9,10-anthraquinones with varying functionalities.

### 5.1.1 Commercially Available Anthraquinone

Initial attempts used the 1,4-diamino-2,3-dichloroanthracene-9,10-dione (**16**) as starting material, as this would allow installation of the important sulphonic acid functionality through substitution of the chlorides with sulphite, and the two aniline amino-groups could be used for attachment of the required handles. For the sulphonation the effect of the counterion was studied as both sodium and potassium sulphite can be used. Interestingly, it was found that when using sodium sulphite, high temperatures gave the desired disulfonic acid (**17**). However, it was observed that the reaction was reversible and cooling the reaction to rt, regenerated the di-chloride, see figure 5.7. Rewardingly, when using potassium as the counterion the reaction proceeded, and the desired product could be isolated. This observation may be explained by the ionic strength of the K-Cl bond (dissociation energy 4.43 eV) compared to the Na-Cl (dissociation energy 4.26 eV)[142].

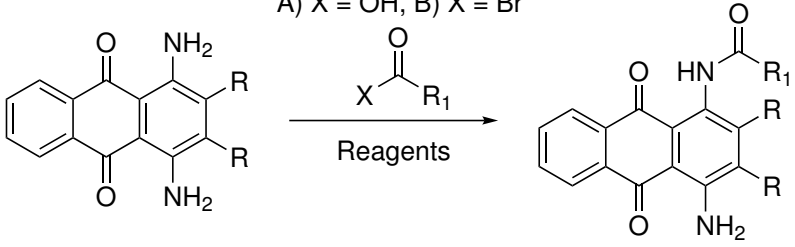
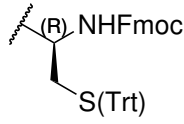
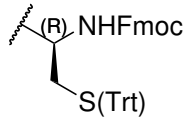
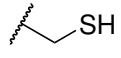
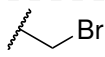
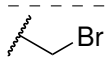
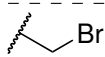


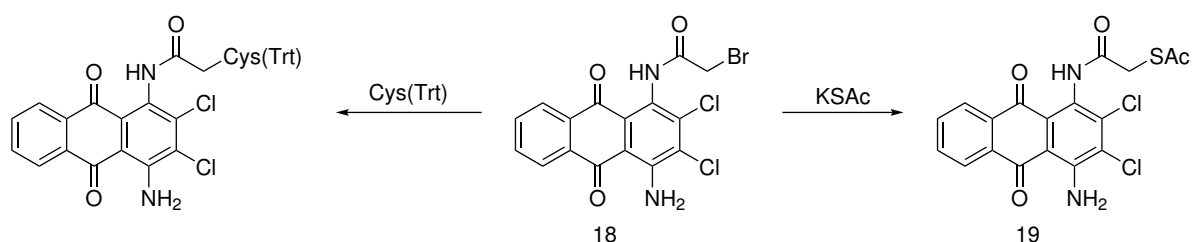
**Figure 5.7:** Addition of the sulphonic acid groups using either  $\text{Na}_2\text{SO}_3$  (reversible) or  $\text{K}_2\text{SO}_3$  (irreversible).

With a method in hand to install the sulphonic acid group, methods to install the required thiol handle was next investigated. Two acylation approaches were taken, A) peptide coupling and B) acetylation with bromoacetyl bromide, which was tried with both the chloride substituted analogue (**16**) and the analogue with the sulphonic acid functionalities installed (**17**). Tabel 5.2 presents an overview of the couplings investigated. First attempt was using a trityl (Trt), Fmoc protected serine under basic conditions; however, no product formation was observed. Second attempt utilized bromoacetyl bromide, which is a very reactive acylation reagent as the bromide is a very good leaving group. Fortunately, the reaction with bromoacetyl bromide was successful (compound **18**) when using basic conditions at low temperature (table 5.2 reaction 4).

It was next tried to substitute the bromo on the  $\alpha$ -carbonyl with Cys(Trt) (allyl protected on the carboxylic acid) and potassium thioacetate (KSAc). While the reaction with Cys(Trt) was unsuccessful, the substitution with KSAc proceeded nicely to give the product (**19**), see figure 5.8.

**Table 5.2:** Reaction conditions tested for acetylation.

<div style="text-align: center;">  <p>Method A) X = OH, B) X = Br</p> <p>Reagents</p> </div>					
Sample	R	R1	Method	Conditions	Comments
1	SO <sub>3</sub> H		A	DIPEA, 50°C	No reaction
2	Cl		A	DIPEA, 50°C	No reaction
3	Cl		A	0°C	No reaction
4	Cl		B	DIPEA, 0°C	Worked, 98%
5	Cl		B	0°C	Worked but not clean
6	SO <sub>3</sub> H		B	DIPEA, 0°C → rt	Worked but not clean

**Figure 5.8:** Substitution of bromo group on the  $\alpha$ -carbonyl.

It was then attempted to install the second handle in a similar fashion by reacting the 2-(acetylthio)acetamide functionalized anthraquinone (**19**) with bromoacetyl bromide, followed by substitution with tert-butyl protected glycine to install the carboxylic acid handle, see figure 5.9. Unfortunately, it was not possible to isolate the desired product.

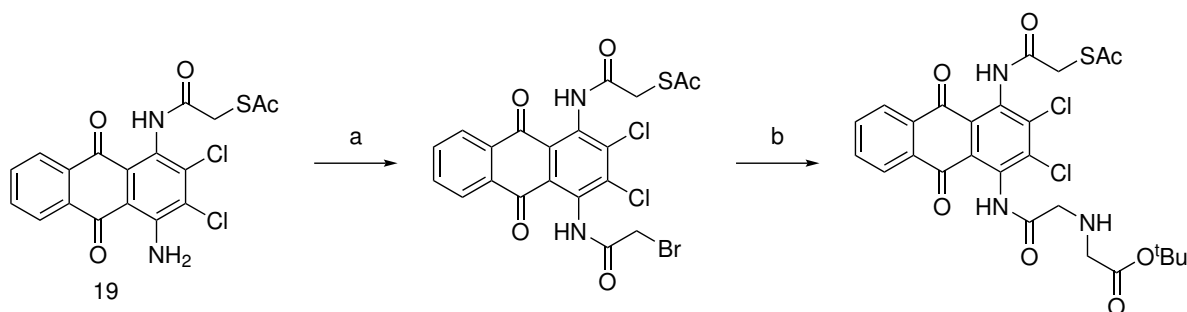


**Figure 5.9:** Instalment of second handle. a) bromo acetyl bromide. b) *t*BuO-Gly-NH<sub>2</sub>.

### 5.1.2 Ullmann Condensation

The strategy was changed and instead the use of sodium 1-amino-4-bromo-9,10-dioxo-9,10-dihydroanthracene-2-sulfonate (**20**) as starting material was investigated. This anthraquinone already contains the sulphonic acid group, and two functional groups for attachment of the required handles. Additionally, has it previously been used in an Ullmann type condensation[143] or more specific the Ullmann amine synthesis[144] using metallic copper (Cu(0)) and microwave (MW) heating[145, 146], see figure 5.10.

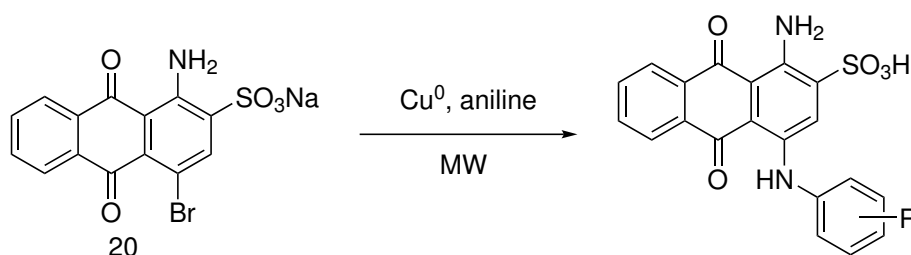


**Figure 5.10:** Ullmann condensation reaction using Cu(0) and MW heating.

This Ullmann cross-coupling mechanism has been investigated[147–152] for many years. Experimental evidence shows that many copper species can be used successfully[148], but still the mechanism is not fully understood[153]. It is generally agreed[147, 148, 154, 155] that Cu(I) is the active intermediate and the reaction is most likely initiated by an oxidation[148, 155] of Cu(0) to Cu(I) by atmospheric oxygen[155]. Through an oxidative addition, the Cu(I) is inserted in between the anthraquinone and the bromide proposedly as the Cu(III) species[143, 148, 151, 156–159] (other mechanism has also been discussed including Cu(II)[152]). The aniline is introduced to the cycle by a ligand exchange with the bromide, and lastly a reductive elimination releases the product, illustrated on figure 5.11. It is worth noting that the exact mechanism may depend on the substrate, as the optimal copper species and medium also dependent on the substrate[153]. For the 2-sulphonate anthraquinone, Müller et al. found that Cu(0) was the optimal catalyst[153], with an aqueous buffer as the medium using MW as

the heat source.

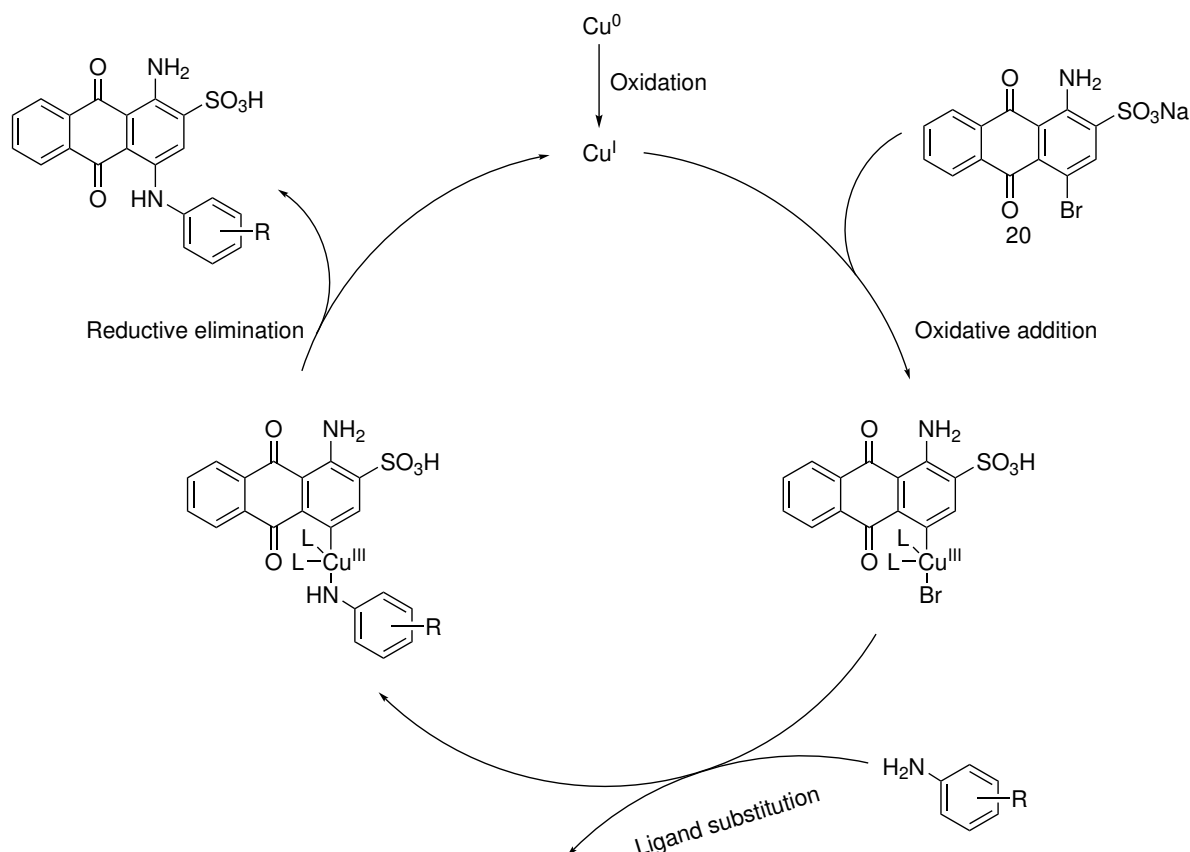


**Figure 5.11:** Proposed Cross-Coupling mechanism for the Ullmann condensation.

Inspired by the work of Müller et al.[146] addition of both an acid-handle (AQ acid, **21**) and an ester-handle (AQ ester, **22**), see figure 5.12, was investigated. It was observed that along with the desired product, a side product was formed due to hydrolysis of the starting material giving the corresponding 1-amino-4-hydroxy-9,10-dioxo-9,10-dihydroanthracene-2-sulfonate (**23**). To further investigate the reaction, aiming to limit formation of the side product, a series of parameters was alternated. These included reaction time, order of reagents added and pH, but without seeing any effect on the ratio of product to biproduct formation.

After consultation with Prof. Müller, it was found that the freshness of the aqueous buffer used as solvent, was of high importance[160–162]. Rewardingly, when the buffer components (A (base) and B (acid)) was freshly made and kept cold, until being mixed just before the reaction was started, the reaction proceeded satisfyingly.

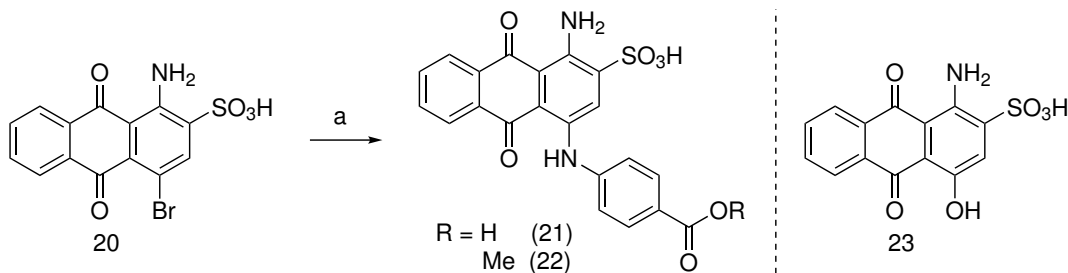


**Figure 5.12:** Ullmann condensation as described by Müller et al.[146]. a) aniline derivative, Cu(0), phosphate buffer, MW, 120°C, 20 min.

### 5.1.2.1 Handles on opposite sides

In the original design (figure 5.3 page 40), the thiol handle (for electrode binding) and the acid/ester handle (for functionalization to attach the enzyme) was placed on each side of the anthraquinone. Two different pathways were investigated.

**Pathway 1;** adding the thiol handle before the Ullmann condensation, see figure 5.13. As described before (section 5.1.1) installation of the thiol was done through an acylation with bromo acetyl bromide followed by substitution with KSAC. However, even though formation of product was observed by mass-spectrometry it could not be confirmed by NMR.

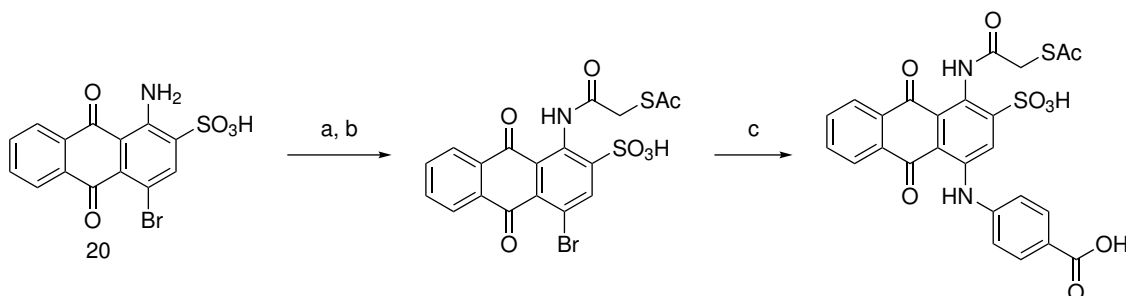


**Figure 5.13:** Pathway 1: instalment of the thiol handle using bromo acetyl bromide and KSAC, followed by the Ullmann condensation. a) bromo acetyl bromide. b) KSAC. c) Aniline derivative, Cu(0), phosphate buffer, MW, 120°C, 20 min.

**Pathway 2;** installation of the thiol handle after the Ullmann condensation. Again, the Ullmann condensation was proceeded as previously described. For the thiol-handle installation a series of reactions were investigated, see overview on figure 5.14.

As no product formation was observed for any of the reactions, they will not be further discussed here. A short summary of the reactions can be found in the experimental section chapter 7 page 75. One potential explanation for the low reactivity of the amino group ortho to the sulphonic acid may be the formation of a zwitter-ion between the sulphonate and the



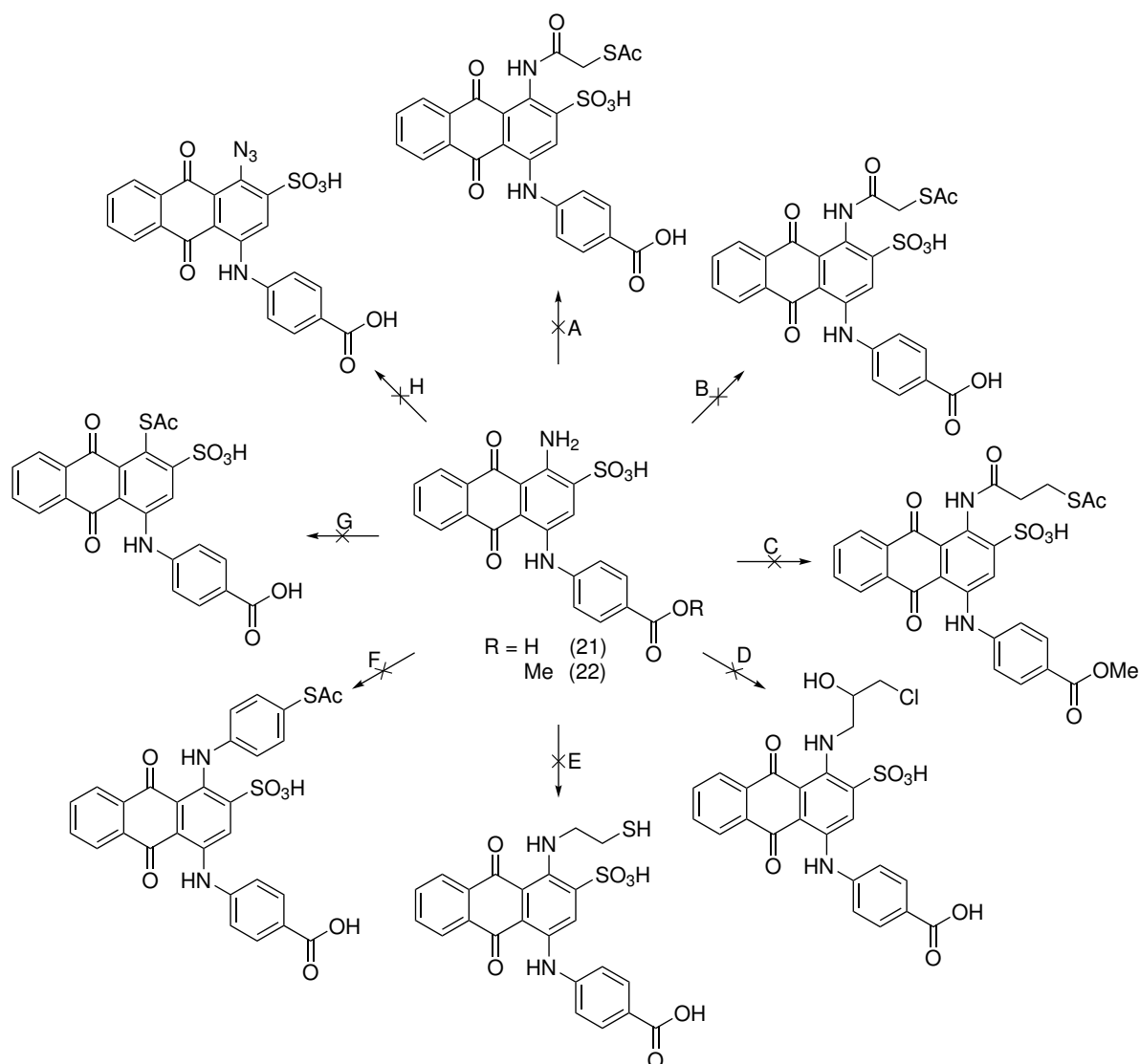


**Figure 5.14:** Pathway 2: first the Ullmann condensation followed by addition of the thiol handle through: A) Bromoacetyl and KSac, B) TCFH amide coupling, C) Acryloyl chloride then KSac, D) Epoxy, E) Thiirane, F) Ullmann conditions, G) Diazotization then KSac, H) Diazotization then  $N_3$ . See details in chapter 7.

anilinium ( $pK_{aH}$  4.6[136]), see figure 5.15, resulting in a significant decrease in nucleophilicity.

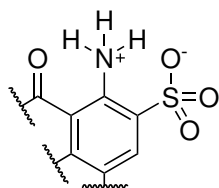


**Figure 5.15:** Zwitter-ion between the sulphonate and the anilinium.

## 5.1.2.2 Handles on the same side

The strategy was changed to install both handles via an Ullmann reaction. The appropriately decorated aniline (**25**) species was prepared from methyl 3-amino-5-bromobenzoate (**24**) by substituting the bromide with thioacetate, to give methyl 3-(acetylthio)-5-aminobenzoate (**25**), under cross-coupling conditions using  $\text{Pd}_2(\text{dba})_3$ ,  $\text{CyPF-}^t\text{Bu}$  and heating, see figure 5.16A. The Ullmann condensation proceeded as prior described, see figure 5.16B, to give the 4-((3-(acetylthio)-5-(methoxycarbonyl)phenyl)amino)-1-amino-9,10-dioxo-9,10-dihydroanthracene-2-sulfonic acid (**26**).

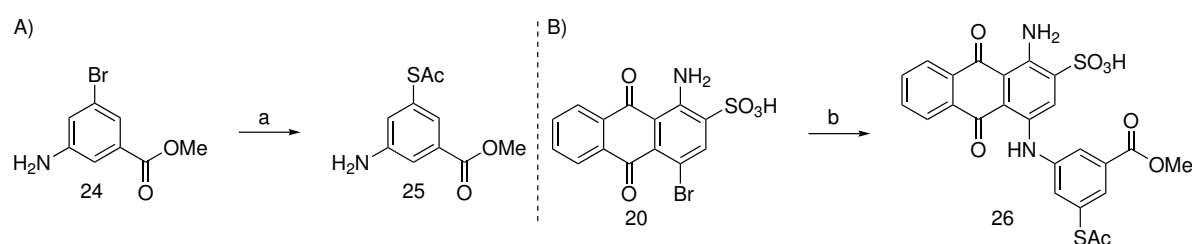


**Figure 5.16:** A) Synthesis of aniline derivative, a) KSAc,  $\text{Pd}_2(\text{dba})_3$ ,  $\text{CyPF-}^t\text{Bu}$ , toluene, reflux, 24 hours. B) Ullmann condensation, b) Aniline derivative,  $\text{Cu}(0)$ , phosphate buffer, MW,  $120^\circ\text{C}$ , 20 min.

For the electrochemical studies both the free carboxylic acid (**27**) and the protected methyl-ester (**28**) was of interest. To identify conditions allowing for selective deacetylation of the thiol without affecting the ester, different conditions (1 M HCl, 1 M NaOH, 6 M HCl and 6 M NaOH,  $80^\circ\text{C}$  for 4 hours) were tested. The results are shown in figure 5.17. While 1 M NaOH resulted in full deprotection (**27**), rewardingly, 1 M HCl allowed selective removal of the thiol acetyl-group to give **28**. With a scaffold for the anthraquinone design in hand studies of the electrochemical properties were initiated.

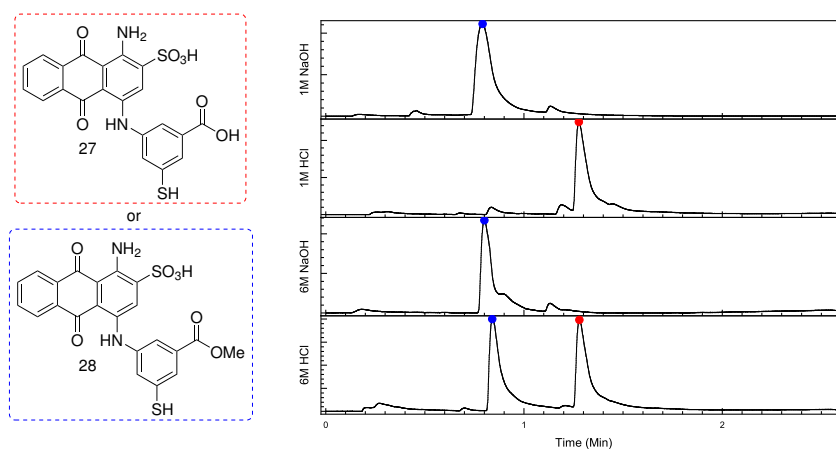


**Figure 5.17:** Selective deprotection study of **26**.

## 5.2 Electrochemical Study in Solution

First electrochemical study was of the AQ acid (**21**) and the AQ ester (**22**) in solution, to get an idea of the electron transfer properties of the anthraquinone design. The thiol was left out to prevent monolayer formation on the gold surface.

### 5.2.1 Experimental Set-up

For all electrochemical studies a three-electrode system was used; consisting of the working electrode (WE, red), the reference electrode (RE, blue) and the counter electrode (CE, black), see figure 5.18.

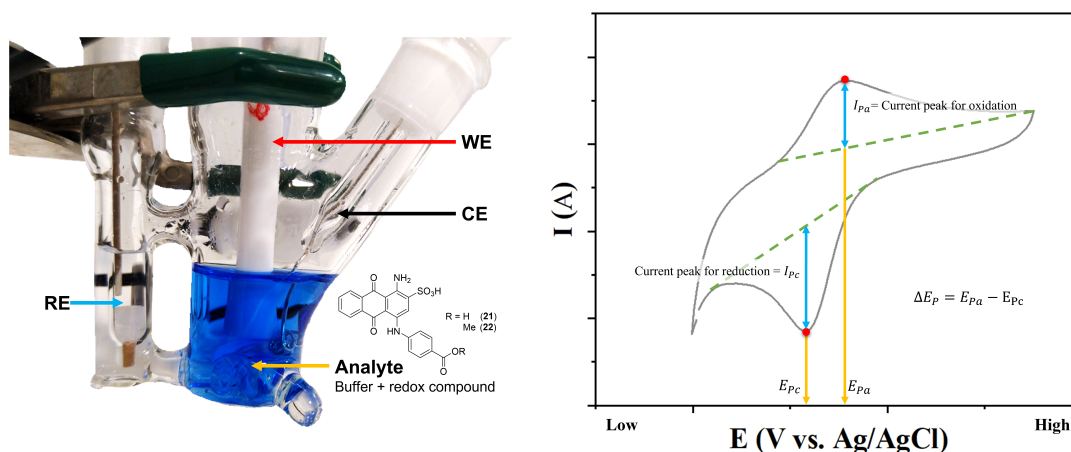


**Figure 5.18:** Left: the electrochemical three-electrode set-up used. Right: a general CV with the relevant information illustrated.

The potential is measured between the working electrode and the reference electrode, while the current is measured between the working electrode and the counter electrode[163]. The reference is an Ag/AgCl-type electrode and the counter is a platinum-type electrode. The working electrode is a nanoporous gold electrode (NPG) which is prepared as described by Xiao et al.[164] using a dealloying method, see details in experimental section chapter 7 page 75.

For all electrochemical studies, cyclic voltammetry (CV) was used for analysis as this provides a full description of redox properties, peak heights, and positions. In a CV program the potential applied ranges from low to high and back to low in a cycle, and the output read is the current provided. The method gives a diagram showing the oxidation and reduction current-peaks of the analyte, the potential-separation of peaks  $I_{Pc}$  and  $I_{Pa}$  is due to diffusion[163] of the analyte on/off the electrode and is calculated by  $\Delta E_P = E_{Pa} - E_{Pc}$ . For a reversible system

it should be 57 mV[163] at 25°C, a system is reversible when both oxidation and reduction peaks are present.

### 5.2.2 Recording CVs or Measuring CVs

The CV diagrams, at scan rate 20 mV/s, for both redox compounds at each pH[127] is displayed in figure 5.19, diagrammed as the current density ( $\mu\text{A cm}^{-2}$ ) against the potential applied (V). At first it appears that the AQ acid has well defined oxidation and reduction peaks, however for the AQ ester the oxidation peak is less defined. This is an indication that AQ acid undergoes quasi-reversible redox process, while less reversible with AQ ester.

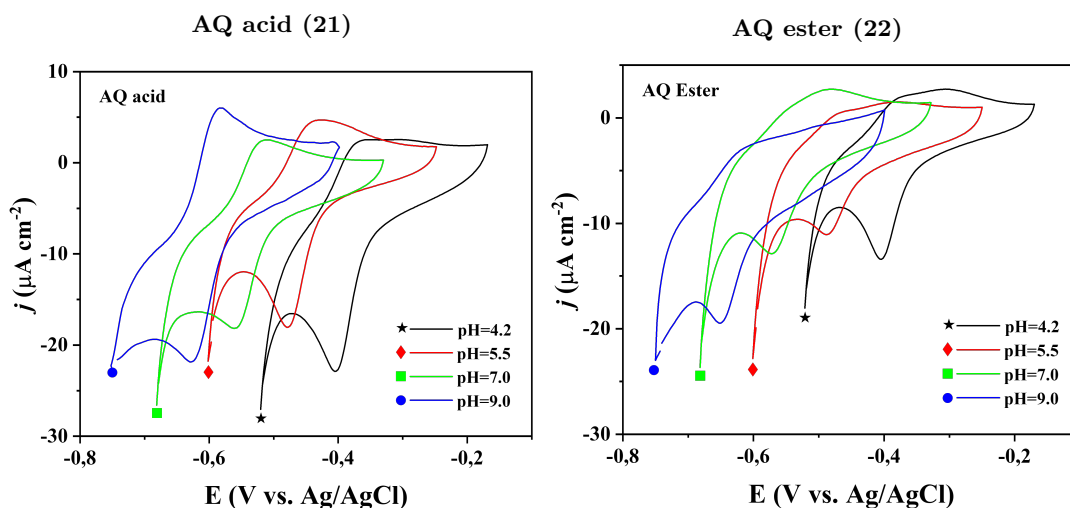


Figure 5.19: CVs of AQ acid (21) and AQ ester (22) for all four pHs at 20 mV s<sup>-1</sup>.

These data points are later used to find the electron transfer rate constant ( $k_s$ ), which gives an overall idea of the speed of the electron transfer with between the redox compound and the electrode[165]. However, to ascertain the required parameters, which will briefly be introduced in section 5.2.3, more CVs were recorded at different scan rates which are shown in figure 5.20 and 5.21.

### 5.2.3 Data Processing

The theory behind the method of calculating the electron transfer rate constant was introduced by R. A. Marcus[166] in 1956[167] and is known as the Marcus Theory. Since then many additions to the field has been made for specific systems and conditions. The Randles–Ševčík equation 5.1 describes the relation between scan rate ( $\nu$ ) and peak current ( $I_p$ ), suitable for

a diffusion-controlled redox process. The equation also includes the number of electrons ( $n$ ), surface area ( $A$ ), electrolyte concentration ( $c$ ), and diffusion coefficient ( $D$ ),

$$I_p = 0.4463nFAc \left( \frac{nF\nu D}{RT} \right)^{1/2} \quad (5.1)$$

the constants are:  $F$  the Faraday constant ( $96485 \text{ C mol}^{-1}$ ) and  $R$  the gas constant ( $8.314 \text{ J K}^{-1} \text{ mol}^{-1}$ ), and often the temperature,  $T$ , is  $298 \text{ K}$ , giving the known simplified version equation 5.2.

$$I_p = 2.69 \cdot 10^5 n^{3/2} A D^{1/2} c \nu^{1/2} \quad (5.2)$$

Other constant components determined by the experiment setup is: the number of electrons ( $n = 2$  for AQ), the surface area of the electrode ( $A = 0.125663706 \text{ cm}^2$ , see equation 5.4), and the concentration of the redox compound in the electrolyte ( $c = 0.07 \text{ mM} = 7 \cdot 10^{-8} \text{ mol cm}^{-3}$ ). This leaves the peak current ( $I_p [\text{A}]$ ), the scan rate ( $\nu [\text{V s}^{-1}]$ ) and the diffusion coefficient of the redox compound ( $D [\text{cm}^2 \text{ s}^{-1}]$ ), to give equation 5.3:

$$I_p = 0.006692759 D^{1/2} \nu^{1/2} \quad (5.3)$$

To normalize the values to the accessible surface area, the current is replaced with the current density ( $j [\text{A cm}^{-2}]$ ), dividing the measured current with the surface area ( $A$ )

$$A = \pi r^2 = \pi (2 \text{ mm})^2 = \pi (0.2 \text{ cm})^2 = 0.125663706 \text{ cm}^2 \quad (5.4)$$

$$j_p = \text{current density} = \frac{I_p}{A} \quad (5.5)$$

To give the relation between the current density and the scan rate

$$j_p = 0.053259283 D^{1/2} \nu^{1/2} \quad (5.6)$$

The current density peak at the cathode ( $j_{pc}$ ) gives the diffusion coefficient of the oxidation ( $D_O$ ) and at the anode ( $j_{pa}$ ) for the reduction ( $D_R$ ). By plotting  $j_p$  against  $\nu$  the slope can be used to calculate the diffusion coefficients for the redox compound (equation 5.7), for convenience the current density and the scan rate is in  $\mu\text{A cm}^{-2}$  and  $\text{mV s}^{-1}$  respectively.

$$D = \left( \frac{\text{slope}_{j_p}}{53259.28} \right)^2 \quad (5.7)$$

$D_O$  and  $D_R$  can then be used to estimate the electron transfer rate constant ( $k_s$ ) with the Nicholson's method[168], suitable for a diffusion-controlled redox process. The relation between diffusion coefficient and the electron transfer rate is written as equation 5.8:

$$\Psi = \frac{\left(\frac{D_O}{D_R}\right)^{\alpha/2} k_s}{\sqrt{\pi \frac{nF\nu}{RT} D_O}} \quad (5.8)$$

From Nicholson's method  $\alpha$ , a transfer coefficient, is set to 0.5.  $\Psi$  is a kinetic parameter and is related to the peak separation ( $\Delta E_p$ ) as described in table 1 in Nichol's article from 1965[168],  $\Psi$  is read from the graph using  $\Delta E_p$ . Later Lavagnini et al.[169] derived a function describing the relation between  $\Psi$  and  $\Delta E_p$ [165], see equation 5.9.

$$\Psi = \frac{-0.6288 + 0.0021 E_p n}{1 - 0.017 E_p n} \quad (5.9)$$

For this method the  $\Delta E_p$  value cannot go below 58.9 mV as the function is a hyperbole towards this value, also the upper range goes to 299.4 mV where the curve intersects the x-axis. The electron transfer rate can then be isolated in equation 5.8, to give equation 5.10, and calculated from the 20 mV/s scan rate, presented in figure 5.19.

$$k_s = \frac{\Psi}{\left(\frac{D_O}{D_R}\right)^{\alpha/2} \sqrt{\pi \frac{nF}{RT} D_O \nu^{-1/2}}} \quad (5.10)$$

$D_O$  and  $D_R$  will for most systems be equal because the oxidation/reduction reaction is reversible. When alternating the scan rate, it affects not only the current peak height but also the position[165, 170] due to the thickness of the diffusion layer. This is true for quasi-reversible systems[171], where the peak separation increases with the scan rate[165]. The scan rates tested are 10, 30, 50, 100 and 200 mV/s. In figure 5.20 and 5.21 the current density is plotted against the potential at the different scan rates, along with the diffusion coefficients calculated for each pH, for AQ acid (**21**) and AQ ester (**22**) respectively.

## AQ acid (21)

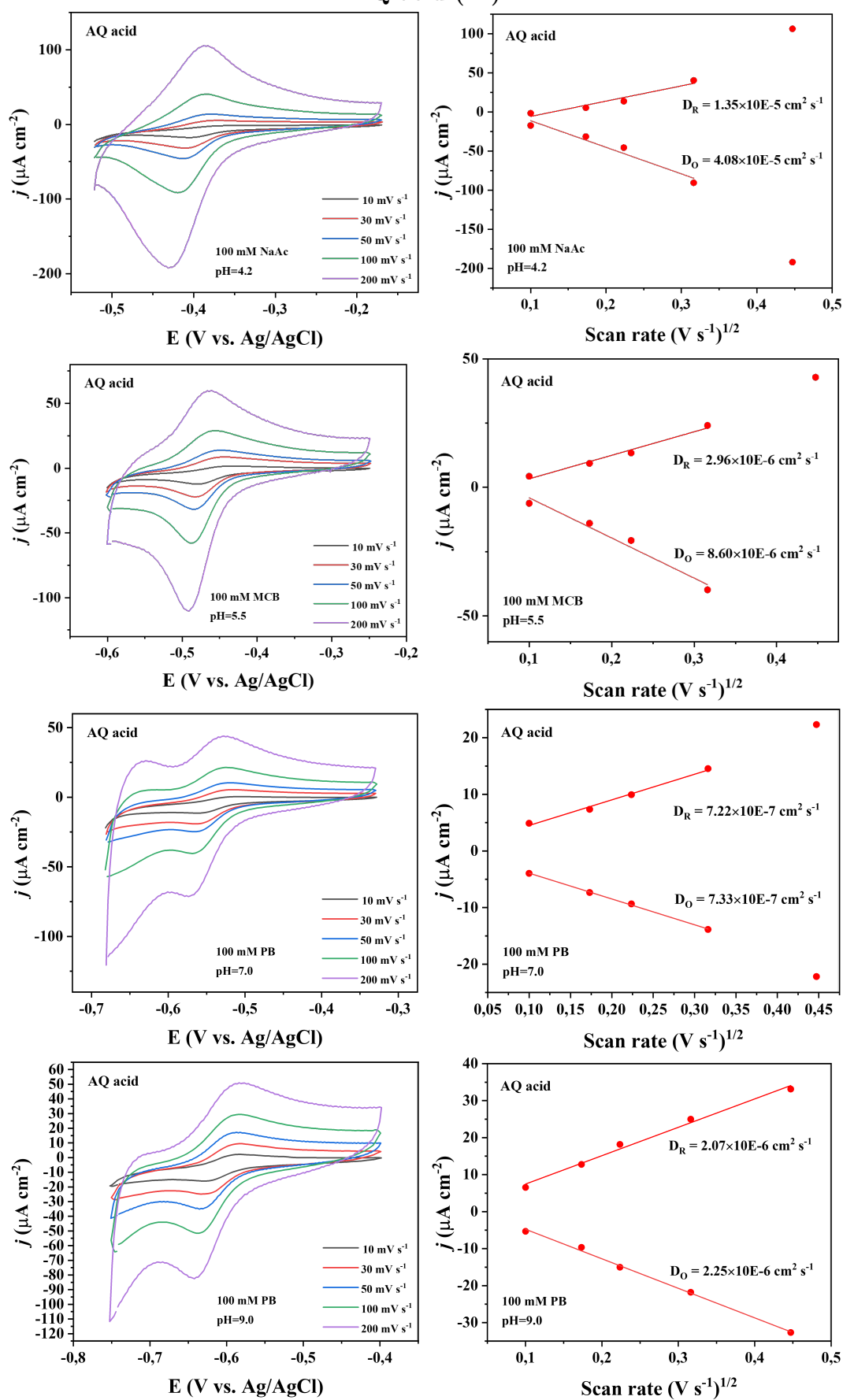


Figure 5.20: Collected CVs of AQ acid (21) and diffusion coefficient graphs.

## AQ ester (22)

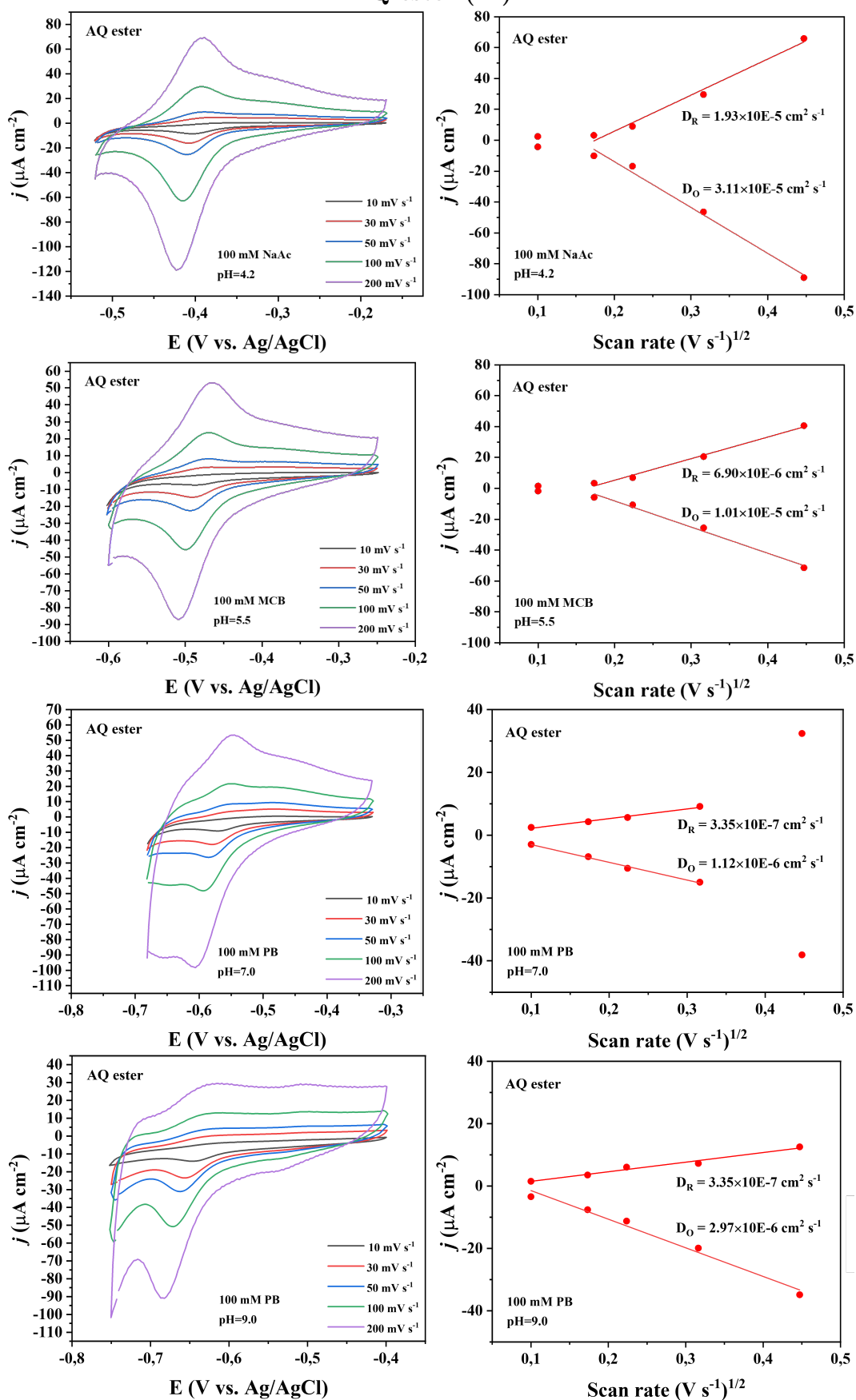


Figure 5.21: Collected CVs of AQ ester (22) and diffusion coefficient graphs.



After finding the diffusion coefficient for both oxidation and reduction at each pH, then the electron transfer rate can be calculated by equation 5.10 derived above, and data from the 20 mV/s scan rate, presented in figure 5.19. The calculations are seen in table 5.3.

**Table 5.3:** Calculation of electron transfer rate constants.

Compound [pH]	$D_O$ ( $\text{cm}^2 \text{s}^{-1}$ )	$D_R$ ( $\text{cm}^2 \text{s}^{-1}$ )	$\Psi^*$	$k_s$ ( $\text{cm s}^{-1}$ )*	Std. of $k_s$
AQ acid [4.2]	4.08E <sup>-5</sup>	1.35E <sup>-5</sup>	2.23	0.0239	0.00618
AQ acid [5.5]	8.60E <sup>-6</sup>	2.96E <sup>-6</sup>	2.82	0.0140	0.01329
AQ acid [7.0]	7.33E <sup>-7</sup>	7.22E <sup>-7</sup>	1.61	0.0030	0.00046
AQ acid [9.0]	2.25E <sup>-6</sup>	2.07E <sup>-6</sup>	2.41	0.0078	0.00183
AQ ester [4.2]	3.11E <sup>-4</sup>	1.93E <sup>-5</sup>	2.33	0.0295	0.00848
AQ ester [5.5]	1.01E <sup>-5</sup>	6.90E <sup>-6</sup>	$\Delta E_{pn}$ out of range		
AQ ester [7.0]	1.12E <sup>-6</sup>	3.35E <sup>-7</sup>	0.28	0.00046	0.000077
AQ ester [9.0]	2.97E <sup>-6</sup>	3.35E <sup>-7</sup>	6.50	0.00055	**

\* Mean value of 1-3 scans (all experiments are run three times, however not all data could be used)

\*\* Only one dataset usable

Both the AQ acid (**21**) and the AQ ester (**22**) showed optimal electron transfer rate constant, just above 0.02 cm/s, at pH 4.2. This is a reasonable value compared to other compounds in the literature[172–174], see figure 5.22, therefore it was decided to continue to work with this core, next with the thiol present.

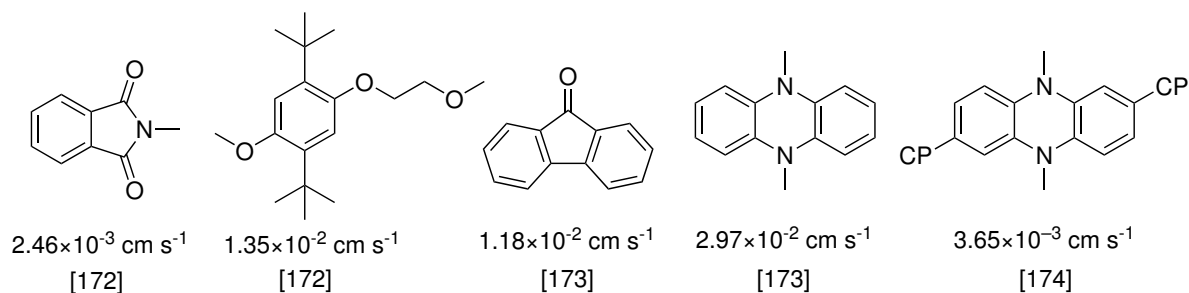


**Figure 5.22:** Electron transfer rate constants from literature.

## 5.3 Electrochemical Study of AQOMe (28)

The electrochemical studies of the AQOMe (28) were performed by PhD Xiaomei Yan, the study and results can be found in a recent paper[175]. In this study a self-assessment monolayer (SAM) was formed with the thiol-functionalized anthraquinone on the gold NPG, by soaking the electrode in a AQOMe solution as described in the experimental chapter 7 section 7.3. SAMs provide an enhanced control and can eliminate the mass diffusion layer component as the molecule is covalently attached to the electrode. It also allows for fixed lengths[127] and designed packing[127]. From the results presented in the paper, it could be concluded that the AQOMe showed overall well-defined SAM and promising electron transfer properties. However, when analysing the molecule in solution at pH 7.0 and 9.0 a second redox pair was observed, see figure 5.23.

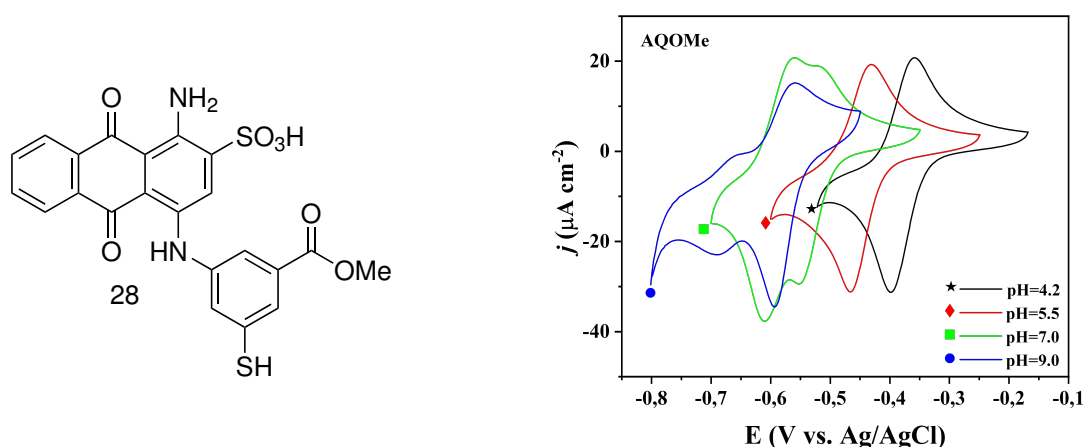


**Figure 5.23:** AQOMe (28) and its CVs from electrochemical study in solution obtained by PhD Xiaomei Yan.

To further investigate the origin of this peak, four compounds were synthesized: AQSH (29) without the ester, AQO<sup>t</sup>Bu (30) to see if it originates from hydrolysis of the ester to the carboxylic acid, AQOMe-dA (31) to see if it was the zwitterion of aniline, and AQaSH (32) with an aliphatic thiol to see if the thiophenol was responsible for the extra peak.

### 5.3.1 Synthesis of AQOMe Derivatives

Washkuhn et al. published a study[176] of the hydrolysis stability of different benzoate esters and based on this study, it was decided to synthesise the tertbutyl (tBu) ester, as this showed one of the lowest hydrolysis rates.

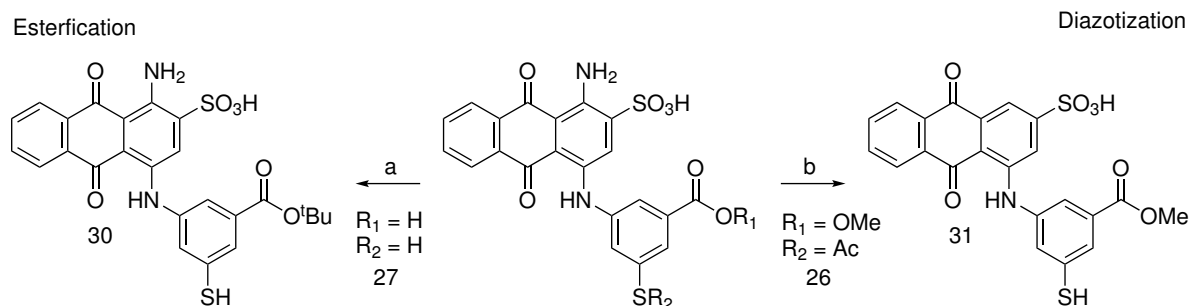


**Figure 5.24:** Synthesis of *t*Bu derivative (**30**) and the de-aminated (**31**). a) *t*BuOH, MgSO<sub>4</sub>, H<sub>2</sub>SO<sub>4</sub>, DCM, rt, overnight. b) NaNO<sub>2</sub>, 1 M HCl, 0°C, 1 hour then Zn, EtOH.

The esterification was done under acidic conditions[177] with tert-butanol and MgSO<sub>4</sub>. To synthesise AQOMe-dNH<sub>2</sub> (**31**) without the primary aniline, a diazotization reaction was done on the thioacetate protected AQOMe (**26**). To get the analogue functionalised with an aliphatic thiol, AQaSH (**32**), the AQ acid (**21**) was reacted with S-(2-aminoethyl) ethanethioate hydrochloride (**33**) in an amide coupling using PyBOP and N-ethylmorpholine. Afterwards the thioacetate was deprotected with 1 M HCl to give the free thiol (**32**), see figure 5.25.

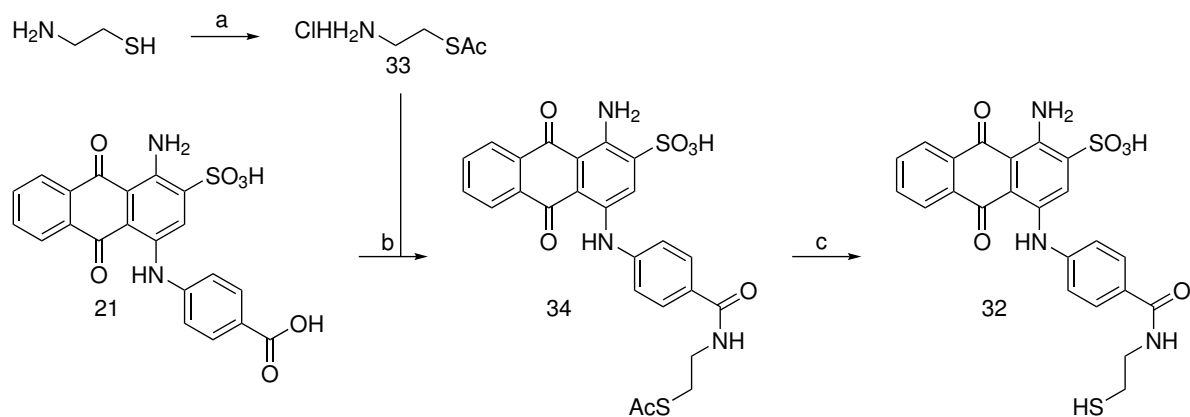


**Figure 5.25:** Synthesis of the aliphatic derivative (**32**). a) AcCl, TFA, 0°C, 1 hour. b) PyBOP, NEM, DMF, rt, overnight. c) 1 M HCl, MeOH, 80°C, overnight.

The synthesis of AQSH (**29**), without the ester functionality, is described in chapter 6. Interestingly the colour of the anthraquinone in solution changes from purple to dark blue when replacing the thiophenol with an aliphatic thiol, see figure 5.26.

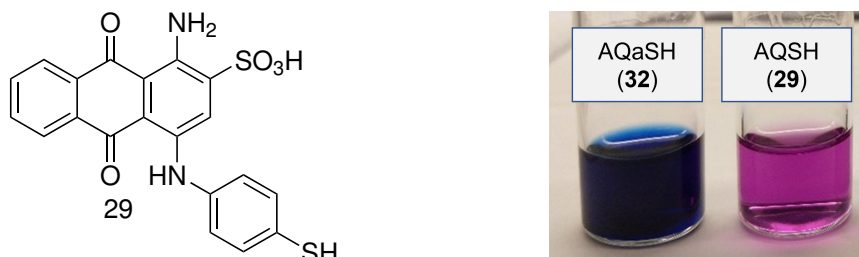


**Figure 5.26:** Left: AQSH (29). Right: picture of AQuSH (32, blue) and AQSH (29, purple) in solution.

### 5.3.2 Electrochemical Study of AQOMe Derivatives in Solution

The CV diagrams<sup>1</sup> of each derivative, at all four pH, is displayed in figure 5.27, depicted as current density ( $\mu\text{A cm}^{-2}$ ) vs potential applied (V) at 20 mV/s (scan rate). By qualitative analysis it could be concluded that only the aliphatic thiol (AQuSH, 32) had a single peak-pair, thereby confirming that the thiophenol group gave rise to the second redox pair.

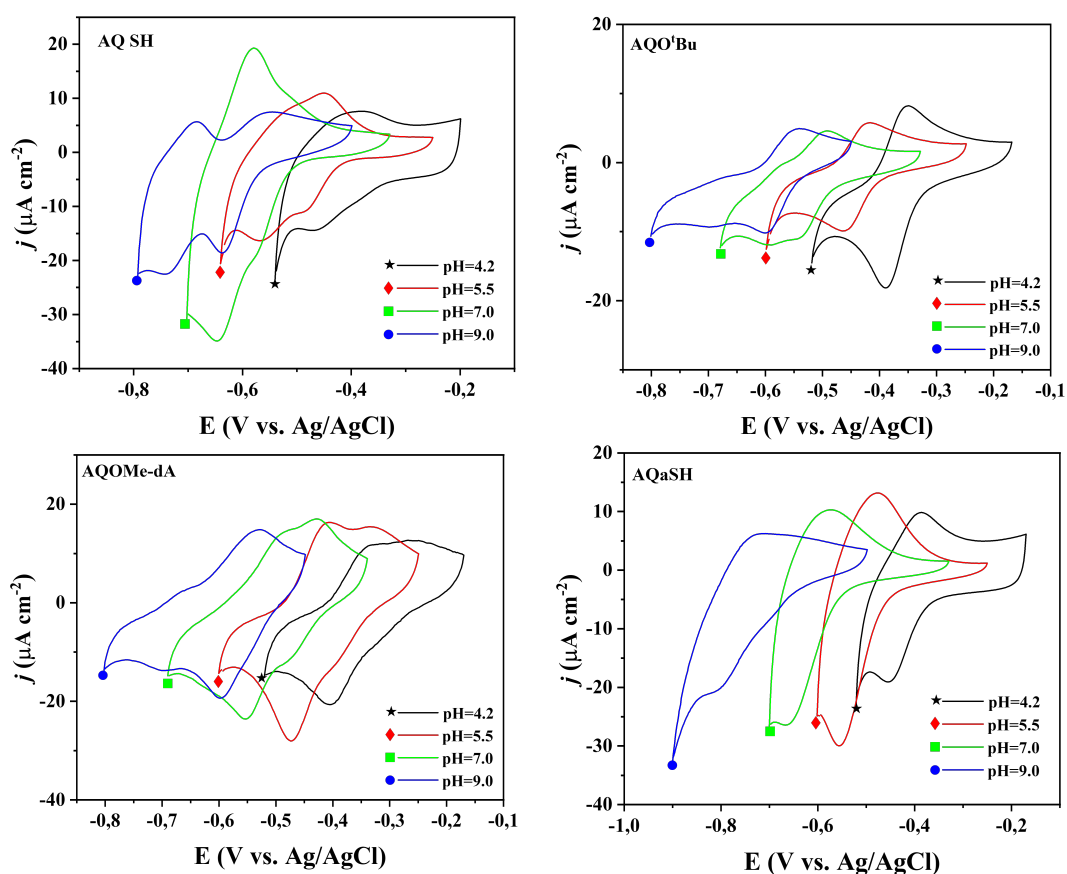


**Figure 5.27:** CVs of AQOMe derivatives in solution.

<sup>1</sup>Dataset for AQOMe-dA (31) and AQO'Bu (30) was obtained by PhD Xiaomei Yan.

Berberova et al.[178] reported that thiophenol anions can fragment to the corresponding radical species and dimerize. The formation of the dimer of AQSH could explain the second redox peak. That the extra peak only appears at pH 7.0 and 9.0 fits with the pK<sub>a</sub> of thiophenol being 6.6[179], therefore, at these pH's the thiophenol will be mostly on the deprotonated form. As the thiol is only installed to obtain the SAM on the gold surface of the electrode, this will not affect their later use as bridging molecules.

## 5.4 Addition of the Protein Handle

The redox-active molecule was designed to have a handle for later conjugation to the biomolecule. This was done by reacting DBCO-amine with the anthraquinone (**27**) benzoic acid functionality, in an amide coupling, to give compound **35**, see figure 5.28.

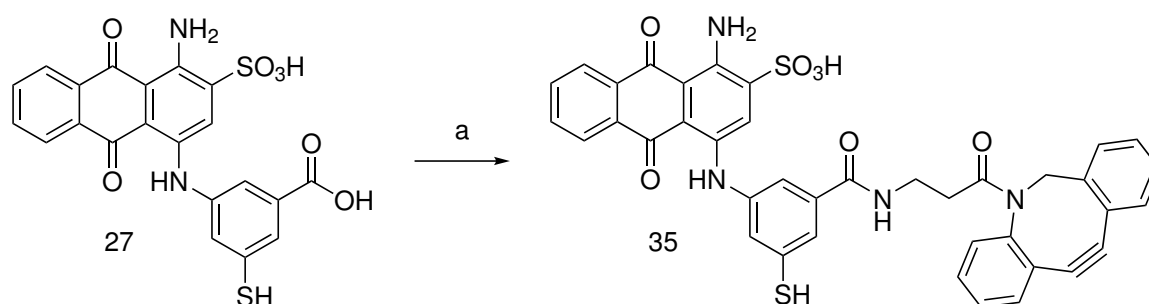


**Figure 5.28:** Synthetic step to add the click-handle DBCO-amine. a) DBCO-amine, COMU, DIPEA, DMSO, 0°C → rt, overnight.

The DBCO-amine unit consist of a strained alkyne handle that can be used in copper-free strain-promoted azide–alkyne cycloaddition (SPAAC) reactions. Due to the very strained nature of the alkyne, it will in the presence of a good 1,3-dipole act as a dipolarophile and initiate a Huisgen 1,3-dipolar cycloaddition, see figure 5.30. A 1,3-dipole has a unit of three atoms which share a dipole[180], this can be generally written as <sup>+</sup>a-b-c<sup>-</sup>, where a is valence incomplete and positively charged, and c has an unshared electron pair and are negatively charged. This property applies for the azido group, which is more specifically an ambiphilic dipole. This means that the roles of HOMO/LUMO is controlled by the substituents of the dipolarophile as the HOMO/LUMO of the two pairs are very similar, see figure 5.29. If the substituents are EDGs it will raise the HOMO, giving the 1,3-dipole the role of the LUMO, and if they are EWGs it will lower the LUMO making the 1,3-dipole the HOMO component[181]. Computational studies[182] of the azido group has shown that the electron distribution likely has the inner-most nitrogen bearing the negative charge at most times.

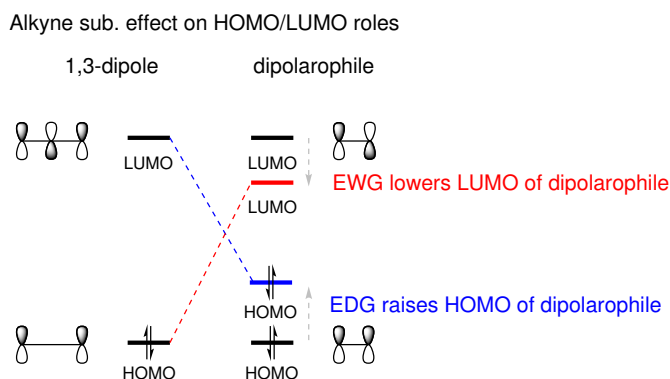


**Figure 5.29:** HOMO/LUMO influenced by substituents of dipolarophile, inspired by [183].

The DBCO-alkyne is very symmetric and therefore both regioisomers will be formed during the click-reaction[184–186], see figure 5.30.

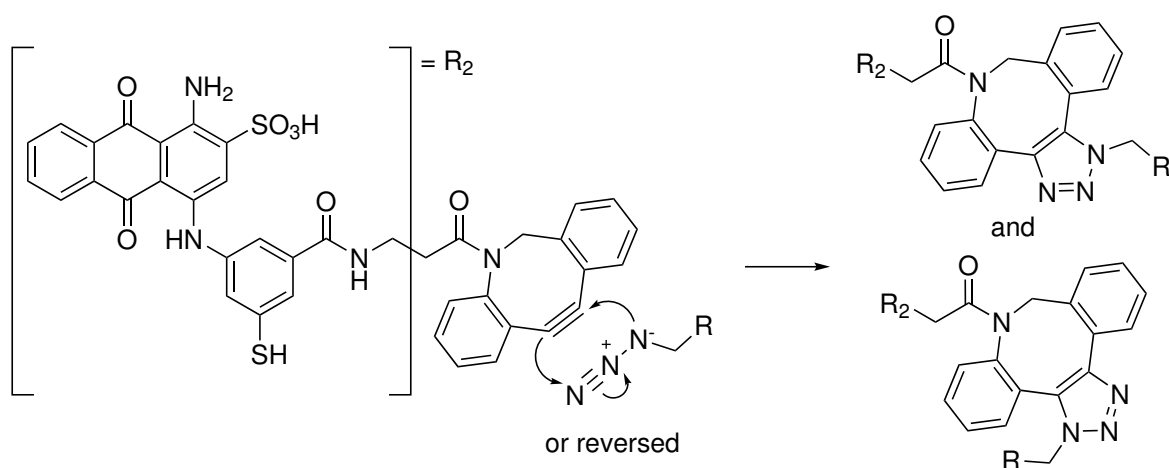


**Figure 5.30:** Huisgen 1,3-dipolar cycloaddition between the DBCO-unit and an azido-handle.

## 5.5 Summary

The lead anthraquinone structure has shown promising electrochemical properties and therefore the next step is to investigate its interaction with the respective enzyme and its function as an electron bridge. The results from this investigation is presented in chapter 6.



## CHAPTER 6

# Anthraquinone as an Electron Bridge for Enzyme

As introduced in chapter 1 and chapter 5, conjugates of proteins and organic molecules can be used to transfer electrons and create a current. In this chapter the anthraquinones' properties as an electrode-anchored electron bridge via non-covalent binding to redox enzymes are investigated.

Redox enzymes interact with its substrate to perform an oxidation/reduction reaction[187, 188]. In a mediated electron transfer mechanism, an oxidizing enzyme oxidizes its substrate and accepts the electron(s), followed by transfer of the electron(s) from the enzyme to an electron mediator, and lastly the mediator will transfer the electron(s) to the electrode's anode, see figure 6.1. For a reducing enzyme this would be the opposite; electrons will be transferred from a cathode to the mediator, and then to the enzyme, which reduces the substrate. Examples in literature can be found where both types of enzymes have been used in synergy to create a flow battery[131, 173].

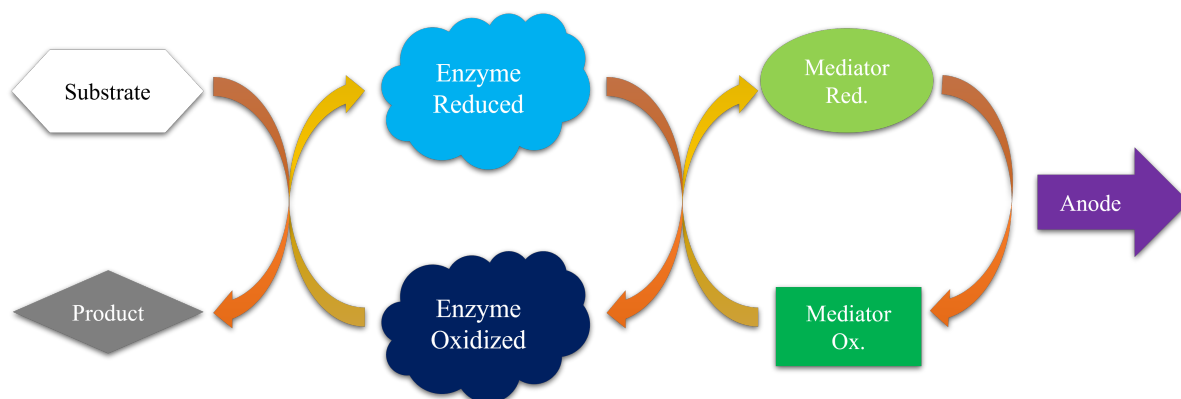


**Figure 6.1:** Schematic overview of the oxidation/reduction between the conjugate components.



It has previously been shown by Cosnier et al.[189] that an anthraquinone can non-covalently bind to a hydrophobic pocket, close to the T1 copper centre, of the enzyme laccase. They demonstrated that the anthraquinone bound to a carbon nanotube cathode functioned as a bridge between the enzyme and the cathode. Here, the anthraquinone serves as an electron transfer “bridge”. A similar hydrophobic pocket exists in the enzyme fructose dehydrogenase (FDH)[190].

In this chapter the impact of the substituents ( $R_1$  and  $R_2$ ), see figure 6.2, on the anthraquinones redox properties and the effects on its interaction with the respective enzyme is investigated. The electrode used in this study is a glassy carbon electrode modified with a nanoporous gold (NPG) surface, which afterwards has been covered with a monolayer of a thiol functionalized anthraquinone (AQ). The NPG-AQ is then combined with the enzyme, to give the final complex (NPG-AQ-E) as illustrated in figure 6.2 (for FDH). Orientation of the enzyme is of high importance[39] as the distance between the redox centre and the electrode should not exceed 20 Å[191, 192] for direct electron transfer. An anchored bridge molecule can be designed to assist in the orientation of the enzyme and control the distance.

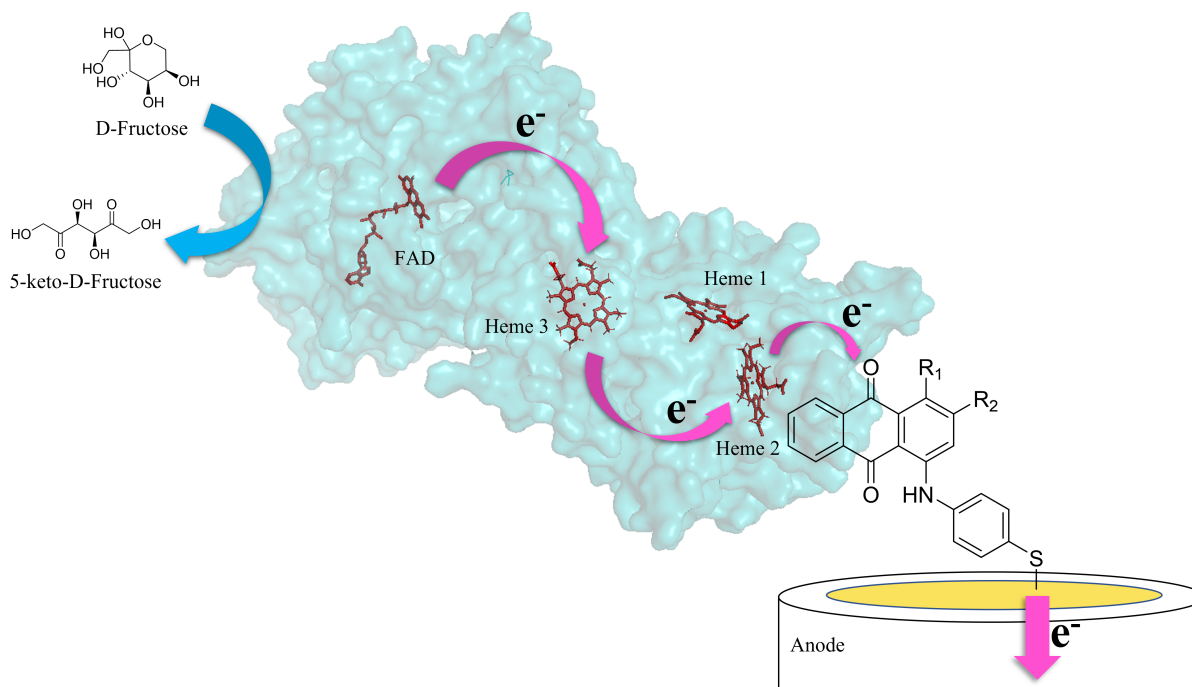


**Figure 6.2:** Schematic illustration of NPG-AQ-Enzyme (FDH Homology model, adapted with permission from Xinxin Xiao [188]) electrode. For a good electron transfer the heme 2 group needs to be close to the electrode.

## 6.1 Design and Synthesis of Anthraquinones

For studying the non-covalent interaction with the enzyme, four new analogues were synthesised based on the design from chapter 5. A thiol-functionalization is needed for attachment to the gold surface. The new analogues are the AQ containing; only the thiol handle (AQdd, **36**), the thiol handle and the 1-NH<sub>2</sub> (AQdS, **37**), as well as the thiol handle and the 2-SO<sub>3</sub>H (AQdA, **38**). Lastly the AQ containing the thiol handle and both the 1-NH<sub>2</sub> and 2-SO<sub>3</sub>H functional groups (AQSH, **29**) was prepared, see figure 6.4. The AQdd is similar to the AQ used in the article by Cosnier et al.[189].

Learning from chapter 5, the Ullmann condensation was used to attach the thiophenol, giving AQSH (**29**) and from this, the other analogues could be synthesized by orthogonal removal of one functional group at a time (figure 6.4). First the S-acetyl protected 4-aminothiophenol (**39**) needed for the Ullmann condensation was synthesised in three steps, see figure 6.3, from the 4-aminothiophenol (**40**). It proved to be important for the yield of the Ullmann reaction that the thiol was protected. Therefore, first the amino group of 4-aminothiophenol was Boc-protected (**41**), followed by acetyl protection of the thiophenol (**42**). The Boc-protection group was then selectively removed to give the S-(4-aminophenyl) ethanethioate (**39**).

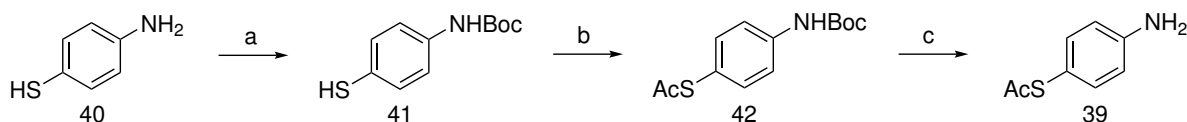


**Figure 6.3:** Synthesis of S-(4-aminophenyl) ethanethioate (**39**). a) Boc<sub>2</sub>O, H<sub>2</sub>O, rt, 24 hours. b) AcCl, NEt<sub>3</sub>, DCM, 0°C, 30 min. c) TFA, rt, 30 min.

To synthesize the AQ-derivatives, see figure 6.4, 1-amino-4-bromoanthraquinone-2-sulfonic acid sodium salt (**20**) was reacted with S-(4-aminophenyl) ethanethioate (**39**) in an Ullmann condensation to give the AQSH (**29**). Synthesis of AQdA (**38**) could be achieved by selectively removing the amino group in a diazotization reaction, while the sulphonic acid was selectively removed using glucose and base[193], to give the AQdS (**37**). In this reaction the glucose act as a reducing agent which leads to formation of H<sub>2</sub>O<sub>2</sub> and thereby OH-radicals, which can mediate the desulphonylation, as reported by Li et al.[194].

The four anthraquinones prepared showed distinct colour differences, relating to their different properties of the compounds[195, 196]. Figure 6.5 shows a 5 mM solution of each of the compounds. AQSH (**29**) has a light purple colour, whereas when the electron donating aniline is removed (AQdA, **38**) the purple colour becomes darker. Then when the sulphonic acid is removed (AQdS, **37**) a drastic change is seen as the solution becomes orange, and lastly, the

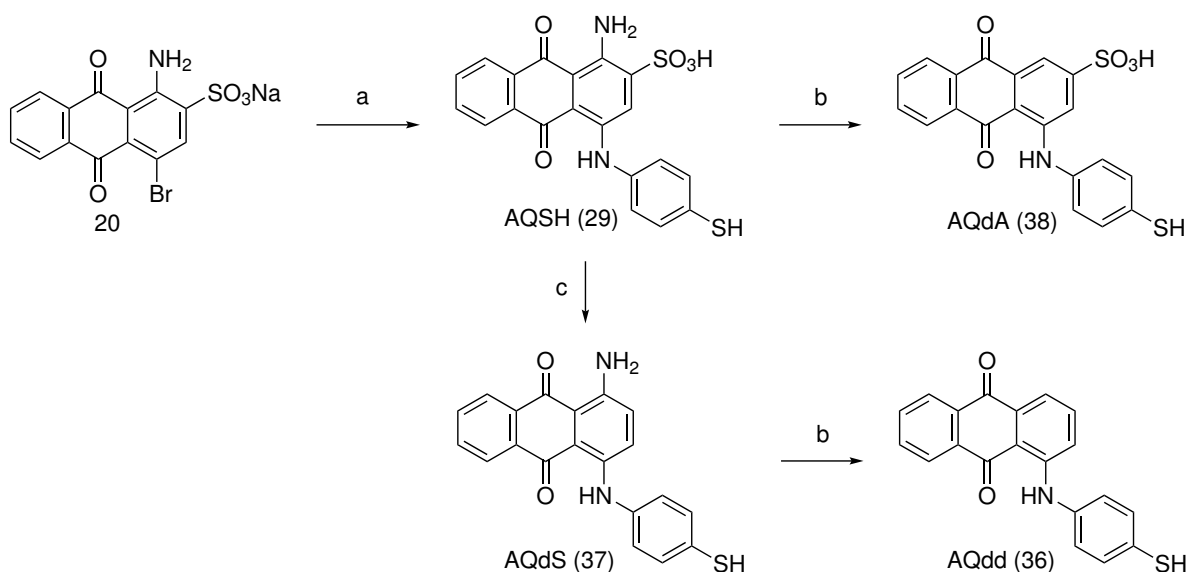


**Figure 6.4:** Synthesis of AQ derivatives. a) **39**, Cu(0), phosphate buffer, MW, 120°C, 20 min. b) NaNO<sub>2</sub>, 1M HCl, 0°C, 20 sec. then Zn, EtOH. d) glucose, 30 M NaOH, H<sub>2</sub>O, 80°C, 30 min.

unsubstituted AQdd (**36**) shows almost no colour. The colour change is an indication of the change in orbital overlap and electrons contributing to the system[197].

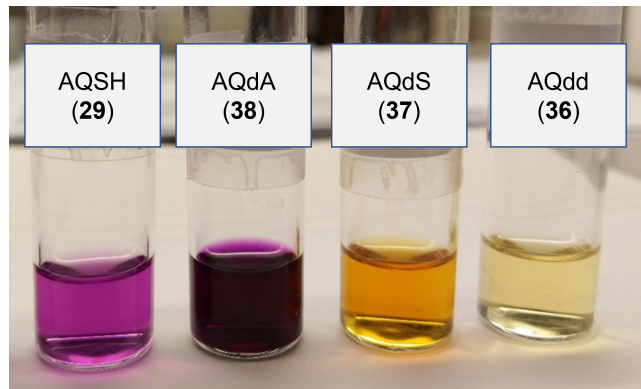


**Figure 6.5:** Picture of AQ derivative in 5 mM solutions.

## 6.2 Electrochemical Study as Monolayer

The setup is identical to the one used in chapter 5, consisting of the three electrodes; reference electrode (Ag/AgCl), counter electrode (platinum wire) and working electrode (NPG-AQ-E, as described earlier), preparation details can be found in chapter 7. Again, cyclic voltammetry (CV) is used for testing the electrochemical system.

Each electrode functionalized with different AQs were analysed under four different conditions: (1) pure buffer solution as a reference, (2) buffer solution with enzyme substrate ( $O_2$  for laccase and fructose for FDH), to analyse the direct electron transfer (DET) from the enzyme, through the AQ, to the electrode. (3) Buffer solution with a mediator present (ABTS or FeMeOH) for the mediated electron transfer (MET) reference, and (4) buffer solution with mediator and enzyme substrate to analyse the MET where the electron transfer goes around the AQ (and possibly also other centres through the enzyme[188, 198])[199]. MET provides information about the amount of catalytic active enzyme loaded in total.

### 6.2.1 Laccase

Inspired by the previously mentioned paper by Cosnier et al.[189], the anthraquinones interactions with the laccase enzyme was studied. Laccase contains a hydrophobic pocket, close to the T1 copper centre, which an anthraquinone has been demonstrated to non-covalently bind to. The substrate of laccase is  $O_2$  which is reduced to  $H_2O$  by donation of 4 electrons[200] from the enzyme, with the electrons coming from the cathode though the mediator.

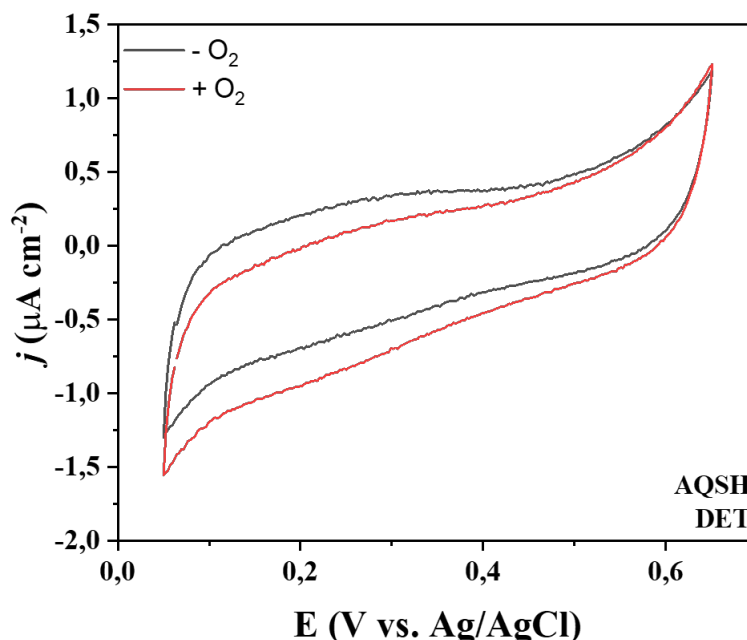


**Figure 6.6:** CV from laccase study with AQSH (29).

ABTS is a well-known mediator for laccase[201–203]. The colourless ABTS gives an electron to the oxidized enzyme, retuning the enzyme to its reduced state. The resulting  $ABTS^{\cdot+}$  has a blue-greenish strong colour, see figure 6.7A-D.

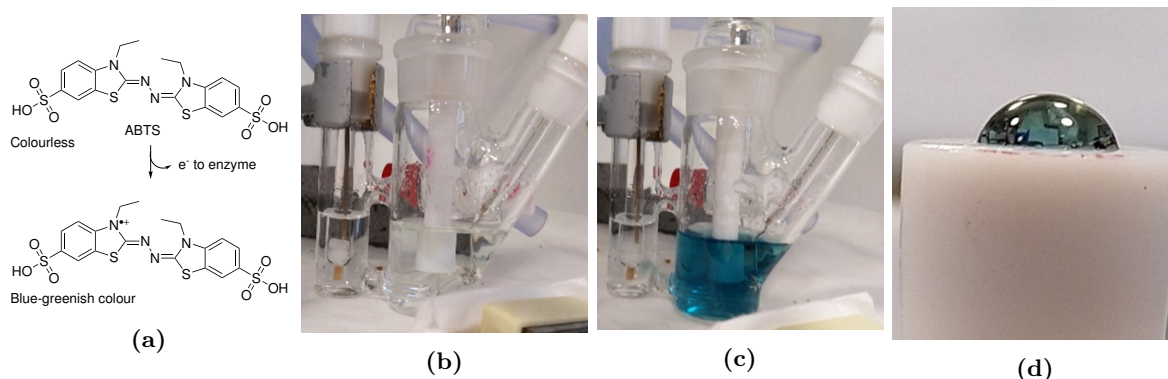


**Figure 6.7:** ABTS as an electron mediator for laccase. (a) the reaction, (b) initial (colour of ABTS), (c) after reaction (colour of ABTS<sup>•+</sup>), (d) a drop of ABTS solution on the electrode with enzyme and O<sub>2</sub> (from the air) shows the enzyme being present and active.

After several attempts, studies with the laccase enzyme was stopped. The enzyme was seen to be present and active on the electrode (as confirmed with ABTS, figure 6.7), however, it did not interact with any of the anthraquinones. Instead, experiments were continued with the enzyme fructose dehydrogenase (FDH).

## 6.2.2 Fructose dehydrogenase

FDH is a sugar oxidating enzyme responsible for the oxidation of D-fructose to 5-keto-D-fructose (see figure 6.2), in a process where the enzyme gains 2 electrons[199]. These electrons are then transferred through the bridge molecule (here the anthraquinone) to the electrode. A homology model of FDH[188] is seen on figure 6.2, illustrating the electrons' movement from the substrate through the enzyme (via FAD, heme 3 and heme 2[188]) to the anthraquinone. With FDH it was possible to obtain a signal for both DET and MET. CV diagrams for all anthraquinone derivatives can be seen in figure 6.1 as the current density ( $\mu\text{A cm}^2$ ) against the potential applied (V).

The output signal is highly dependent on the enzyme orientation on the electrode, and without a covalent bond this will never be consistent. To illustrate this a series of diagrams from the same anthraquinone, AQdS, on different electrodes are shown individually on table 6.2. This clearly demonstrates the value of developing controlled and site-selective strategies, for production of consistent bioconjugates in electrocatalytic applications.

**Table 6.1:** FDH CV datasets for AQ derivatives. The reference without any enzyme substrate is marked as “-FT” and with 100 mM substrate (fructose) as “+FT”.

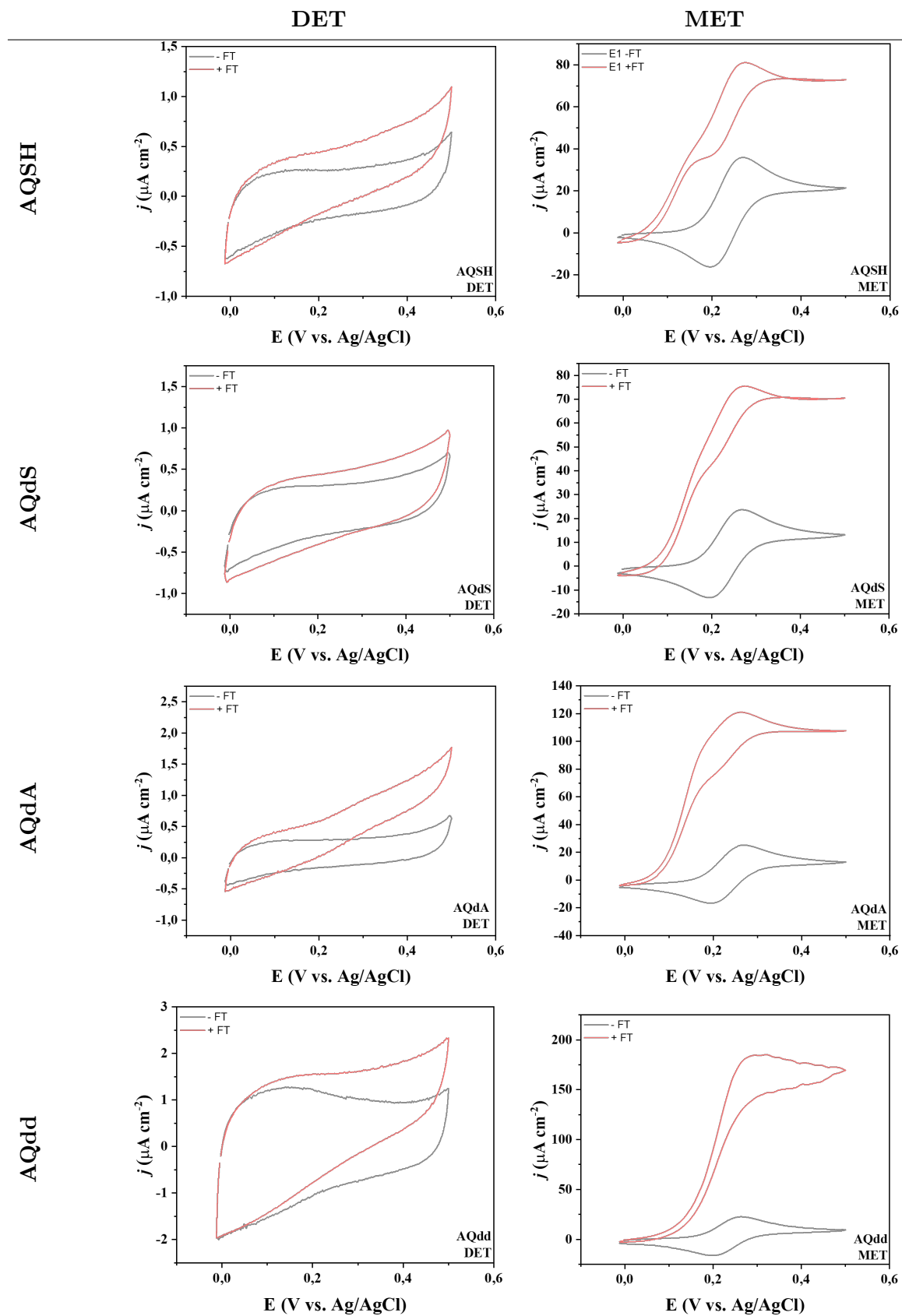
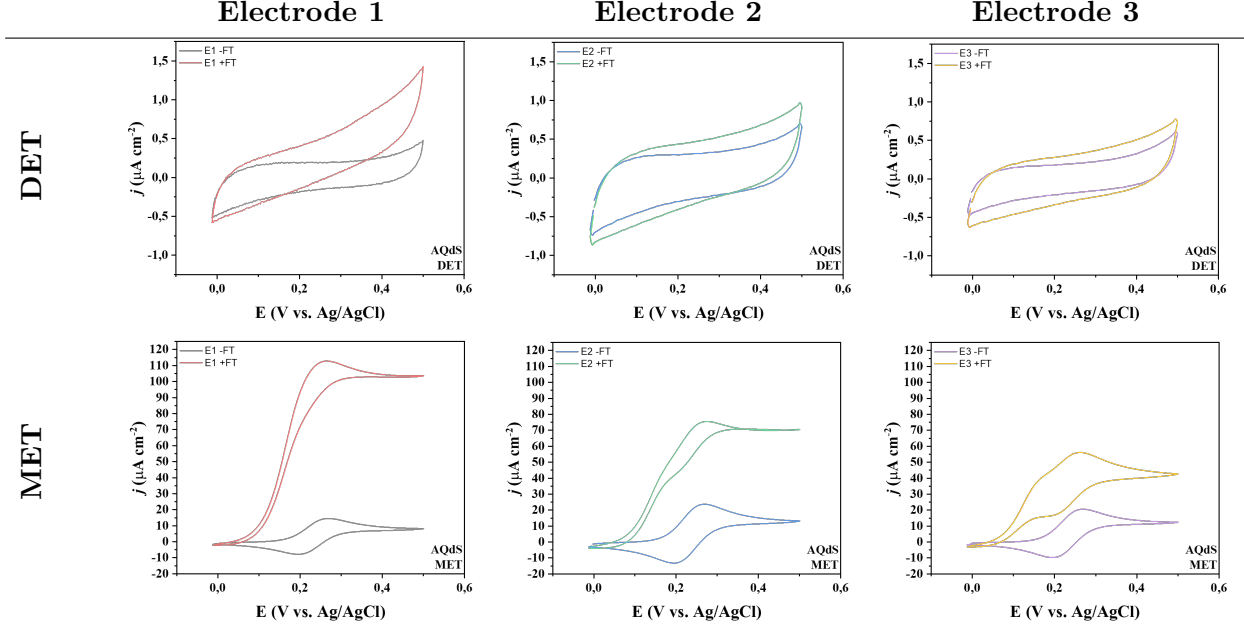


**Table 6.2:** FDH CV datasets for different electrodes with AQdS (37). The baseline without any enzyme substrate is marked as “-FT” and with 100 mM substrate (fructose) as “+FT”.



The electrocatalytic current ( $\Delta j$ ) is the difference at DET between the output with enzyme-substrate (+) and the baseline without (-) at the right switching potential[39, 204], gives a relative picture of the anthraquinones ability as an electron bridge. The same difference at MET gives a relative picture of the amount of enzyme loaded onto the electrode, see both on figure 6.8.

$$\Delta j_{DET} = j_{DET+(0.5V)} - j_{DET-(0.5V)} \quad (6.1)$$

$$\Delta j_{MET} = j_{MET+(0.5V)} - j_{MET-(0.5V)} \quad (6.2)$$

The ratio between the two  $\Delta j$ s gives an idea of how good a direct mediator the anthraquinone is compared to the loading of enzyme, a high ratio would indicate that a lot of electrons are transferred with a low enzyme loading, see figure 6.9. This is called the DET-capable fraction ( $\chi_{DET}$ ) and is displayed as percentage.

$$\chi_{DET} = \frac{\Delta j_{DET}}{\Delta j_{MET}} \cdot 100 \quad (6.3)$$

For the AQs tested it was the AQdA (38) that showed the overall best properties as a bridge molecule. This is reasonable[205] when comparing to the discussing from chapter 5,

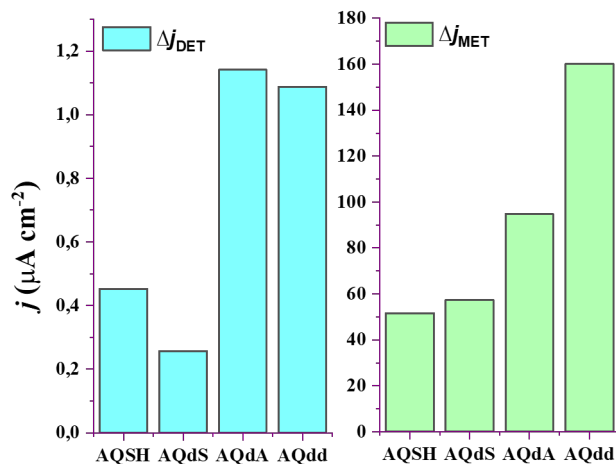


Figure 6.8: Left:  $\Delta j_{\text{DET}}$ , right:  $\Delta j_{\text{MET}}$ .

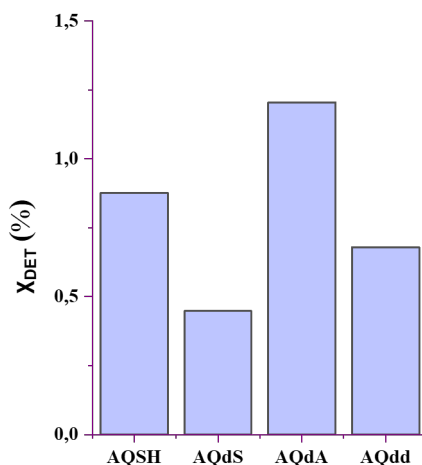


Figure 6.9: DET-capable fraction ( $\chi_{\text{DET}}$ ).

as the sulphonic acid enhances the redox potential by elongating the conjugated system[125], and without the aniline its polarity is probably better matching the hydrophobic pocket of the enzyme than AQSH (**29**). AQdd (**36**) was predicted to fit the pocket best, as it is very similar to the bare anthraquinone, which has been shown to bind in enzymatic hydrophobic pockets[189, 190]; however, with a relatively weak redox potential compared to the other analogues. AQdS (**37**) has the EDG  $-\text{NH}_2$  which lowers the redox potential by donation of lone-pair electron to the system[124, 205].

### 6.2.3 Comparison with Mercaptoethanol

To validate the setup and procedure, a SAM of mercaptoethanol (BME) was tested under similar conditions, as it has shown to bind the enzyme, and have a good surface coverage[188]. As seen on the CV diagrams, figure 6.10, there is a good signal from the enzyme. In comparison



to the AQs the  $\Delta j_{DET}$  is  $160 \text{ A cm}^{-2}$ .

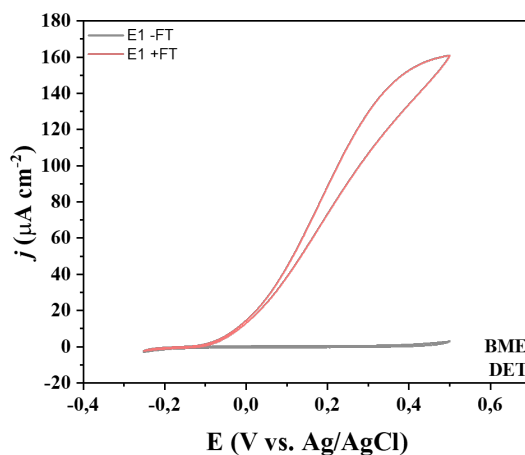


**Figure 6.10:** CV dataset of the set-up validation with mecaptopoethanol. The reference without any enzyme substrate is marked as “-FT” and with 100 mM substrate (fructose) as “+FT”.

## 6.3 Future Work

Among the investigated anthraquinones, the AQdA (**38**) was found to have promising properties, for further development. Going forward, the next step would be to optimize the rather low surface coverage of the AQ on the gold surface, or the disorder[127] of the formed monolayer. Here it would be feasible to investigate the instalment of a spacer between the anthraquinone and the electrode. Based on the design of the spacer, it is possible to tune the overall electronic properties as desired. Examples of reported spacers are alkanes, conjugated systems, or peptides, which all possess different properties[127]. The alkane chain is flexible and can bend to allow the AQ to move closer to the electrode surface during electron transfer, whereas the conjugated is more rigid but can function as an electronic road for the electron transfer (either electron hopping or tunnelling[127]). The peptide spacer is inspired by biological electron transfer, and multiple movement mechanisms has been proposed (contraction/bending, helix conversion and hopping along the backbone)[127].

Another challenge, mentioned in chapter 1, is the orientation and amount of enzyme immobilized on the electrode. Here a solution would be to covalently bind the enzyme to the anthraquinone in the right orientation through bioconjugation[39]. The concept and benefits of site-selective bioconjugation was presented in chapter 2 and a promising site-selective bioconjugation technique that could be used was presented in chapter 3.

# CHAPTER 7

## Experimental Section Part II

---

General Methodologies relevant for all experimental work can be found in appendix A.  
Details for figure 5.14 page 48.

- Reaction **A** and **C** both utilizes very electrophilic acid halogenides, which has previously shown good results. However, a second reaction was observed most likely at the electrophile position, before KSAc was added.
- Reaction **B** was an attempt to do an amide coupling using the TCFH as it has previously been seen in the group to react well with anilines.
- Reaction **D** and **E** used a strained three-membered ring which was to be opened by the nucleophilic attack from the aniline, some precipitation was formed, possibly polymerization of the epoxy-reagent.
- Reaction **F** was an attempt to do an Ullmann coupling with reversed roles (of the anthraquinone and benzene) compared to the reaction introduced prior.
- Reaction **G** and **H** was a diazotization, forming the diazonium-ion which is a good leaving group, followed by a substitution on the aniline position with either -SAc or -N<sub>3</sub> respectively, however only the deaminated was found.

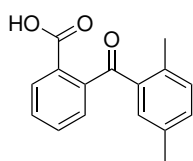
### 7.1 Synthesis of Compounds in Chapter 5

#### General procedure for the $\mu$ wave mediated Ullmann condensation

Sodium 1-amino-4-bromo-9,10-dioxo-9,10-dihydroanthracene-2-sulfonate (**20**, 1 eq.), the appropriate aniline (1.1 eq.) and Cu(0) powder (0.25 eq.) was added to a microwave vial equipped with a stirring bar. The buffer was preferred as described by Bargi and Müller[160]. Buffer A: Na<sub>2</sub>HPO<sub>4</sub>·10H<sub>2</sub>O (CAS 10039-32-4), 0.2 mol, pH 9.67, 7.16 g per 100 mL milli-Q water. Buffer B: NaH<sub>2</sub>PO<sub>4</sub>·2H<sub>2</sub>O (CAS 13472-35-0), 0.12 mol, pH 4.17, 1.82 g per 100 mL

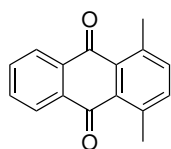
milli-Q water. The two buffers are added to the microwave vial just prior to running the experiment (4:1 of A:B, 25 mL/mmol anthraquinone). The capped microwave vial as heated to 120° for 20 min in a microwave reactor at 80 W. Subsequently concentrated before purification on a reverse phase (RF) dry column plug (water as eluent till hydrolysed red biproduct (**23**) has been collected, then decrease polarity by gradual addition of ACN).

### 2-(2,5-dimethylbenzoyl)benzoic acid (**14A**)

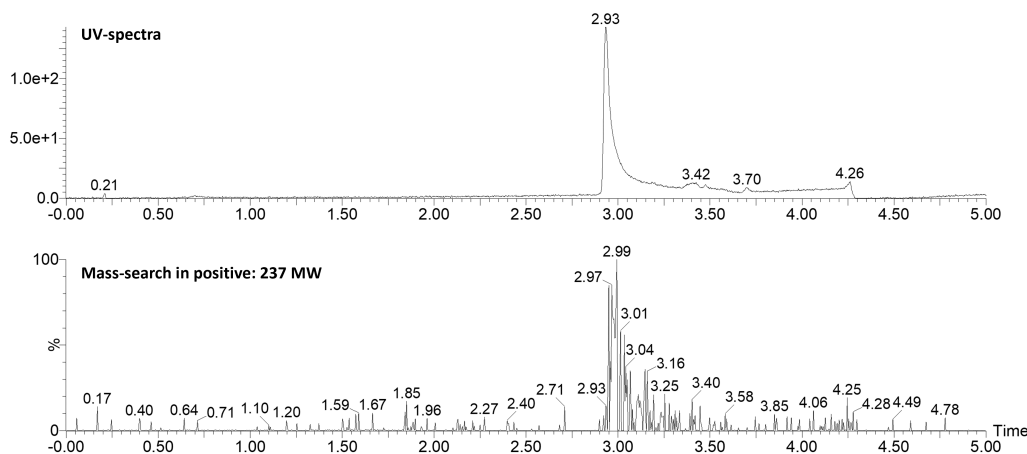


Procedure: Modified from [206]. In a dried round bottom flask was phthalic anhydride (1 g, 6.75 mmol, 1 eq.) and p-xylene (0.92 mL, 7.43 mmol, 1.1 eq.) dissolved in dry DCM (2.87 mL/mmol phthalimide anhydride). Anhydrous  $\text{AlCl}_3$  (1.8 g, 13.5 mmol, 2 eq.) was added slowly over 10 minutes (colour change was observed from yellow, to orange then red) and then the mixture was heated to 40°C. After 4 hours TLC showed that all p-xylene had been used but some phthalimide anhydride was still present, therefore was an additional 0.3 mL p-xylene added. After an hour showed TLC full completion and the reaction mixture was allowed to cool to room temperature. The mixture was slowly added 10% sulphuric acid, then the white precipitate was collected by suction-filtration and dried until the “gum”-like precipitate became dry crystalline powder (**14A**, 1.59 g, 92%).  $^1\text{H}$  NMR (400 MHz, DMSO)  $\delta$  12.90 (s, 1H), 7.90 (dd,  $J = 7.6, 1.4$  Hz, 1H), 7.73 – 7.57 (m, 3H), 7.42 (dd,  $J = 7.4, 1.4$  Hz, 1H), 7.29 – 7.19 (m, 2H), 6.91 (d,  $J = 1.7$  Hz, 1H), 2.48 (s, 3H), 2.17 (s, 3H).  $^{13}\text{C}$  NMR (101 MHz, DMSO)  $\delta$  198.89, 167.87, 142.91, 137.29, 136.27, 134.85, 132.77, 132.48, 132.08, 131.43, 130.87, 130.48, 130.06, 128.43, 20.84, 20.79. HRMS (ESI)  $m/z$ :  $[\text{C}_{16}\text{H}_{14}\text{O}_3 - \text{H}]^-$  Calcd 253.0870; Found 253.0826.

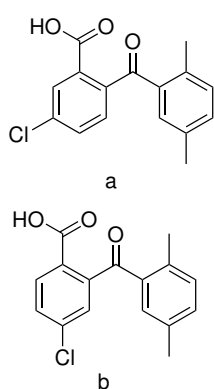
### 1,4-dimethylantracene-9,10-dione (**14**)



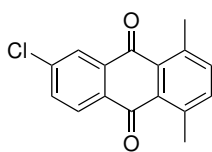
Procedure: As by [206]. The benzoyl-benzoic acid (**14A**, 1.55 g, 6.11 mmol, 1 eq.) was dissolved in conc. sulphuric acid ( $\text{H}_2\text{SO}_4$ , 0.96 mL/mmol **14A**) and heated to 100°C for 1 hour, then TLC showed full conversion. The warm reaction mixture was then poured onto ice, and after the ice has melted can the precipitate be collected by suction filtration. The precipitate was washed excessively with water, and afterwards redissolved in DCM and washed once with water. Anhydrous  $\text{Na}_2\text{SO}_4$  was used to dry the organic phase, which gave the dimethyl anthraquinone (762 mg, 53%) as a dark brown glittery solid. It was not possible to redissolve the compound for NMR, but mass was confirmed by LCMS (calculated  $[\text{C}_{16}\text{H}_{12}\text{O}_2 + \text{H}]^+$  Calcd 237.09):



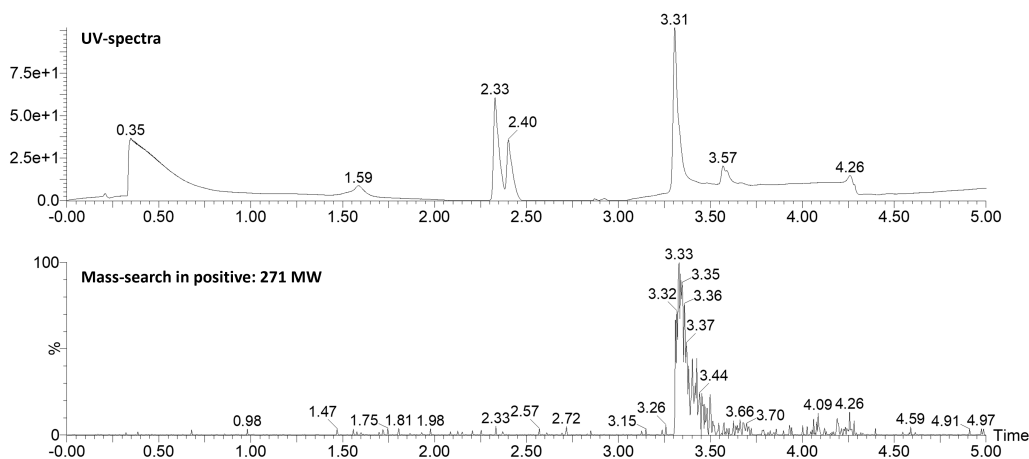
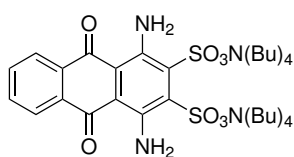
### 5 or 4-chloro-2-(2,5-dimethylbenzoyl)benzoic acid (**15A**)



Procedure: As described for compound **14A**. In a dried round bottom flask was 4-chlorophthalic anhydride (1.3 g, 7.12 mmol, 1 eq.) and p-xylene (1 mL, 7.83 mmol, 1.1 eq.) dissolved in dry DCM (2.87 mL/mmol phthalimide anhydride). Anhydrous AlCl<sub>3</sub> (1.9 g, 14.24 mmol, 2 eq.) was added slowly over 10 minutes. After 5 hours at 40°C showed TLC full conversion of the starting material to two new peaks. The mixture was allowed to cool to room temperature, before slow addition of 10% sulphuric acid, the organic phase was isolated by a separation funnel and evaporated to give a white solid. The solid was then washed with 10% sulphuric acid and then extensively with water, to give the product mixture (**15A**, 1.79 g, 87% - based on NMR integrals 40% **a** and 60% **b**). <sup>1</sup>H NMR (400 MHz, DMSO) δ 7.95 (d, J = 8.4 Hz, 1H **b**), 7.90 (d, J = 2.2 Hz, 1H **a**), 7.80 (dd, J = 8.4, 2.2 Hz, 1H **a**), 7.73 (dd, J = 8.4, 2.1 Hz, 1H **b**), 7.57 (d, J = 2.1 Hz, 1H **b**), 7.50 (d, J = 8.4 Hz, 1H **a**), 7.33 – 7.23 (m, 4H), 6.96 (s, 2H), 2.53 (s, 6H), 2.21 (s, 6H). <sup>13</sup>C NMR (101 MHz, DMSO) δ 197.78, 197.12, 166.86, 166.70, 144.93, 141.35, 137.57, 136.89, 136.63, 136.56, 136.35, 135.07, 135.04, 135.01, 133.11, 133.06, 133.02, 132.31, 132.19, 132.16, 132.14, 131.71, 131.54, 130.52, 130.32, 129.65, 129.27, 128.12, 20.91, 20.79. HRMS (ESI) *m/z*: [C<sub>16</sub>H<sub>13</sub>ClO<sub>3</sub> - H]<sup>-</sup> Calcd 287.0480; Found 287.0430 and 287.0431.

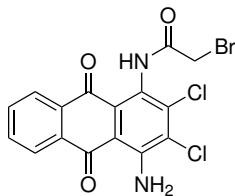
**6-chloro-1,4-dimethylantracene-9,10-dione (15)**

Procedure: The benzoyl-benzoic acid mix (**15A**, 1.77 g, 6.13 mmol, 1 eq.) was dissolved in conc. sulphuric acid ( $\text{H}_2\text{SO}_4$ , 1.63 mL/mmol **15A**) and heated to 135°C for 6 hours, then TLC showed full conversion. The warm reaction mixture was then poured onto ice, and after the ice has melted can the precipitate be collected by suction filtration. The precipitate was washed excessively with water, and afterwards redissolved in EtOAc and washed once with water. Anhydrous  $\text{Na}_2\text{SO}_4$  was used to dry the organic phase, which gave the dimethyl chloro anthraquinone (369.9 mg, 22%) as a black solid. It was not possible to redissolve the compound for NMR, but mass was confirmed by LCMS (calculated  $[\text{C}_{16}\text{H}_{11}\text{ClO}_2 + \text{H}]^+$  Calcd 271.72):

**1,4-diamino-2,3-bis(((tetrabutylamino)oxy)sulfonyl)anthracene-9,10-dione (17)**

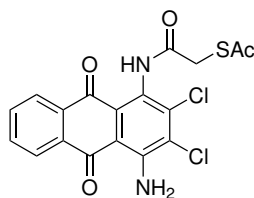
Procedure: The 1,4-diamino-2,3-dichloroanthracene-9,10-dione (**16**, 503 mg, 1.64 mmol, 1 eq.) was dissolved in DMF:H<sub>2</sub>O (2:1, 13.7 mL/mmol **16**) and added  $\text{K}_2\text{SO}_3$  (7.7 g, 49 mmol, 30 eq.). Under stirring was the mixture heated to 95°C overnight. The next day was the mixture cooled to room temperature before filtered and extracted with EtOAc and tetrabutylammonium hydrogen sulphate ( $(\text{Bu})_4\text{N}(\text{HSO}_4)$ ). The organic phase was concentrated and filtered through a short silica dry column (heptane → EtOAc + 10% MeOH) to give the tetrabutylammonium salt of the di-sulphonate (**17**, 676.5 mg, 47%).  $^1\text{H}$  NMR (400 MHz, DMSO)  $\delta$  8.29 – 8.20 (m, 2H), 7.85 – 7.76 (m, 2H), 3.21 – 3.12 (m, 19H), 1.56 (dq,  $J$  = 11.9, 7.6, 6.0 Hz, 19H), 1.31 (h,  $J$  = 7.4 Hz, 20H), 0.93 (t,  $J$  = 7.3 Hz, 28H).  $^{13}\text{C}$  NMR (101 MHz, DMSO)  $\delta$  181.72, 181.66, 162.77, 146.08, 144.22, 143.29, 134.79, 134.35, 132.93, 132.83, 127.10, 126.36, 108.93, 57.99, 23.52, 19.68, 13.96. HRMS (ESI)  $m/z$ :  $[\text{C}_{14}\text{H}_{10}\text{N}_2\text{O}_8\text{S}_2 - \text{SO}_3]^-$  Calcd 317.0238; Found 317.0203.

**N-(4-amino-2,3-dichloro-9,10-dioxo-9,10-dihydroanthracen-1-yl)-2-bromoacetamide (18)**



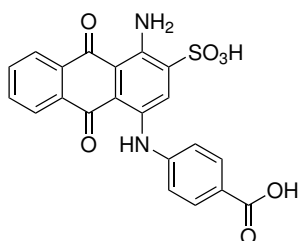
Procedure: The 1,4-diamino-2,3-dichloroanthracene-9,10-dione (**16**, 254 mg, 0.8 mmol, 1 eq.) was dissolved in dry DCM (25 mL/mmol anthraquinone) and added DIPEA (0.16 mL, 1.1 eq.). The solution was cooled to 0°C and under stirring was bromoacetyl bromide (0.07 mL, 1 eq.) added dropwise, afterwards was the mixture allow to warm up to room temperature and stir overnight. The reaction mixture was diluted with DCM before wash with 2 M HCl, then water, sat. NaHCO<sub>3</sub>, and twice brine, the organic phase was then dried over Na<sub>2</sub>SO<sub>4</sub>, and evaporated to dryness to give the bromoacetamide product (**18**, 308.6 mg, 98%). <sup>1</sup>H NMR (400 MHz, DMSO)  $\delta$  10.25 (s, 1H), 8.16 (dd, *J* = 7.4, 1.7 Hz, 1H), 8.05 (dd, *J* = 7.2, 1.8 Hz, 1H), 7.95 – 7.80 (m, 2H), 4.17 (s, 2H). <sup>13</sup>C NMR (101 MHz, DMSO)  $\delta$  184.46, 183.08, 165.97, 147.83, 142.24, 134.90, 134.55, 133.78, 133.55, 133.51, 126.80, 126.74, 124.33, 123.84, 111.98, 29.72.

**S-(2-((4-amino-2,3-dichloro-9,10-dioxo-9,10-dihydroanthracen-1-yl)amino)-2-oxoethyl) ethanethioate (19)**



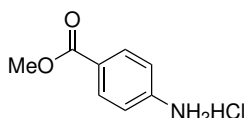
Procedure: Starting from 1,4-diamino-2,3-dichloroanthracene-9,10-dione (**16**, 1 g, 3.26 mmol, 1 eq.) dissolved in dry DCM (24.5 mL/mmol anthraquinone), added dry DIPEA (0.63 mL, 3.58 mmol, 1.1 eq.) and cooled to 0°C before dropwise addition of bromoacetyl bromide (0.63 mL, 3.26 mmol, 1 eq.). After two hours at 0°C was potassium thioacetate (KSAc, 3.72 g, 32.56 mmol, 10 eq.) added and the reaction mixture was allowed to stir for an additional hour. The organic solution was then washed with 2 M HCl, water, sat. NaHCO<sub>3</sub>, and twice brine, before being dried over Na<sub>2</sub>SO<sub>4</sub>, and concentrated. The crude mix was purified by a dry column plug in DCM, to give the ethanethioate anthraquinone (**19**, 453.1 mg, 33% from dichloro) as a red solid, and unreacted starting material (**16**) was also recovered (715.5 mg, 71%). <sup>1</sup>H NMR (400 MHz, DMSO)  $\delta$  10.10 (s, 1H), 8.15 (dd, *J* = 7.4, 1.7 Hz, 1H), 8.06 – 8.01 (m, 1H), 7.92 – 7.81 (m, 2H), 3.91 (s, 2H), 2.43 (s, 3H). <sup>13</sup>C NMR (101 MHz, DMSO)  $\delta$  194.65, 184.43, 183.15, 167.17, 147.71, 142.23, 134.88, 134.53, 133.75, 133.72, 133.51, 126.81, 126.71, 126.52, 124.33, 111.89, 33.28, 30.66. HRMS (ESI) *m/z*: [C<sub>18</sub>H<sub>12</sub>Cl<sub>2</sub>N<sub>2</sub>O<sub>2</sub>S - H]<sup>-</sup> Calcd 420.9822; Found 420.9719.

#### 4-((4-amino-9,10-dioxo-3-sulfo-9,10-dihydroanthracen-1-yl)amino)benzoic acid (**21**)



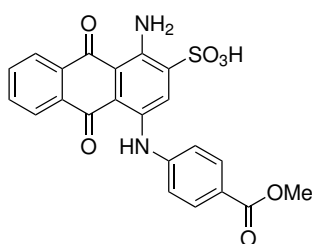
Procedure: General procedure for the  $\mu$ wave mediated Ullmann condensation (described in the beginning of this section). Starting from sodium 1-amino-4-bromo-9,10-dioxo-9,10-dihydroanthracene-2-sulfonate (**20**, 80 mg), 4-aminobenzoic acid (30 mg), Cu(0) powder (3.1 mg), 4 mL buffer A and 1 mL buffer B. The dark blue product was isolated (22.7 mg, 26%) by RF plug.  $^1\text{H}$  NMR (400 MHz, MeOD)  $\delta$  8.41 (s, 1H), 8.36 – 8.27 (m, 2H), 8.04 (d,  $J$  = 8.1 Hz, 2H), 7.86 – 7.75 (m, 2H), 7.34 (d,  $J$  = 8.1 Hz, 3H). HRMS (ESI)  $m/z$ :  $[\text{C}_{21}\text{H}_{14}\text{N}_2\text{O}_7\text{S} + \text{H}]^+$  Calcd 439.0594; Found 439.0596.

#### Methyl 4-aminobenzoate hydrochloride (**22A**)

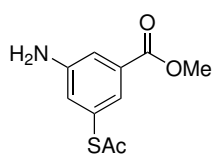


Procedure[207] 4-aminobenzoic acid (7 g, 51.04 mmol, 1 eq.) was dissolved in methanol (5 mL/mmol) at 0°C and dropwise added thionyl chloride ( $\text{SOCl}_2$ , 7.45 mL, 102.09 mmol, 2 eq.). Afterwards was the ice bath removed, the flask was equipped with a condenser, and an oil bath was used to heat the reaction to reflux. After three hours LCMS showed completion, the reaction was cooled to rt, and the solvent removed *in vacuo* to give a HCl-precipitation of the methylester product (**22A**, 9.37 g, 98%).  $^1\text{H}$  NMR (400 MHz,  $\text{D}_2\text{O}$ )  $\delta$  8.00 (d,  $J$  = 8.3 Hz, 2H), 7.36 (d,  $J$  = 8.3 Hz, 2H), 3.83 (s, 3H).  $^{13}\text{C}$  NMR (101 MHz,  $\text{D}_2\text{O}$ )  $\delta$  168.11, 135.82, 131.23, 129.32, 122.61, 52.77.

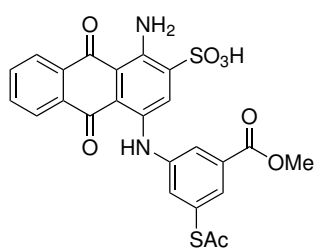
#### 1-amino-4-((4-(methoxycarbonyl)phenyl)amino)-9,10-dioxo-9,10-dihydroanthracene-2-sulfonic acid (**22**)



Procedure: General procedure for the  $\mu$ wave mediated Ullmann condensation (described in the beginning of this section). Starting from sodium 1-amino-4-bromo-9,10-dioxo-9,10-dihydroanthracene-2-sulfonate (**20**, 322 mg), methyl 4-aminobenzoate hydrochloride (**22A**, 164 mg), Cu(0) powder (30 mg), 16 mL buffer A and 4 mL buffer B. The dark blue product was isolated (245.9 mg, 15%) by RF plug.  $^1\text{H}$  NMR (400 MHz, DMSO)  $\delta$  11.73 (s, 1H), 8.30 – 8.20 (m, 2H), 8.14 (s, 1H), 7.97 (d,  $J$  = 8.1 Hz, 2H), 7.91 – 7.83 (m, 2H), 7.34 (d,  $J$  = 8.1 Hz, 2H), 3.85 (s, 2H).  $^{13}\text{C}$  NMR (101 MHz, DMSO)  $\delta$  184.01, 182.72, 166.23, 145.36, 145.26, 142.42, 137.78, 134.53, 134.13, 133.78, 133.50, 131.44, 126.57, 124.27, 123.83, 120.48, 114.79, 110.24, 52.38. HRMS (ESI)  $m/z$ :  $[\text{C}_{22}\text{H}_{16}\text{N}_2\text{O}_7\text{S} + \text{H}]^+$  Calcd 453.0751; Found 453.0757.

**Methyl 3-(acetylthio)-5-aminobenzoate (25)**

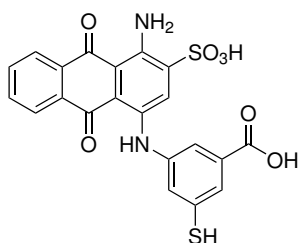
Procedure: This procedure was published, see [175]. Toluene (15 mL/mol aniline) was degassed with a nitrogen flow in a dry three-necked round-bottomed flask equipped with a condenser and a stir bar, before addition of methyl 3-amino-5-bromobenzoate (**24**, 2.5 g, 10.87 mmol, 1 eq.), followed by addition of  $\text{Pd}_2(\text{dba})_3$  (509 mg, 0.56 mmol, 0.05 eq.) and  $\text{CyPF-}^t\text{Bu}$  (604.9 mg, 1.09 mmol, 0.1 eq.). The mixture was allowed to stir under a nitrogen atmosphere at room temperature for 5 min resulting in a dark red coloured solution. Potassium thioacetate (KSAc, 2.48 g, 21.73 mmol, 2 eq.) was then added and the mixture refluxed for 24 hours. Full conversion was confirmed by TLC. After cooling to room temperature,  $\text{Et}_2\text{O}$  was added, and the reaction filtered to remove precipitated salt. The filtrate was concentrated *in vacuo* and the mixture was purified by flash chromatography (DCM:Acetone, 95:5) to yield 1.7 g (71 %) of the desired product (**25**).  $^1\text{H}$  NMR (400 MHz, Chloroform- $d$ )  $\delta$  7.49 (q,  $J = 1.0, 0.6$  Hz, 1H), 7.41 (dd,  $J = 2.4, 1.5$  Hz, 1H), 6.96 (dd,  $J = 2.4, 1.5$  Hz, 1H), 5.32 (d,  $J = 0.5$  Hz, aniline\*), 3.91 (d,  $J = 0.6$  Hz, 3H), 2.44 (d,  $J = 0.6$  Hz, 3H).  $^{13}\text{C}$  NMR (101 MHz, Chloroform- $d$ )  $\delta$  193.69, 166.32, 146.72, 132.00, 129.08, 125.44, 124.89, 117.16, 52.27, 30.26. \*The aniline protons did not integrate to the expected two protons due to rapid exchange. Also, it was observed that the chemical shift of the signal varied. HRMS (ESI)  $m/z$ :  $[\text{C}_{10}\text{H}_{11}\text{NO}_3\text{S} + \text{H}]^+$  Calcd 226.0532; Found 226.0533.

**4-((3-(acetylthio)-5-(methoxycarbonyl)phenyl)amino)-1-amino-9,10-dioxo-9,10-dihydroanthracene-2-sulfonic acid (26)**

Procedure[175]: General procedure for the microwave mediated Ullmann condensation. Starting from sodium 1-amino-4-bromo-9,10-dioxo-9,10-dihydroanthracene-2-sulfonate (**20**, 323 mg), methyl 3-(acetylthio)-5-aminobenzoate (**25**, 215 mg), Cu(0) powder (30 mg), 16 mL buffer A and 4 mL buffer B. The violet product (871.3 mg, 52%) was isolated by RF plug from four combined identical reactions.  $^1\text{H}$  NMR (400 MHz, DMSO)  $\delta$  10.37 (s, 1H), 8.40 (t,  $J = 1.8$  Hz, 1H), 8.27 – 8.20 (m, 2H), 8.04 (t,  $J = 1.8$  Hz, 1H), 7.95 – 7.88 (m, 2H), 7.72 (t,  $J = 1.8$  Hz, 1H), 7.43 (s, 1H), 3.87 (s, 3H), 2.08 (s, 3H).  $^{13}\text{C}$  NMR (101 MHz, DMSO)  $\delta$  183.83, 182.79, 166.49, 150.46, 147.52, 139.06, 134.51, 134.27, 134.03, 133.88, 132.96, 132.32, 131.18, 128.50, 126.73, 126.69, 124.45, 122.80, 115.82, 112.90, 52.59, 24.64. HRMS (ESI)  $m/z$ :  $[\text{C}_{24}\text{H}_{18}\text{N}_2\text{O}_8\text{S}_2 - \text{H}]^-$  Calcd 525.0432; Found 525.0324.



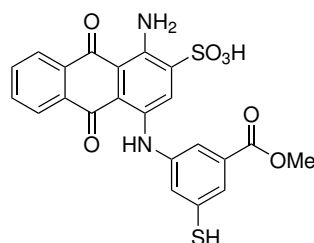
### 3-((4-amino-9,10-dioxo-3-sulfo-9,10-dihydroanthracen-1-yl)amino)-5-mercapto benzoic acid (**27**)



Procedure: 4-((3-(acetylthio)-5-(methoxycarbonyl)phenyl)amino)-1-amino-9,10-dioxo-9,10-dihydroanthracene-2-sulfonic acid (**26**, 104.5 mg, 0.2 mmol, 1 eq.) was dissolved in 1M NaOH (70 mL/mmol **26**) and added methanol (7.5 mL/mmol **26**) in a microwave vial equipped with a stir bar. The vial was capped and heated to 80°C in an oil bath, after 3.5 hours showed LCMS full deprotection of both the thiol

group and the carboxylic acid. The solvent was removed, and the compound purified on RF dry column plug (water → ACN) and afterwards freeze dried to give the mercaptobenzoic acid product as a dark purple solid (41.6 mg, 47%). <sup>1</sup>H NMR (400 MHz, DMSO) δ 9.72 (s, 1H), 8.30 – 8.16 (m, 2H), 7.97 – 7.83 (m, 2H), 7.65 (s, 1H), 7.30 – 7.27 (m, 2H), 6.71 (t, J = 2.0 Hz, 1H), 5.20 (s, 2H). <sup>13</sup>C NMR (101 MHz, DMSO) δ 183.75, 182.55, 170.73, 149.49, 147.47, 142.49, 138.93, 134.36, 134.27, 133.81, 133.18, 133.07, 132.57, 131.27, 127.90, 126.71, 126.64, 124.41, 120.82, 117.16, 112.71. HRMS (ESI) *m/z*: [C<sub>21</sub>H<sub>14</sub>N<sub>2</sub>O<sub>7</sub>S<sub>2</sub> - H]<sup>-</sup> Calcd 469.0170; Found 469.0079.

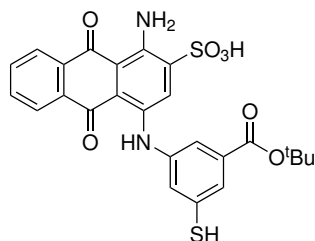
### 1-amino-4-((3-mercapto-5-(methoxycarbonyl)phenyl)amino)-9,10-dioxo-9,10-dihydroanthracene-2-sulfonic acid (**28**)



Procedure: 4-((3-(acetylthio)-5-(methoxycarbonyl)phenyl)amino)-1-amino-9,10-dioxo-9,10-dihydroanthracene-2-sulfonic acid (**26**, 586.4 mg, 1.11 mmol, 1 eq.) was dissolved in 1M HCl (45 mL/mmol **26**) and added methanol (7.2 mL/mmol **26**) in a microwave vial equipped with a stir bar. The vial was capped and heated to 80°C in an oil bath overnight. LCMS the following day confirmed full

deprotection of the thiol group, which precipitates and was collected by suction filtration and afterwards freeze dried to give the 3-mercapto-5-(methoxycarbonyl)phenyl product as a dark purple solid (**28**, 403 mg, 75%). <sup>1</sup>H NMR (400 MHz, DMSO) δ 8.30 – 8.16 (m, 2H), 8.00 – 7.84 (m, 3H), 7.63 (s, 1H), 7.61 (s, 1H), 7.51 (s, 1H), 7.37 (s, 1H), 3.86 (s, 3H). <sup>13</sup>C NMR (101 MHz, DMSO) δ 183.90, 182.94, 165.78, 147.63, 143.08, 139.07, 135.52, 134.61, 134.26, 133.94, 132.92, 132.51, 132.36, 129.62, 129.18, 128.61, 128.20, 126.73, 119.97, 113.09, 52.94. HRMS (ESI) *m/z*: [C<sub>22</sub>H<sub>16</sub>N<sub>2</sub>O<sub>7</sub>S<sub>2</sub> + H]<sup>+</sup> Calcd 485.0472; Found 485.0484.

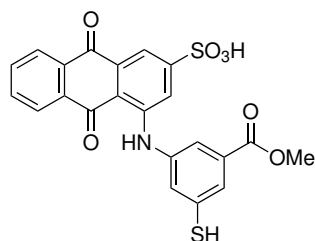
**1-amino-4-((3-(tert-butoxycarbonyl)-5-mercaptophenyl)amino)-9,10-dioxo-9,10-dihydroanthracene-2-sulfonic acid (30)**



Procedure[177]: DCM (40 mL/mmol **27**),  $\text{MgSO}_4$  (30.7 mg, 0.255 mmol, 4 eq.) and  $\text{H}_2\text{SO}_4$  (4  $\mu\text{L}$ , 0.06 mmol, 1 eq.) was stirred for 15 min before addition of the 3-((4-amino-9,10-dioxo-3-sulfo-9,10-dihydroanthracen-1-yl)amino)-5-mercaptobenzoic acid (**27**, 30 mg, 0.06 mmol, 1 eq.) and tertbutyl alcohol (31  $\mu\text{L}$ , 0.32 mmol, 5 eq.).

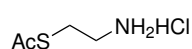
The reaction mixture was allowed to stir overnight, the solvent was then removed and the compound was purified by RF dry column plug and freeze dried to give the tert-butoxycarbonyl product (**30**, 19.4 mg, 58%).  $^1\text{H}$  NMR (400 MHz, DMSO)  $\delta$  8.30 – 8.15 (m, 2H), 7.98 – 7.84 (m, 2H), 7.56 (s, 1H), 7.29 (s, 1H), 7.21 (s, 1H), 6.97 (s, 1H), 1.24 (s, 9H).  $^{13}\text{C}$  NMR (101 MHz, DMSO)  $\delta$  183.83, 182.80, 167.35, 147.56, 139.11, 134.51, 134.29, 134.06, 133.88, 133.29, 132.98, 132.39, 131.00, 130.11, 128.59, 126.74, 126.69, 117.18, 112.90, 70.25, 29.49, 29.29, 29.17. HRMS (ESI)  $m/z$ :  $[\text{C}_{25}\text{H}_{22}\text{N}_2\text{O}_7\text{S}_2 - \text{H}]^-$  Calcd 525.0796; Found 525.0680.

**4-((3-mercapto-5-(methoxycarbonyl)phenyl)amino)-9,10-dioxo-9,10-dihydroanthracene-2-sulfonic acid (31)**



Procedure[208]: 4-((3-(acetylthio)-5-(methoxycarbonyl)phenyl)-amino)-1-amino-9,10-dioxo-9,10-dihydroanthracene-2-sulfonic acid (**26**, 49.7 mg, 0.09 mmol, 1 eq.) was dissolved in 1 M HCl (67 mL/mmol **26**) and cooled to 0°C.  $\text{NaNO}_2$  (7.1 mg, 0.1 mmol, 1.1 eq.) solution in water (5.6 mL/mmol **26**) was then added dropwise, and after one hour was Zn (71 mg, 1.09 mmol, 11.5 eq.) in ethanol (22.2 mL/mmol **26**) added. The mixture was concentrated and purified by RF dry column plug (water  $\rightarrow$  ACN) to give the deaminated product (**31**, 17.5 mg, 36%).  $^1\text{H}$  NMR (400 MHz, DMSO)  $\delta$  9.68 – 9.63 (m, 1H), 8.27 – 8.17 (m, 3H), 8.07 (s, 1H), 8.00 – 7.82 (m, 3H), 7.71 – 7.66 (m, 1H), 7.43 (s, 1H), 3.89 (s, 3H).  $^{13}\text{C}$  NMR (101 MHz, DMSO)  $\delta$  183.92, 182.96, 165.95, 147.54, 140.21, 139.12, 135.63, 135.25, 134.60, 134.49, 134.28, 133.94, 132.93, 132.06, 131.59, 131.03, 130.48, 130.07, 128.95, 126.75, 126.72, 113.08, 52.90. HRMS (ESI)  $m/z$ :  $[\text{C}_{22}\text{H}_{15}\text{NO}_7\text{S}_2 - \text{H}]^-$  Calcd 468.0217; Found 468.0134.

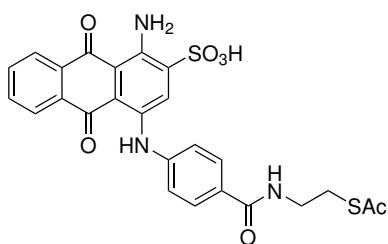
**S-(2-aminoethyl) ethanethioate hydrochloride (33)**



Procedure: Under nitrogen atmosphere was 2-aminoethantio (4 g, 51.85 mmol, 1 eq.) added in portions to TFA (0.5 mL/mmol 2-aminoethantio) at 0°C under vigorous stirring. Afterwards was acetyl chloride (8.2 mL, 103.7 mmol, 2 eq.)

added dropwise to the cooled solution, which was allowed to stir for an hour before addition of Et<sub>2</sub>O and precipitation of the product. The HCl form of the product was collected by suction filtration and wash with Et<sub>2</sub>O (4.8 g, 59%). <sup>1</sup>H NMR (400 MHz, DMSO)  $\delta$  3.10 (t, *J* = 8.2 Hz, 2H), 2.91 (t, *J* = 8.2 Hz, 2H), 2.37 (s, 3H). <sup>13</sup>C NMR (101 MHz, D<sub>2</sub>O)  $\delta$  200.12, 39.22, 29.96, 25.99.

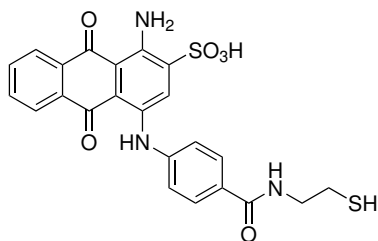
**4-((4-((2-(acetylthio)ethyl)carbamoyl)phenyl)amino)-1-amino-9,10-dioxo-9,10-dihydroanthracene-2-sulfonic acid (**34**)**



Procedure: 4-((4-amino-9,10-dioxo-3-sulfo-9,10-dihydroanthracen-1-yl)amino)benzoic acid (**21**, 20 mg, 0.046 mmol, 1 eq.) was dissolved in DMF (38 mL/mmol **21**), then added N-ethylmorpholine (NEM, 8.6  $\mu$ L, 0.273 mmol, 6 eq.) and Py-BOP (26.6 mg, 50.18 mmol, 1.1 eq.). After 20 minutes was S-(2-aminoethyl) ethanethioate hydrochloride (**33**, 11 mg, 73

mmol, 1.6 eq.) added and the reaction mixture was allowed to stir overnight. LCMS showed that the reaction was not complete, therefore was additional **33**, NEM and PyBOP added to the mixture and the reaction was left overnight. The following day LCMS showed full conversion and the DMF was removed. The compound was purified by RF dry column plug (water  $\rightarrow$  ACN) to give a mix of the product (**34**) and the S-(2-aminoethyl) ethanethioate. It was chosen to continue with the thiol deprotection without further purification.

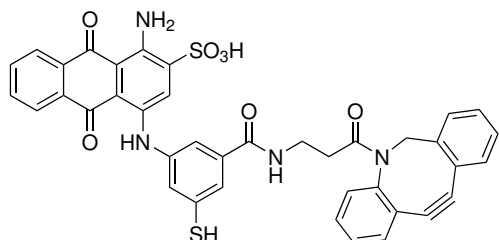
**1-amino-4-((4-((2-mercaptoethyl)carbamoyl)phenyl)amino)-9,10-dioxo-9,10-dihydroanthracene-2-sulfonic acid (**32**)**



Procedure: The crude mix of 4-((4-((2-(acetylthio)ethyl)carbamoyl)phenyl)amino)-1-amino-9,10-dioxo-9,10-dihydroanthracene-2-sulfonic acid (**34**) and S-(2-aminoethyl) ethanethioate was dissolved in 1 M HCl (0.076 mL/ $\mu$ mol **34**) and methanol (0.0076 mL/ $\mu$ mol **34**), and heated to 80°C overnight.

Next day the solvent was removed by air flow, and the crude compound was purified by RF dry column plug (water  $\rightarrow$  ACN) to give the product (**32**, 22 mg, 97%). <sup>1</sup>H NMR (400 MHz, MeOD)  $\delta$  8.25 (s, 1H), 7.96 – 7.88 (m, 2H), 7.74 – 7.59 (m, 4H), 7.09 (d, *J* = 8.4 Hz, 2H), 4.84 (s, 0H), 3.76 (t, *J* = 6.1 Hz, 2H), 3.14 (t, *J* = 6.1 Hz, 2H). <sup>13</sup>C NMR (101 MHz, MeOD)  $\delta$  183.63, 182.80, 168.69, 143.94, 142.65, 138.64, 138.47, 133.48, 133.11, 132.91, 128.54, 127.88, 126.07, 125.71, 123.82, 120.40, 113.50, 110.67, 40.01, 23.68.

**1-amino-4-((3-((3-(11,12-didehydrodibenzo[b,f]azocin-5(6H)-yl)-3-oxopropyl)carbamoyl)-5-mercaptophenyl)amino)-9,10-dioxo-9,10-dihydroanthracene-2-sulfonic acid (35)**

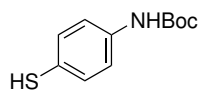


Procedure[209]: 4-((3-mercapto-5-(methoxycarbonyl)-phenyl)amino)-9,10-dioxo-9,10-dihydroanthracene-2-sulfonic acid (**27**, 50.5 mg, 107.3  $\mu\text{mol}$ ) was dissolved in DMSO (11.67 mL/ $\mu\text{mol}$  **27**), then added dibenzocyclooctyne-amine (DBCO-amine, CAS: 1255942-06-3, 44.6 mg, 161

$\mu\text{mol}$ , 1.5 eq.) and DIPEA (37  $\mu\text{L}$ , 214.7  $\mu\text{mol}$ , 2 eq.). The reaction mixture was placed on ice and COMU<sup>®</sup> (69 mg, 161  $\mu\text{mol}$ , 1.5 eq.) was added, then the reaction was allowed to warm to room temperature with continued stirring overnight. Afterwards was DMSO removed by airflow and the crude residue was first moderately purified by RF dry column plug (water  $\rightarrow$  ACN), followed by preparative HPLC of the fractions containing product, lastly freeze dried to give the product. <sup>1</sup>H NMR (400 MHz, DMSO)  $\delta$  10.24 (s, 1H), 8.40 (t,  $J = 5.6$  Hz, 1H), 8.28 – 8.20 (m, 2H), 8.08 (t,  $J = 1.8$  Hz, 1H), 7.95 – 7.86 (m, 2H), 7.65 – 7.58 (m, 2H), 7.51 – 7.25 (m, 6H), 7.21 (s, 1H), 7.08 (s, 1H), 6.95 (s, 1H), 5.05 (d,  $J = 14.0$  Hz, 1H), 3.62 (d,  $J = 14.0$  Hz, 1H), 3.16 – 3.03 (m, 1H), 2.61 – 2.52 (m, 2H), 2.02 – 1.92 (m, 1H). <sup>13</sup>C NMR (101 MHz, DMSO)  $\delta$  183.84, 182.87, 170.61, 165.32, 151.85, 148.82, 147.56, 141.01, 139.14, 136.63, 134.58, 134.29, 133.91, 133.73, 132.93, 132.85, 132.25, 130.03, 129.50, 128.68, 128.62, 128.49, 128.16, 127.73, 127.25, 126.73, 125.68, 122.94, 121.80, 114.72, 112.94, 108.62, 55.31, 36.42, 24.54. HRMS (ESI)  $m/z$ : [ $\text{C}_{39}\text{H}_{28}\text{N}_4\text{O}_7\text{S}_2 - \text{H}$ ]<sup>−</sup> Calcd 727.1327; Found 727.1194.

## 7.2 Synthesis of Compounds in Chapter 6

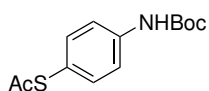
**tert-butyl (4-mercaptophenyl)carbamate (41)**



Procedure: 4-aminobenzenethiol (**40**, 1 g, 7.99 mmol, 1 eq.) was dissolved in water (1 mL/ $\mu\text{mol}$ ) and added Boc anhydride ( $\text{Boc}_2\text{O}$ , 2 g, 8.79 mmol, 1.1 eq.), which was allowed to stir for 24 hours at room temperature. The product had precipitated and was collected by suction filtration, washed with water, redissolved in EtOAc, dried over  $\text{Na}_2\text{SO}_4$ , and evaporated to give the Boc-protected product as a pale-yellow solid (1.8 g, *quant.*). <sup>1</sup>H NMR (400 MHz, DMSO)  $\delta$  7.47 (d,  $J = 8.5$  Hz, 1H), 7.42 – 7.32 (m, 2H), 7.22 – 7.15 (m, 1H), 1.47 (s, 9H). <sup>13</sup>C NMR (101 MHz, DMSO)  $\delta$  153.17, 140.46, 131.20, 130.02, 119.19, 79.84, 28.58, 28.53, 27.33. HRMS (ESI)  $m/z$ : [ $\text{C}_{11}\text{H}_{15}\text{NOS} - \text{H}$ ]<sup>−</sup> Calcd 224.0751;

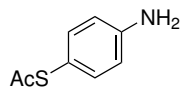
Found 224.0725.

### S-(4-((tert-butoxycarbonyl)amino)phenyl) ethanethioate (**42**)



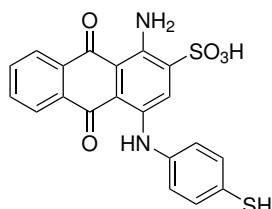
Procedure[210]: Tert-butyl (4-mercaptophenyl)carbamate (**41**, 1.8 g, 8 mmol, 1 eq.) was dissolved in DCM (1 mL/mmol **41**) and NEt<sub>3</sub> (2.25 mL, 16 mmol, 2 eq.), cooled to 0°C, and then added acetyl chloride (625 µL, 8.8 mmol, 1.1 eq.). After 30 min. was the reaction complete, confirmed by LCMS, and sat. NaHCO<sub>3</sub> was used to quench the remaining acetyl chloride (still on ice!). The mixture was then extracted with DCM (2x) and the combined organic phase was dried over Na<sub>2</sub>SO<sub>4</sub> and evaporated to give the Boc-protected ethanethioate product (2.2 g, *quant.*) as an off-white solid. <sup>1</sup>H NMR (400 MHz, DMSO) δ 9.60 (s, 1H), 7.54 (d, J = 8.5 Hz, 2H), 7.29 (d, J = 8.5 Hz, 2H), 2.39 (s, 3H), 1.49 (s, 9H). <sup>13</sup>C NMR (101 MHz, DMSO) δ 194.87, 153.10, 141.40, 135.61, 120.18, 119.06, 79.93, 30.40, 28.53. HRMS (ESI) *m/z*: [C<sub>13</sub>H<sub>17</sub>NO<sub>3</sub>S - H]<sup>-</sup> Calcd 226.0856; Found 266.0815.

### S-(4-aminophenyl) ethanethioate (**39**)



Procedure: S-(4-((tert-butoxycarbonyl)amino)phenyl) ethanethioate (**42**, 2.14 g, 8 mmol, 1 eq.) was dissolved in TFA (1.74 mL/mmol **42**) and allowed to stir for 30 min. at room temperature, before dilution with DCM (29 mL/mmol **42**). The organic solution was then washed with 1 M NaOH (29 mL/mmol **42**), the basic aqueous phase then extracted with additional DCM (13 mL/mmol **42**). The combined organic phase was dried over Na<sub>2</sub>SO<sub>4</sub> and evaporated to give the Boc-deprotected ethanethioate product (761.4 mg, 57%). <sup>1</sup>H NMR (400 MHz, DMSO) δ 7.02 (d, J = 8.4 Hz, 2H), 6.60 (d, J = 8.4 Hz, 2H), 5.53 (s, 2H), 2.32 (d, J = 0.8 Hz, 3H). <sup>13</sup>C NMR (101 MHz, DMSO) δ 196.55, 150.75, 136.20, 114.73, 114.63, 30.02. HRMS (ESI) *m/z*: [C<sub>11</sub>H<sub>15</sub>NO<sub>2</sub>S - H]<sup>-</sup> Calcd 224.0751; Found 224.0725.

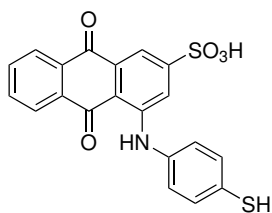
### 1-amino-4-((4-mercaptophenyl)amino)-9,10-dioxo-9,10-dihydroanthracene-2-sulfonic acid (AQSH, **29**)



Procedure: General procedure for the µwave mediated Ullmann condensation (described in the beginning of this section). Starting from sodium 1-amino-4-bromo-9,10-dioxo-9,10-dihydroanthracene-2-sulfonate (**20**, 321 mg), S-(4-aminophenyl) ethanethioate (**39**, 176 mg), Cu(0) powder (14 mg), 16 mL buffer A and 4 mL buffer B. The de-acetylated purple product (266 mg, 79%) was isolated by RF plug. <sup>1</sup>H NMR (400 MHz, DMSO) δ 9.69 (s, 1H), 8.27 – 8.18 (m, 2H), 7.93 – 7.84 (m, 2H), 7.62 (s, 1H), 7.19 – 7.14 (m, 2H), 6.68 – 6.63 (m, 2H), 5.58 (s, 2H), 2.09 (d, J = 0.9 Hz, 1H). <sup>13</sup>C NMR (101

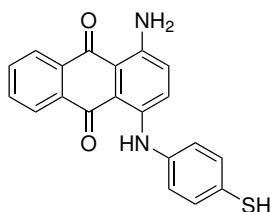
MHz, DMSO)  $\delta$  183.80, 182.47, 150.62, 147.33, 139.01, 137.19, 134.98, 134.83, 134.30, 134.25, 133.78, 133.06, 131.66, 127.43, 126.71, 126.62, 115.90, 115.42, 114.63, 112.86. HRMS (ESI)  $m/z$ :  $[\text{C}_{20}\text{H}_{14}\text{N}_2\text{O}_5\text{S}_2 - \text{H}]^-$  Calcd 425.0271; Found 425.0301.

**4-((4-mercaptophenyl)amino)-9,10-dioxo-9,10-dihydroanthracene-2-sulfonic acid (AQdA, **38**)**



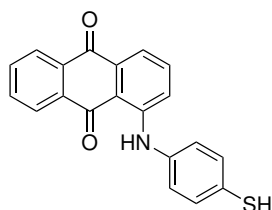
Procedure[208]: 1-amino-4-((4-mercaptophenyl)amino)-9,10-dioxo-9,10-dihydroanthracene-2-sulfonic acid (**29**, 50.0 mg, 0.1 mmol, 1 eq.) was dissolved in 1 M HCl (50 mL/mmol **29**) and cooled to 0°C.  $\text{NaNO}_2$  (17 mg, 0.1 mmol, 1.1 eq.) solution in water (5 mL/mmol **29**) was then added dropwise, and after 20 sec. was Zn (77 mg, 1 mmol, 10 eq.) in ethanol (50 mL/mmol anthraquinone) added. The mixture was concentrated and purified by RF dry column plug (water  $\rightarrow$  ACN) to give the deaminated product (**38**, 9.9 mg, 21%) and recovered starting material (**29**, 31.4 mg, 63%).  $^1\text{H}$  NMR (400 MHz, DMSO)  $\delta$  8.30 – 8.16 (m, 2H), 8.00 – 7.84 (m, 2H), 7.61 – 7.48 (m, 6H).  $^{13}\text{C}$  NMR (101 MHz, DMSO)  $\delta$  183.86, 182.81, 147.50, 139.11, 135.48, 134.50, 134.28, 133.88, 133.22, 132.99, 132.06, 131.31, 130.42, 129.85, 128.46, 126.74, 126.69, 112.94. HRMS (ESI)  $m/z$ :  $[\text{C}_{20}\text{H}_{13}\text{NO}_5\text{S}_2 + \text{H}]^+$  Calcd 412.0308; Found 412.0309.

**1-amino-4-((4-mercaptophenyl)amino)anthracene-9,10-dione (AQdS, **37**)**



Procedure[193]: 1-amino-4-((4-mercaptophenyl)amino)-9,10-dioxo-9,10-dihydroanthracene-2-sulfonic acid (**29**, 60.0 mg, 0.128 mmol, 1 eq.) was suspended in water (4.4 mL/mmol **29**), then added 30 NaOH (0.5 mL/mmol **29**) and heated to 80°C. A glucose solution (30 mg, 0.17 mmol, 1.3 eq.) in water (1.3 mL/mmol **29**) was added dropwise, and after 30 min. the reaction was removed from the heat and allowed to cool to room temperature while more water was added. The mixture was concentrated and purified by RF dry column plug (water  $\rightarrow$  ACN) followed by a normal phase dry column plug (EtOAc:heptane (50:50)  $\rightarrow$  EtOAc) to give the desulphonated product (**37**, 39.2 mg, 80%) as an orange solid.  $^1\text{H}$  NMR (400 MHz, DMSO)  $\delta$  8.67 – 8.60 (m, 1H), 8.41 (dd,  $J = 7.9, 1.5$  Hz, 1H), 8.04 (d,  $J = 9.2$  Hz, 1H), 7.93 – 7.82 (m, 1H), 7.77 (td,  $J = 7.6, 1.1$  Hz, 1H), 7.34 – 7.24 (m, 3H), 6.76 (d,  $J = 8.4$  Hz, 2H), 5.72 (s, 2H).  $^{13}\text{C}$  NMR (101 MHz, DMSO)  $\delta$  181.54, 158.48, 151.54, 151.23, 144.90, 137.35, 134.57, 133.81, 133.14, 132.92, 131.81, 130.78, 127.96, 127.74, 124.63, 122.08, 120.96, 118.61, 115.64, 114.78. HRMS (ESI)  $m/z$ :  $[\text{C}_{20}\text{H}_{14}\text{N}_2\text{O}_2\text{S} + \text{H}]^+$  Calcd 347.0849; Found 347.2306.

### 1-((4-mercaptophenyl)amino)anthracene-9,10-dione (AQdd, **36**)



Procedure: 1-amino-4-((4-mercaptophenyl)amino)anthracene-9,10-dione (AQdS, **37**, 20 mg, 0.058 mmol, 1 eq.) was dissolved in 1 M HCl (50 mL/mmol **37**) and cooled to 0°C. NaNO<sub>2</sub> (8 mg, 0.12 mmol, 2 eq.) solution in water (5 mL/mmol **37**) was then added dropwise, and after 1 min. was Zn (40 mg, 0.58 mmol, 10 eq.) in ethanol (50 mL/mmol **37**) added. The mixture was concentrated and purified by RF dry column plug (heptane → EtOAc → methanol → ACN → DMF) to give the deaminated desulphonated product (**36**, 7 mg, 37%) as a pale orange solid. <sup>1</sup>H NMR (400 MHz, DMSO) δ 8.72 (dd, J = 7.6, 1.1 Hz, 1H), 8.54 (dd, J = 7.3, 1.3 Hz, 1H), 8.39 (dtt, J = 24.0, 8.3, 7.6, 1.3 Hz, 2H), 8.04 (t, J = 8.3, 7.3 Hz, 1H), 7.94 (dd, J = 7.6, 1.2 Hz, 1H), 7.78 (dd, J = 7.6, 1.1 Hz, 1H), 7.20 (br. s, 2H), 6.65 (br. s, 2H). HRMS (ESI) *m/z*: [C<sub>20</sub>H<sub>13</sub>NO<sub>2</sub>S + H]<sup>+</sup> Calcd 332.0740; Found 332.0884.

## 7.3 Electrochemical Preparation

The instrument used for obtaining electrochemical data is an AUTOLAB potentiostat. The laccase enzyme was provided by Anne S. Meyer from DTU Bioengineering and the FDH enzyme was bought from Sorachim.

### 7.3.1 Preparation of Electrodes

The reference electrode, Ag/AgCl, was kept in a saturated KCl solution and the counter electrode, platinum wire, was cleaned with a hydrogen flame before use. For the working electrode see figure 7.1. The Au/Ag leaves was cut in 0.7x0.7 cm squares and transferred by a small glass plate to a water bath containing milli-Q water before being transferred to a bath with concentrated nitric acid, the bath was sealed and placed in 30°C water bath for 30 min. Meanwhile, the bare glassy carbon electrodes (GCE) were first mechanically polished with aluminium oxide slurry (particle size 1 μm → 0.3 μm → 0.05 μm), then sonicated in a cold bath for 2x 3 min with absolute ethanol and 2x 3 min with milli-Q water to remove particles. After the 30 min, the Au leaves were transferred to one milli-Q water bath followed by another, before one-by-one being transferred to a taller bath where the leaves was deposited on the polished GCE by having the GCE approach the leaf on the water surface from below (full schematic illustration on figure 7.1). The GCEs with the leaves was left to dry overnight. The following day the gold film that did not connect with the carbon surface was removed by a toothpick and a moist soft tissue, before electrode activation in degassed 1 M sulphonic

acid. Once again, the, now activated, NPGs were allowed to dry overnight. Common for all experiments is that the solvent/analyte solution, is degassed by bubbling argon through for 30 min.

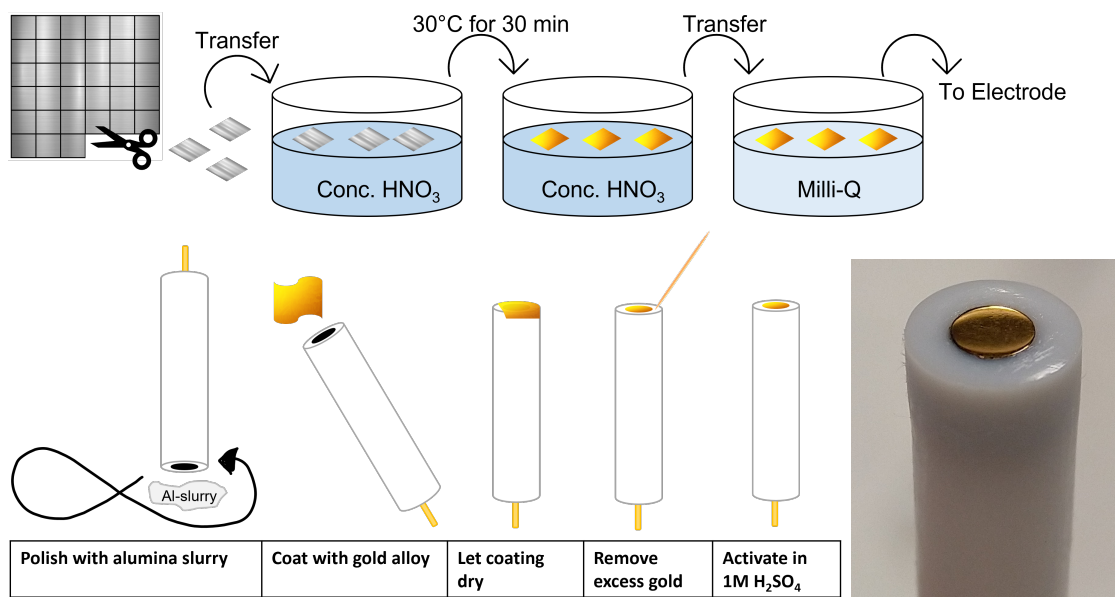


**Figure 7.1:** Schematic illustration of the preparation of the working electrode (WE).

The activation and further cleaning of the electrode in 1 M sulphonic acid is done by running a CV program with 15 cycles of oxidation-reduction of the gold surface. On the CV diagrams, the three gold faces (100, 110, 111) can be seen in oxidation peaks and a sharp reduction peak verifying its cleanness, see figure 7.2.

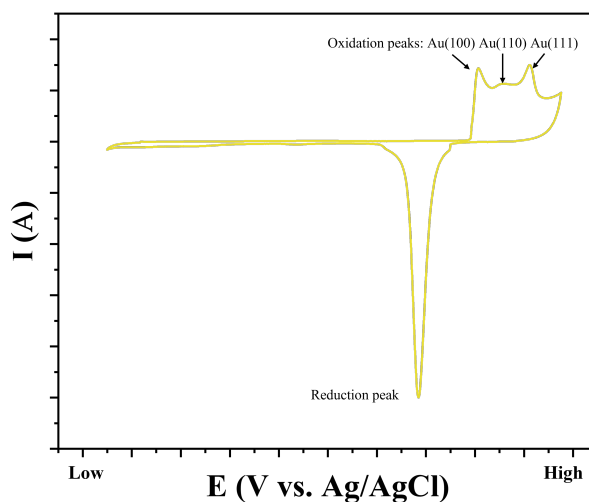


**Figure 7.2:** CV dataset from the activation of the NPG in 1 M sulphonic acid. Observed are the three faces of gold (100, 110, 111) and the reduction peak.

During monolayer studies additional steps are needed for the electrode preparation. After



the activation, the NPGs were soaked in an anthraquinone solution (1-5 mM) overnight. When soaking the electrode in the AQ-solution the thiol of the AQs will bind to the gold surface. The AQs will over time cover the whole surface to form a so-called self-assembled monolayer (SAM). The following day, the electrode is washed in an ethanol beaker for 20 min and afterwards in a milli-Q water beaker for another 20 min, before allowed to dry overnight. Lastly the, now anthraquinone coated, NPGs were submersed in an enzyme solution (0.6 mg/mL buffer) and kept in the fridge overnight. The following day the enzyme-anthraquinone modified NPG electrodes were washed in cold buffer solution before being used in electrochemical study, see figure 7.3.

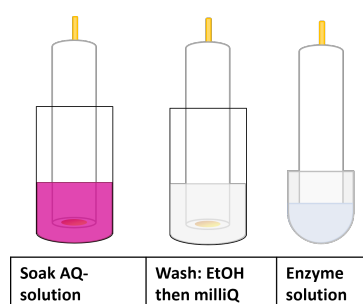


**Figure 7.3:** Continued preparation of the WE with the anthraquinone monolayer and enzyme attachment.

### 7.3.2 Preparation of Solutions

**Solution Studies:** The anthraquinone stock solutions needs to be 1.5 mM, the solid compound is dissolved in ethanol and then added milli-Q in the relation 2:1 (EtOH:milli-Q). When added to the buffer solution at testing the final concentration was 0.07 mM. Four buffers were prepared and adjusted to different pHs; 100 mM sodium acetate buffer (NaAc) pH 4.2, 100 mM McIlvaine buffer (MCB) pH 5.5, 100 mM phosphate buffer (PB) pH 7.0, and 100 mM PB pH 9.

**Monolayer Studies:** The anthraquinone soaking-solutions needs to be 1-5 mM, the solid compound is dissolved in ethanol and then added milli-Q in the relation 2:1 (EtOH:milli-Q). The mediator for laccase MET, 2,2'-azino-bis(3-ethylbenzothiazoline-6-sulfonic acid (ABTS), is dissolved in milli-Q to give a 50 mM stock concentration. The mediator for FDH MET, ferrocene-MeOH (FeMeOH), is dissolved in milli-Q using sonification so that the stock concentration is 5 mM. The substrate for FDH, fructose, was dissolved in milli-Q to reach 2 M for the stock. For the laccase testing a phosphate buffer was prepared at 200 mM with pH adjusted to 5.0. For the FDH testing a McIlvaine buffer was prepared at 100 mM with pH adjusted to 5.5. The final concentrations during experiments for ABTS, FeMeOH and fructose are 0.2 mM, 0.5 mM and 100 mM respectively.

# CHAPTER 8

## Conclusion

---

In this PhD project, two important elements for developing efficient light energy harvesting conjugates was investigated. This includes developing methods to ensure correct enzyme-on-electrode orientation as well as a bridging-molecule allowing efficient electron-transfer.

In Part I, two novel strategies allowing site-selective bioconjugation on proteins containing natural amino acids was investigated. Both methods utilize the site-specificity provided by the phosphorylating PKA kinase enzyme. The first strategy utilizes an unnatural ATP analogue, successfully synthesized in four steps, allowing direct installation of an azido handle for further functionalization. Unfortunately, due to time limitations, the investigation was not completed, but it was concluded that the strategy processes good potential and therefore should be further investigated. The second strategy utilized an efficient phosphorylation using the kinase enzymes natural substrate (ATP), followed by a pyrophosphorylation reaction with a phosphorimidazolide reagent, allowing installation of the desired azide-handle. Both the phosphorylation and the pyrophosphorylation individually proceeded with great satisfaction. The phosphorimidazolide reagent proved to be very stable in an aqueous environment, allowing investigation of a two-reaction-one-pot strategy. Hereby, it was possible to achieve a 41% product formation (determined by HPLC) and the plans for further optimization has been presented.

In Part II, the development of an anthraquinone-based electron transfer bridge to connect the enzyme and the gold-covered electrode, was presented. Through different synthetic approaches, a procedure for preparation of an anthraquinone containing both a thiol-handle (for electrode binding) and a handle for further protein functionalisation was developed. The molecule possessed good electrochemical properties. The anthraquinone design was tested in solution, where good electron transfer rate constants were observed. Also, good interaction with the fructose dehydrogenase enzyme was demonstrated. The anthraquinone was shown to form a monolayer on the gold-surface of the electrode, allowing non-covalent interaction with the enzyme. Different substitution patterns on the anthraquinone were investigated allowing design of an electron-transfer bridge for further studies.



# APPENDIX A

## General Methodologies

---

All solvents were of HPLC quality from either Sigma-Aldrich or VWR Chemicals these and other commercially available reagents were used without further purification. The dry solvents DCM, Et<sub>2</sub>O, ACN and DMF were obtained from the in-house PureSolve<sup>TM</sup> MD-7 Solvent Purification System, from Innovative Technology were Al<sub>2</sub>O<sub>3</sub> was used as the stationary phase. Dry MeOH was purchased from Sigma-Aldrich. For dry reaction glassware was flame-dried, and cooled under dry N<sub>2</sub> atmosphere before use. Room temperature is approximately 23°C. Chemicals have been bought from Sigma-Aldrich, Combi-Blocks, Fluorochem and Fisher Scientific.

<sup>1</sup>H-NMR, <sup>13</sup>C-NMR, COSY, HSQC, <sup>31</sup>P-NMR spectra were recorded on Bruker Ascend spectrometer with a Prodigy cryoprobe operating at 400 MHz or 800 MHz for <sup>1</sup>H-NMR and 101 MHz for <sup>13</sup>C-NMR. The specific deuterated solvent is stated for each compound. Chemical shifts (δ) are reported in ppm downfield from TMS ( = 0) using solvent resonance as the internal standard (chloroform-d, <sup>1</sup>H: 7.26 ppm, <sup>13</sup>C: 77.16 ppm; dimethylsulfoxide-d<sub>6</sub>, <sup>1</sup>H: 2.50 ppm, <sup>13</sup>C: 39.52 ppm)[211]. Coupling constants (J) are reported in Hz and the field is reported in each case. Multiplicities are reported as singlet (s), broad singlet (br. s), doublet (d), doublet of doublets (dd), doublet of triplets (dt), doublet of doublet of doublets (ddd), doublet of doublet of triplets (ddt), triplet (t), triplet of doublets (td), quartet (q), pentet (p), septet (sep) and multiplets (m).

**Evaporation** of the solvents were performed using a Heidolph Laborota 4000 efficient under reduced pressure (*in vacuo*) at different temperatures depending on the boiling point of the solvents.

**N<sub>2</sub> atmosphere** was used in experiments for obtaining an inert atmosphere in reactions that would otherwise react with water resulting in undesired side-reactions. N<sub>2</sub> atmosphere was achieved by applying a rubber septum to the reagent flask and hereafter adding a constant N<sub>2</sub> inlet through a Schlenk line.

**Flash chromatography** was performed using Merck Geduran Silica gel 60 Å (particle size 40-63 μm) as the stationary phase. The chromatography method which was used, followed the general method developed by Still *et al.* [212]. The eluent systems used are specified for

each product, and are given as a volume ratio.

**Reverse phase chromatography** was performed using C18 silica gel, which was washed with methanol before use, in a dry column vacuum set-up.

**TLC** was performed using Merck Aluminum Sheets which were precoated with silica gel 60 F<sub>254</sub>. By placing spots on the TLC plates containing the different compounds/products in solution, then the compounds could be separated. The spots were developed using UV-light or a suitable staining agent, e.g. KMnO<sub>4</sub>-solution (40 g potassium carbonate, 6 g potassium permanganate, 600 mL H<sub>2</sub>O and 5 mL 10% NaOH).

**Microwave reactions** was performed using a Initiator from Biotage, with proper vials and caps also purchased from Biotage.

**UPLC/MS** analysis was run on Waters AQUITY UPLC system equipped with PDA and either a SQD or a SQD2 electrospray MS detector. Column: Thermo accucore C18 2.6  $\mu$ m, 2.1  $\times$  50 mm. Column temp: 50 °C. Flow rate: 0.6 mL/min. Acid run: Solvent A1 - 0.1% formic acid in water, Solvent B1 - 0.1% formic acid in ACN. Base run: Solvent A2 - 15 mM NH<sub>4</sub>Ac in water, Solvent B2 - 15 mM NH<sub>4</sub>Ac in ACN/water 9:1. Gradient: (short run) 5% B to 100% B in 2.4 min., hold 0.1 min., total run time 2.6 min. (long run) 5% B to 100% B in 3 min., hold 0.1 min., total run time 5 min.

**IR** (Infrared) analysis was performed on a Bruker Alpha FT-IR spectrometer from 4000 to 400 cm<sup>-1</sup> of a neat sample.

**Preparative HPLC** purification was performed on a Waters autopurification system consisting of a 2767 Sample Manager, 2545 Gradient Pump and 2998 PDA detector. Column: XBridge Peptide BEH C18 OBD Prep Column, 130Å, 5  $\mu$ m, 19 mm  $\times$  100 mm. Column temp: Ambient. Flow rate: 20 mL/min. Solvent A2 - 15 mM NH<sub>4</sub>Ac in water, Solvent B2 - 15 mM NH<sub>4</sub>Ac in MeCN/water 9:1. Gradient: 5% B to 20% B in min., hold min., gradient: 20% B to 50% B in min., hold min., gradient: 50% B to 70% B in min., hold min., gradient: 70% B to 100% B in min., hold min., run min., recalibrating the column for min. Total run time - 18 min.

## APPENDIX B

# Additional HPLC-Spectras

---

Spectra of SerUV (2) unmodified.

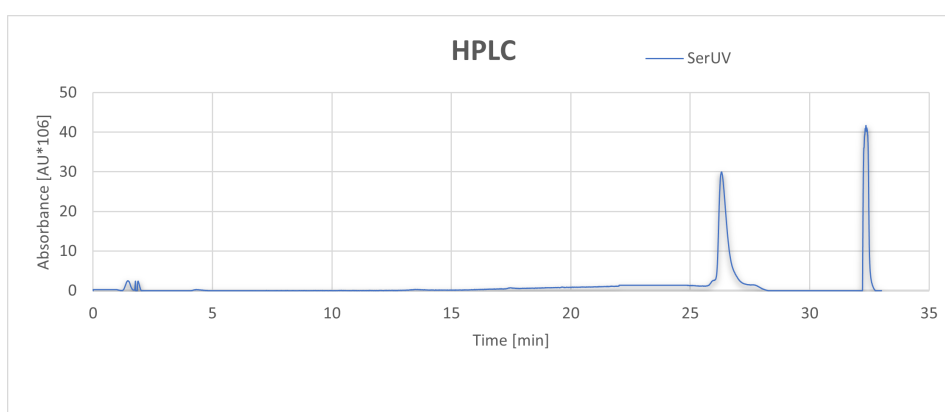


**Figure B.1:** HPLC spectra of SerUV (2).

Spectra of SerPUV (3) unmodified.

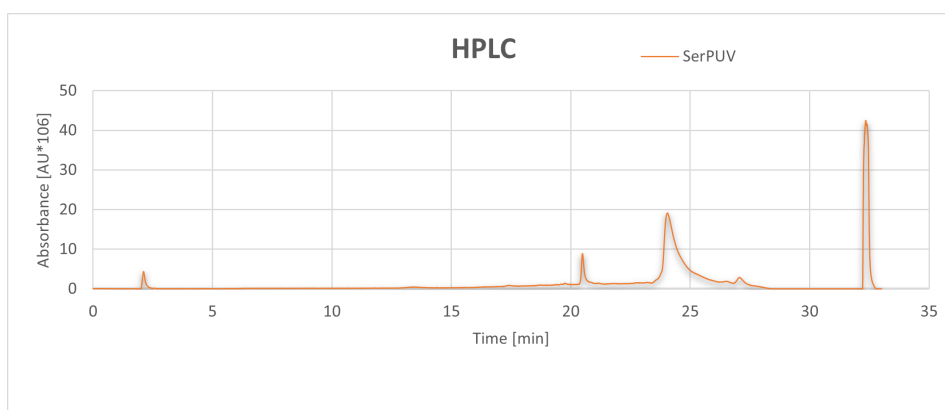


**Figure B.2:** HPLC spectra of SerPUV (3).

### Spectra of the pyrophosphorylated SerPUV (3) (SerPUV-P).

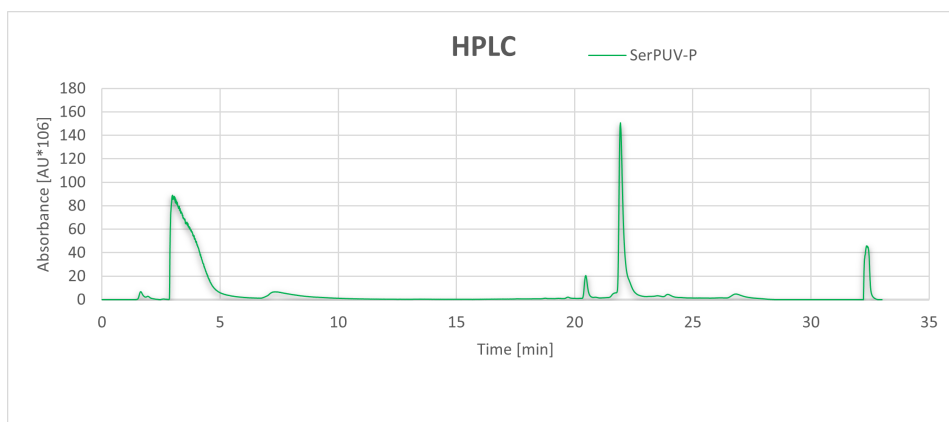


Figure B.3: HPLC spectra of SerPUV-P.

### Study of the pyrophosphorylation reaction using either ZnCl<sub>2</sub> or MgCl<sub>2</sub>.

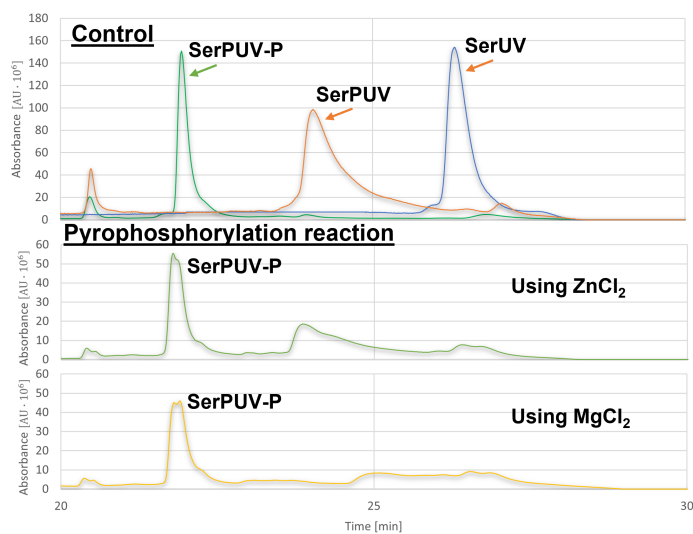
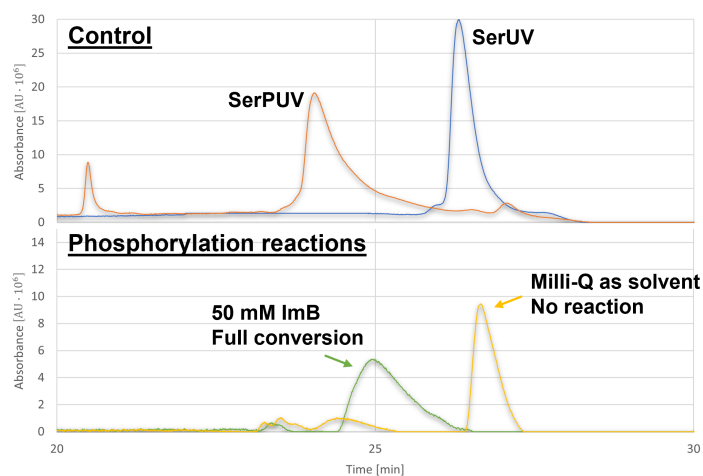
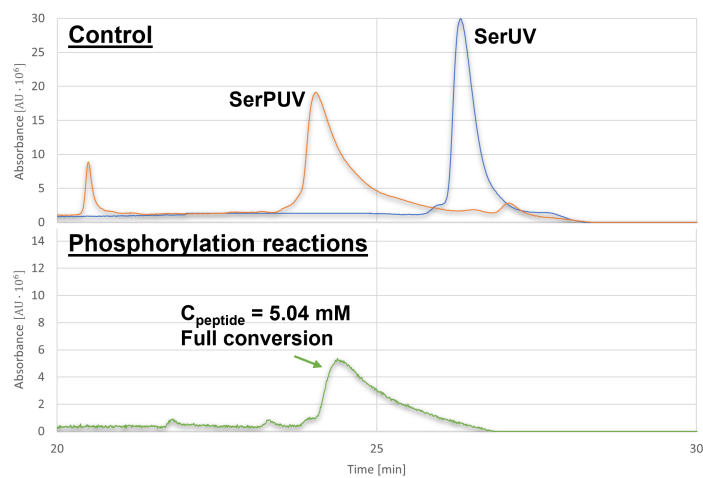


Figure B.4: HPLC results from pyrophosphorylation using either ZnCl<sub>2</sub> or MgCl<sub>2</sub>.

**Phosphorylation with kinase in 50 mM ImB or milli-Q water.****Figure B.5:** HPLC results from phosphorylation in either 50 mM ImB or milli-Q.**Phosphorylation with kinase in 5.04 mM peptide concentration.****Figure B.6:** HPLC results from phosphorylation in 5.04 mM peptide concentration.





# APPENDIX C

## List of Publications

---

### Publications from 2019-2021

Qvortrup, K., Hultqvist, L. D., Nilsson, M., Jakobsen, T. H., Jansen, C. U., Uhd, J., Andersen, J. B., Nielsen, T. E., Givskov, M., & Tolker-Nielsen, T. (2019). Small Molecule Anti-biofilm Agents Developed on the Basis of Mechanistic Understanding of Biofilm Formation. *Frontiers in Chemistry*, 7, [742]. <https://doi.org/10.3389/fchem.2019.00742>

Yan, X., Jansen, C. U., Diao, F., Qvortrup, K., Tanner, D. A., Ulstrup, J., & Xiao, X. (2021). Surface-confined redox-active monolayers of a multifunctional anthraquinone derivative on nanoporous and single-crystal gold electrodes. *Electrochemistry Communications*, 124, [106962]. <https://doi.org/10.1016/j.elecom.2021.106962>

Jansen, C. U., & Qvortrup, K. (Accepted/In press). Small Molecule Drugs for Treatment of Alzheimer's Diseases Developed on the Basis of Mechanistic Understanding of the Serotonin Receptors 4 and 6. In *Serotonin and the CNS - New Developments in Pharmacology and Therapeutics* InTechOpen. <https://doi.org/10.5772/intechopen.96381>

Jansen, C. U., Uhd, J., Andersen, J. B., Hultqvist, L. D., Jakobsen, T. H., Nilsson, M., Nielsen, T. E., Givskov, M., Tolker-Nielsen, T., & Qvortrup, K. M. (2021). SAR study of 4-arylaazo-3,5-diamino-1H-pyrazoles: identification of small molecules that induce dispersal of *Pseudomonas aeruginosa* biofilms. *RSC Medicinal Chemistry*, 11(12), 1868-1878. <https://doi.org/10.1039/D1MD00275A>

Andersen, J. B., Hultqvist, L. D., Jansen, C. U., Jakobsen, T. H., Nilsson, M., Rybtke, M., Uhd, J., Fritz, B. G., Seifert, R., Berthelsen, J., Nielsen, T. E., Qvortrup, K., Givskov, M., & Tolker-Nielsen, T. (2021). Identification of small molecules that interfere with c-di-GMP signaling and induce dispersal of *Pseudomonas aeruginosa* biofilms. *NPJ biofilms and microbiomes*, 7(1), [59]. <https://doi.org/10.1038/s41522-021-00225-4>

**Publications in Preparation**

Electrochemical detection of pH-dependent anthraquinone derivatives

Kinase Applied as Novel Bioconjugation Tool

Mechanistic understanding of the photoinduced conversion of indican to indigo

Denim dyeing with chemoenzymatic indican has high sustainability performance

Development of a Convergent Total Synthesis for Exochelin 772SM

# Bibliography

---

- [1] Nikolay Belyakov. “Solar energy.” In: *Sustainable Power Generation*. Elsevier, 2019, pp. 417–438. DOI: 10.1016/b978-0-12-817012-0.00031-1. URL: <https://doi.org/10.1016/b978-0-12-817012-0.00031-1>.
- [2] Juan G. Yañuk et al. “Photosensitizing role of R-phycoerythrin red protein and  $\beta$ -carboline alkaloids in Dye sensitized solar cell. Electrochemical and spectroscopic characterization.” In: *Energy Reports* 6 (2020), pp. 25–36. DOI: 10.1016/j.egyr.2019.10.045. URL: <https://doi.org/10.1016/j.egyr.2019.10.045>.
- [3] Tanja Vidakovic-Koch. “Electron Transfer Between Enzymes and Electrodes.” In: *Bioelectrosynthesis*. Springer International Publishing, 2017, pp. 39–85. DOI: 10.1007/10\_2017\_42. URL: [https://doi.org/10.1007/10\\_2017\\_42](https://doi.org/10.1007/10_2017_42).
- [4] N. Thejo Kalyani and Sanjay J. Dhoble. “Empowering the Future With Organic Solar Cell Devices.” In: *Nanomaterials for Green Energy*. Elsevier, 2018, pp. 325–350. DOI: 10.1016/b978-0-12-813731-4.00010-2. URL: <https://doi.org/10.1016/b978-0-12-813731-4.00010-2>.
- [5] Daniel Antón-García et al. “Photoelectrochemical hybrid cell for unbiased CO<sub>2</sub> reduction coupled to alcohol oxidation.” In: *Nature Synthesis* 1.1 (2022), pp. 77–86. DOI: 10.1038/s44160-021-00003-2. URL: <https://doi.org/10.1038/s44160-021-00003-2>.
- [6] Jan Winsberg et al. “TEMPO/Phenazine Combi-Molecule: A Redox-Active Material for Symmetric Aqueous Redox-Flow Batteries.” In: *ACS Energy Letters* 1.5 (2016), pp. 976–980. DOI: 10.1021/acsenenergylett.6b00413. URL: <https://doi.org/10.1021/acsenenergylett.6b00413>.
- [7] Federico Bella et al. “Boosting the efficiency of aqueous solar cells: A photoelectrochemical estimation on the effectiveness of TiCl<sub>4</sub> treatment.” In: *Electrochimica Acta* 302 (2019), pp. 31–37. DOI: 10.1016/j.electacta.2019.01.180. URL: <https://doi.org/10.1016/j.electacta.2019.01.180>.

- [8] Harry B. Gray and Jay R. Winkler. “Electron tunneling through proteins.” In: *Quarterly Reviews of Biophysics* 36.3 (2003), pp. 341–372. DOI: 10.1017/s0033583503003913. URL: <https://doi.org/10.1017/s0033583503003913>.
- [9] Ana A. Arteni, Ghada Ajlani, and Egbert J. Boekema. “Structural organisation of phycobilisomes from *Synechocystis* sp. strain PCC6803 and their interaction with the membrane.” In: *Biochimica et Biophysica Acta (BBA) - Bioenergetics* 1787.4 (2009), pp. 272–279. DOI: 10.1016/j.bbabi.2009.01.009. URL: <https://doi.org/10.1016/j.bbabi.2009.01.009>.
- [10] Christa L. Colyer et al. “Analysis of cyanobacterial pigments and proteins by electrophoretic and chromatographic methods.” In: *Analytical and Bioanalytical Chemistry* 382.3 (2005), pp. 559–569. DOI: 10.1007/s00216-004-3020-4. URL: <https://doi.org/10.1007/s00216-004-3020-4>.
- [11] Jianfei Ma et al. “Structural basis of energy transfer in *Porphyridium purpureum* phycobilisome.” In: *Nature* 579.7797 (2020), pp. 146–151. DOI: 10.1038/s41586-020-2020-7. URL: <https://doi.org/10.1038/s41586-020-2020-7>.
- [12] Jun Zhang et al. “Structure of phycobilisome from the red alga *Griffithsia pacifica*.” In: *Nature* 551.7678 (2017), pp. 57–63. DOI: 10.1038/nature24278. URL: <https://doi.org/10.1038/nature24278>.
- [13] Noam Adir, Shira Bar-Zvi, and Dvir Harris. “The amazing phycobilisome.” In: *Biochimica et Biophysica Acta (BBA) - Bioenergetics* 1861.4 (2020), p. 148047. DOI: 10.1016/j.bbabi.2019.07.002. URL: <https://doi.org/10.1016/j.bbabi.2019.07.002>.
- [14] Justine Dumay et al. “Phycocerythrins.” In: *Advances in Botanical Research*. Elsevier, 2014, pp. 321–343. DOI: 10.1016/b978-0-12-408062-1.00011-1. URL: <https://doi.org/10.1016/b978-0-12-408062-1.00011-1>.
- [15] Niraj Kumar Singh et al. “The phycobilisomes: an early requisite for efficient photosynthesis in cyanobacteria.” en. In: *EXCLI Journal*; 14:Doc268; ISSN 1611-2156 (2015). DOI: 10.17179/EXCLI2014-723. URL: [https://www.excli.de/vol14/Rastogi\\_Madamwar\\_20022015\\_proof.pdf](https://www.excli.de/vol14/Rastogi_Madamwar_20022015_proof.pdf).
- [16] Vinod K. Kannaujiya, Shanthi Sundaram, and Rajeshwar P. Sinha. “Structural and Functional Significance of Phycobiliproteins.” In: *Phycobiliproteins: Recent Developments and Future Applications*. Springer Singapore, 2017, pp. 21–44. DOI: 10.1007/978-981-10-6460-9\_3. URL: [https://doi.org/10.1007/978-981-10-6460-9\\_3](https://doi.org/10.1007/978-981-10-6460-9_3).

- [17] Jay R. Winkler and Harry B. Gray. "Long-Range Electron Tunneling." In: *Journal of the American Chemical Society* 136.8 (2014), pp. 2930–2939. DOI: 10.1021/ja500215j. URL: <https://doi.org/10.1021/ja500215j>.
- [18] Reginald Garrett. *Biochemistry*. Belmont, CA: Brooks/Cole, Cengage Learning, 2010. ISBN: 0-495-10935-5.
- [19] S. J. UPDIKE and G. P. HICKS. "The Enzyme Electrode." In: *Nature* 214.5092 (1967), pp. 986–988. DOI: 10.1038/214986a0. URL: <https://doi.org/10.1038/214986a0>.
- [20] Hope Adamson, Alan M. Bond, and Alison Parkin. "Probing biological redox chemistry with large amplitude Fourier transformed ac voltammetry." In: *Chemical Communications* 53.69 (2017), pp. 9519–9533. DOI: 10.1039/c7cc03870d. URL: <https://doi.org/10.1039/c7cc03870d>.
- [21] Nicholas D. J. Yates, Martin A. Fascione, and Alison Parkin. "Methodologies for "Wiring" Redox Proteins/Enzymes to Electrode Surfaces." In: *Chemistry - A European Journal* 24.47 (2018), pp. 12164–12182. DOI: 10.1002/chem.201800750. URL: <https://doi.org/10.1002/chem.201800750>.
- [22] Eugenii Katz, Andrew N. Shipway, and Itamar Willner. "The Electrochemical and Photochemical Activation of Redox Enzymes." In: *Electron Transfer in Chemistry*. Wiley-VCH Verlag GmbH, pp. 127–201. DOI: 10.1002/9783527618248.ch50. URL: <https://doi.org/10.1002/9783527618248.ch50>.
- [23] Franziska V. Oberhaus, Dieter Frense, and Dieter Beckmann. "Immobilization Techniques for Aptamers on Gold Electrodes for the Electrochemical Detection of Proteins: A Review." In: *Biosensors* 10.5 (2020), p. 45. DOI: 10.3390/bios10050045. URL: <https://doi.org/10.3390/bios10050045>.
- [24] María Belluzo, María Ribone, and Claudia Lagier. "Assembling Amperometric Biosensors for Clinical Diagnostics." In: *Sensors* 8.3 (2008), pp. 1366–1399. DOI: 10.3390/s8031366. URL: <https://doi.org/10.3390/s8031366>.
- [25] Leland C. Clark and Champ Lyons. "ELECTRODE SYSTEMS FOR CONTINUOUS MONITORING IN CARDIOVASCULAR SURGERY." In: *Annals of the New York Academy of Sciences* 102.1 (2006), pp. 29–45. DOI: 10.1111/j.1749-6632.1962.tb13623.x. URL: <https://doi.org/10.1111/j.1749-6632.1962.tb13623.x>.
- [26] Eun-Hyung Yoo and Soo-Youn Lee. "Glucose Biosensors: An Overview of Use in Clinical Practice." In: *Sensors* 10.5 (2010), pp. 4558–4576. DOI: 10.3390/s100504558. URL: <https://doi.org/10.3390/s100504558>.

- [27] AC Pereira, MGF Sales, and LR Rodrigues. “Biosensors for Rapid Detection of Breast Cancer Biomarkers.” In: *Advanced Biosensors for Health Care Applications*. Elsevier, 2019, pp. 71–103. DOI: 10.1016/b978-0-12-815743-5.00003-2. URL: <https://doi.org/10.1016/b978-0-12-815743-5.00003-2>.
- [28] Meenakshi Choudhary and Kavita Arora. “Electrochemical biosensors for early detection of cancer.” In: *Biosensor Based Advanced Cancer Diagnostics*. Elsevier, 2022, pp. 123–151. DOI: 10.1016/b978-0-12-823424-2.00024-7. URL: <https://doi.org/10.1016/b978-0-12-823424-2.00024-7>.
- [29] Vinita Hooda et al. “Bilirubin enzyme biosensor: potentiality and recent advances towards clinical bioanalysis.” In: *Biotechnology Letters* 39.10 (2017), pp. 1453–1462. DOI: 10.1007/s10529-017-2396-0. URL: <https://doi.org/10.1007/s10529-017-2396-0>.
- [30] Lin Zhang et al. “Rational Design of Enzyme-Modified Electrodes for Optimized Bioelectrocatalytic Activity.” In: *ChemElectroChem* 6.19 (2019), pp. 4980–4984. DOI: 10.1002/ce1c.201901022. URL: <https://doi.org/10.1002/ce1c.201901022>.
- [31] Orr Schlesinger et al. “Electron transfer rate analysis of a site-specifically wired copper oxidase.” In: *Physical Chemistry Chemical Physics* 20.9 (2018), pp. 6159–6166. DOI: 10.1039/c8cp00041g. URL: <https://doi.org/10.1039/c8cp00041g>.
- [32] Dirk Mersch et al. “Wiring of Photosystem II to Hydrogenase for Photoelectrochemical Water Splitting.” In: *Journal of the American Chemical Society* 137.26 (2015), pp. 8541–8549. DOI: 10.1021/jacs.5b03737. URL: <https://doi.org/10.1021/jacs.5b03737>.
- [33] Adrian Ruff, Felipe Conzuelo, and Wolfgang Schuhmann. “Bioelectrocatalysis as the basis for the design of enzyme-based biofuel cells and semi-artificial biophotoelectrodes.” In: *Nature Catalysis* 3.3 (2019), pp. 214–224. DOI: 10.1038/s41929-019-0381-9. URL: <https://doi.org/10.1038/s41929-019-0381-9>.
- [34] Frank Davis and Séamus P.J. Higson. “Biofuel cells—Recent advances and applications.” In: *Biosensors and Bioelectronics* 22.7 (2007), pp. 1224–1235. DOI: 10.1016/j.bios.2006.04.029. URL: <https://doi.org/10.1016/j.bios.2006.04.029>.
- [35] Celine Justino, Armando Duarte, and Teresa Rocha-Santos. “Recent Progress in Biosensors for Environmental Monitoring: A Review.” In: *Sensors* 17.12 (2017), p. 2918. DOI: 10.3390/s17122918. URL: <https://doi.org/10.3390/s17122918>.

- [36] Juntai Liu et al. “Mechanisms of Self-Assembly and Energy Harvesting in Tuneable Conjugates of Quantum Dots and Engineered Photovoltaic Proteins.” In: *Small* 15.4 (2018), p. 1804267. DOI: 10.1002/smll.201804267. URL: <https://doi.org/10.1002/smll.201804267>.
- [37] Laura T. Wey et al. “The Development of Biophotovoltaic Systems for Power Generation and Biological Analysis.” In: *ChemElectroChem* 6.21 (2019), pp. 5375–5386. DOI: 10.1002/celec.201900997. URL: <https://doi.org/10.1002/celec.201900997>.
- [38] Nikolay Kornienko et al. “Advancing Techniques for Investigating the Enzyme–Electrode Interface.” In: *Accounts of Chemical Research* 52.5 (2019), pp. 1439–1448. DOI: 10.1021/acs.accounts.9b00087. URL: <https://doi.org/10.1021/acs.accounts.9b00087>.
- [39] Paolo Bollella and Evgeny Katz. “Enzyme-Based Biosensors: Tackling Electron Transfer Issues.” In: *Sensors* 20.12 (2020), p. 3517. DOI: 10.3390/s20123517. URL: <https://doi.org/10.3390/s20123517>.
- [40] Volkmar Weissig and Tamer Elbayoumi, eds. *Pharmaceutical Nanotechnology*. Springer New York, 2019. DOI: 10.1007/978-1-4939-9516-5. URL: <https://doi.org/10.1007/978-1-4939-9516-5>.
- [41] Pedro M. S. D. Cal, Gonalo J. L. Bernardes, and Pedro M. P. Gois. “Cysteine-Selective Reactions for Antibody Conjugation.” In: *Angewandte Chemie International Edition* 53.40 (2014), pp. 10585–10587. DOI: 10.1002/anie.201405702. URL: <https://doi.org/10.1002/anie.201405702>.
- [42] Christopher D. Spicer and Benjamin G. Davis. “Selective chemical protein modification.” In: *Nature Communications* 5.1 (2014). DOI: 10.1038/ncomms5740. URL: <https://doi.org/10.1038/ncomms5740>.
- [43] Jared A. Shadish and Cole A. DeForest. “Site-Selective Protein Modification: From Functionalized Proteins to Functional Biomaterials.” In: *Matter* 2.1 (2020), pp. 50–77. DOI: 10.1016/j.matt.2019.11.011. URL: <https://doi.org/10.1016/j.matt.2019.11.011>.
- [44] Omar Boutureira and Gonalo J. L. Bernardes. “Advances in Chemical Protein Modification.” In: *Chemical Reviews* 115.5 (2015), pp. 2174–2195. DOI: 10.1021/cr500399p. URL: <https://doi.org/10.1021/cr500399p>.
- [45] Jason W. Chin. “Expanding and reprogramming the genetic code.” In: *Nature* 550.7674 (2017), pp. 53–60. DOI: 10.1038/nature24031. URL: <https://doi.org/10.1038/nature24031>.



- [46] Greg T. Hermanson. "The Reactions of Bioconjugation." In: *Bioconjugate Techniques*. Elsevier, 2013, pp. 229–258. DOI: 10.1016/b978-0-12-382239-0.00003-0. URL: <https://doi.org/10.1016/b978-0-12-382239-0.00003-0>.
- [47] Sung In Lim. "Site-specific bioconjugation and self-assembly technologies for multi-functional biologics: on the road to the clinic." In: *Drug Discovery Today* 25.1 (2020), pp. 168–176. DOI: 10.1016/j.drudis.2019.10.002. URL: <https://doi.org/10.1016/j.drudis.2019.10.002>.
- [48] Rachel M. Lieser et al. "Site-Specific Bioconjugation Approaches for Enhanced Delivery of Protein Therapeutics and Protein Drug Carriers." In: *Bioconjugate Chemistry* 31.10 (2020), pp. 2272–2282. DOI: 10.1021/acs.bioconjchem.0c00456. URL: <https://doi.org/10.1021/acs.bioconjchem.0c00456>.
- [49] Smita B. Gunnoo and Annemieke Madder. "Bioconjugation – using selective chemistry to enhance the properties of proteins and peptides as therapeutics and carriers." In: *Organic & Biomolecular Chemistry* 14.34 (2016), pp. 8002–8013. DOI: 10.1039/c6ob00808a. URL: <https://doi.org/10.1039/c6ob00808a>.
- [50] Erika M. Milczek. "Commercial Applications for Enzyme-Mediated Protein Conjugation: New Developments in Enzymatic Processes to Deliver Functionalized Proteins on the Commercial Scale." In: *Chemical Reviews* 118.1 (2017), pp. 119–141. DOI: 10.1021/acs.chemrev.6b00832. URL: <https://doi.org/10.1021/acs.chemrev.6b00832>.
- [51] Vijay Chudasama, Antoine Maruani, and Stephen Caddick. "Recent advances in the construction of antibody–drug conjugates." In: *Nature Chemistry* 8.2 (2016), pp. 114–119. DOI: 10.1038/nchem.2415. URL: <https://doi.org/10.1038/nchem.2415>.
- [52] Samuel M. Meier-Menches and Angela Casini. "Design Strategies and Medicinal Applications of Metal-Peptidic Bioconjugates." In: *Bioconjugate Chemistry* 31.5 (2020), pp. 1279–1288. DOI: 10.1021/acs.bioconjchem.0c00152. URL: <https://doi.org/10.1021/acs.bioconjchem.0c00152>.
- [53] Mei-Xia Zhao and Er-Zao Zeng. "Application of functional quantum dot nanoparticles as fluorescence probes in cell labeling and tumor diagnostic imaging." In: *Nanoscale Research Letters* 10.1 (2015). DOI: 10.1186/s11671-015-0873-8. URL: <https://doi.org/10.1186/s11671-015-0873-8>.
- [54] Igor L. Medintz et al. "Quantum dot bioconjugates for imaging, labelling and sensing." In: *Nature Materials* 4.6 (2005), pp. 435–446. DOI: 10.1038/nmat1390. URL: <https://doi.org/10.1038/nmat1390>.

- [55] Marissa A. Morales and Jeffrey Mark Halpern. "Guide to Selecting a Biorecognition Element for Biosensors." In: *Bioconjugate Chemistry* 29.10 (2018), pp. 3231–3239. DOI: 10.1021/acs.bioconjchem.8b00592. URL: <https://doi.org/10.1021/acs.bioconjchem.8b00592>.
- [56] Susana Liébana and Guido A. Drago. "Bioconjugation and stabilisation of biomolecules in biosensors." In: *Essays in Biochemistry* 60.1 (2016). Ed. by Pedro Estrela, pp. 59–68. DOI: 10.1042/ebc20150007. URL: <https://doi.org/10.1042/ebc20150007>.
- [57] Yifan Dai et al. "Application of bioconjugation chemistry on biosensor fabrication for detection of TAR-DNA binding protein 43." In: *Biosensors and Bioelectronics* 117 (2018), pp. 60–67. DOI: 10.1016/j.bios.2018.05.060. URL: <https://doi.org/10.1016/j.bios.2018.05.060>.
- [58] Caroline Apel et al. "Protein Modification of Lysine with 2-(2-Styrylcyclopropyl)ethanal." In: *Organic Letters* 21.24 (2019), pp. 10043–10047. DOI: 10.1021/acs.orglett.9b03982. URL: <https://doi.org/10.1021/acs.orglett.9b03982>.
- [59] Chun Ling Tung et al. "Traceless and Chemoselective Amine Bioconjugation via Phthalimidine Formation in Native Protein Modification." In: *Organic Letters* 18.11 (2016), pp. 2600–2603. DOI: 10.1021/acs.orglett.6b00983. URL: <https://doi.org/10.1021/acs.orglett.6b00983>.
- [60] Oleksandr Koniev and Alain Wagner. "Developments and recent advancements in the field of endogenous amino acid selective bond forming reactions for bioconjugation." In: *Chem. Soc. Rev.* 44.15 (2015), pp. 5495–5551. DOI: 10.1039/c5cs00048c. URL: <https://doi.org/10.1039/c5cs00048c>.
- [61] Cláudia S.M. Fernandes et al. "Engineered Protein Variants for Bioconjugation." In: *Biomedical Applications of Functionalized Nanomaterials*. Elsevier, 2018, pp. 105–138. DOI: 10.1016/b978-0-323-50878-0.00005-7. URL: <https://doi.org/10.1016/b978-0-323-50878-0.00005-7>.
- [62] João M. J. M. Ravasco et al. "Bioconjugation with Maleimides: A Useful Tool for Chemical Biology." In: *Chemistry – A European Journal* 25.1 (2018), pp. 43–59. DOI: 10.1002/chem.201803174. URL: <https://doi.org/10.1002/chem.201803174>.
- [63] Anthony J. Rojas, Bradley L. Pentelute, and Stephen L. Buchwald. "Water-Soluble Palladium Reagents for Cysteine S-Arylation under Ambient Aqueous Conditions." In: *Organic Letters* 19.16 (2017), pp. 4263–4266. DOI: 10.1021/acs.orglett.7b01911. URL: <https://doi.org/10.1021/acs.orglett.7b01911>.

- [64] Philipp Ochtrop and Christian Peter Richard Hackenberger. “Recent advances of thiol-selective bioconjugation reactions.” In: *Current Opinion in Chemical Biology* 58 (2020), pp. 28–36. DOI: 10.1016/j.cbpa.2020.04.017. URL: <https://doi.org/10.1016/j.cbpa.2020.04.017>.
- [65] Maik Henkel, Niels Röckendorf, and Andreas Frey. “Selective and Efficient Cysteine Conjugation by Maleimides in the Presence of Phosphine Reductants.” In: *Bioconjugate Chemistry* 27.10 (2016), pp. 2260–2265. DOI: 10.1021/acs.bioconjchem.6b00371. URL: <https://doi.org/10.1021/acs.bioconjchem.6b00371>.
- [66] Smita B. Gunnoo and Annemieke Madder. “Chemical Protein Modification through Cysteine.” In: *ChemBioChem* 17.7 (Mar. 2016), pp. 529–553. DOI: 10.1002/cbic.201500667. URL: <https://doi.org/10.1002/cbic.201500667>.
- [67] Shang Jia, Dan He, and Christopher J. Chang. “Bioinspired Thiophosphorodichloridate Reagents for Chemoselective Histidine Bioconjugation.” In: *Journal of the American Chemical Society* 141.18 (2019), pp. 7294–7301. DOI: 10.1021/jacs.8b11912. URL: <https://doi.org/10.1021/jacs.8b11912>.
- [68] Xiaoping Chen et al. “Histidine-Specific Peptide Modification via Visible-Light-Promoted C–H Alkylation.” In: *Journal of the American Chemical Society* 141.45 (2019), pp. 18230–18237. DOI: 10.1021/jacs.9b09127. URL: <https://doi.org/10.1021/jacs.9b09127>.
- [69] Peter A. Szijj et al. “Tyrosine bioconjugation – an emergent alternative.” In: *Organic & Biomolecular Chemistry* 18.44 (2020), pp. 9018–9028. DOI: 10.1039/d0ob01912g. URL: <https://doi.org/10.1039/d0ob01912g>.
- [70] Mathew W. Jones et al. “Direct Peptide Bioconjugation/PEGylation at Tyrosine with Linear and Branched Polymeric Diazonium Salts.” In: *Journal of the American Chemical Society* 134.17 (2012), pp. 7406–7413. DOI: 10.1021/ja211855q. URL: <https://doi.org/10.1021/ja211855q>.
- [71] Hitoshi Ban, Julia Gavriluk, and Carlos F. Barbas. “Tyrosine Bioconjugation through Aqueous Ene-Type Reactions: A Click-Like Reaction for Tyrosine.” In: *Journal of the American Chemical Society* 132.5 (2010), pp. 1523–1525. DOI: 10.1021/ja909062q. URL: <https://doi.org/10.1021/ja909062q>.
- [72] Julien C. Vantourout et al. “Serine-Selective Bioconjugation.” In: *Journal of the American Chemical Society* 142.41 (2020), pp. 17236–17242. DOI: 10.1021/jacs.0c05595. URL: <https://doi.org/10.1021/jacs.0c05595>.

- [73] Emily A. Hoyt et al. "Contemporary approaches to site-selective protein modification." In: *Nature Reviews Chemistry* 3.3 (2019), pp. 147–171. DOI: 10.1038/s41570-019-0079-1. URL: <https://doi.org/10.1038/s41570-019-0079-1>.
- [74] Dominik Schumacher and Christian PR Hackenberger. "More than add-on: chemoselective reactions for the synthesis of functional peptides and proteins." In: *Current Opinion in Chemical Biology* 22 (2014), pp. 62–69. DOI: 10.1016/j.cbpa.2014.09.018. URL: <https://doi.org/10.1016/j.cbpa.2014.09.018>.
- [75] Timothy L Foley and Michael D Burkart. "Site-specific protein modification: advances and applications." In: *Current Opinion in Chemical Biology* 11.1 (2007), pp. 12–19. DOI: 10.1016/j.cbpa.2006.11.036. URL: <https://doi.org/10.1016/j.cbpa.2006.11.036>.
- [76] Jisoo Park et al. "Methods to generate site-specific conjugates of antibody and protein." In: *Bioorganic & Medicinal Chemistry* 30 (2021), p. 115946. DOI: 10.1016/j.bmc.2020.115946. URL: <https://doi.org/10.1016/j.bmc.2020.115946>.
- [77] Christian B Rosen and Matthew B Francis. "Targeting the N terminus for site-selective protein modification." In: *Nature Chemical Biology* 13.7 (2017), pp. 697–705. DOI: 10.1038/nchembio.2416. URL: <https://doi.org/10.1038/nchembio.2416>.
- [78] Marion Garreau, Franck Le Vaillant, and Jerome Waser. "C-Terminal Bioconjugation of Peptides through Photoredox Catalyzed Decarboxylative Alkynylation." In: *Angewandte Chemie International Edition* 58.24 (2019), pp. 8182–8186. DOI: 10.1002/anie.201901922. URL: <https://doi.org/10.1002/anie.201901922>.
- [79] Xi Chen et al. "Site-Selective Lysine Modification of Native Proteins and Peptides via Kinetically Controlled Labeling." In: *Bioconjugate Chemistry* 23.3 (2012), pp. 500–508. DOI: 10.1021/bc200556n. URL: <https://doi.org/10.1021/bc200556n>.
- [80] Vikas Gupta et al. "Recognition of active and inactive catalytic triads: A template based approach." In: *International Journal of Biological Macromolecules* 46.3 (2010), pp. 317–323. DOI: 10.1016/j.ijbiomac.2010.01.011. URL: <https://doi.org/10.1016/j.ijbiomac.2010.01.011>.
- [81] Charles S. Craik et al. "The Catalytic Role of the Active Site Aspartic Acid in Serine Proteases." In: *Science* 237.4817 (1987), pp. 909–913. DOI: 10.1126/science.3303334. URL: <https://doi.org/10.1126/science.3303334>.

- [82] B.T. Miller and A. Kurosky. “Elevated Intrinsic Reactivity of Seryl Hydroxyl Groups within the Linear Peptide Triads His-Xaa-Ser or Ser-Xaa-His.” In: *Biochemical and Biophysical Research Communications* 196.1 (1993), pp. 461–467. DOI: 10.1006/bbrc.1993.2272. URL: <https://doi.org/10.1006/bbrc.1993.2272>.
- [83] Chi Zhang et al. “Site-Selective Cysteine–Cyclooctyne Conjugation.” In: *Angewandte Chemie International Edition* 57.22 (2018), pp. 6459–6463. DOI: 10.1002/anie.201800860. URL: <https://doi.org/10.1002/anie.201800860>.
- [84] Manuel C. Martos-Maldonado et al. “Selective N-terminal acylation of peptides and proteins with a Gly-His tag sequence.” In: *Nature Communications* 9.1 (2018). DOI: 10.1038/s41467-018-05695-3. URL: <https://doi.org/10.1038/s41467-018-05695-3>.
- [85] Brian L. Carlson et al. “Function and Structure of a Prokaryotic Formylglycine-generating Enzyme.” In: *Journal of Biological Chemistry* 283.29 (2008), pp. 20117–20125. DOI: 10.1074/jbc.M800217200. URL: <https://doi.org/10.1074/jbc.M800217200>.
- [86] Justin D. Cohen, Peng Zou, and Alice Y. Ting. “Site-Specific Protein Modification Using Lipoic Acid Ligase and Bis-Aryl Hydrazone Formation.” In: *ChemBioChem* 13.6 (2012), pp. 888–894. DOI: 10.1002/cbic.201100764. URL: <https://doi.org/10.1002/cbic.201100764>.
- [87] C. Uttamapinant et al. “A fluorophore ligase for site-specific protein labeling inside living cells.” In: *Proceedings of the National Academy of Sciences* 107.24 (2010), pp. 10914–10919. DOI: 10.1073/pnas.0914067107. URL: <https://doi.org/10.1073/pnas.0914067107>.
- [88] Saurabh Bhatia. “Introduction to enzymes and their applications.” In: *Introduction to Pharmaceutical Biotechnology, Volume 2*. IOP Publishing, 2018. DOI: 10.1088/978-0-7503-1302-5ch1. URL: <https://doi.org/10.1088/978-0-7503-1302-5ch1>.
- [89] Naoyuki Sugiyama, Haruna Imamura, and Yasushi Ishihama. “Large-scale Discovery of Substrates of the Human Kinome.” In: *Scientific Reports* 9.1 (2019). DOI: 10.1038/s41598-019-46385-4. URL: <https://doi.org/10.1038/s41598-019-46385-4>.
- [90] David Bradley and Pedro Beltrao. “Evolution of protein kinase substrate recognition at the active site.” In: *PLOS Biology* 17.6 (2019). Ed. by Benjamin E. Turk, e3000341. DOI: 10.1371/journal.pbio.3000341. URL: <https://doi.org/10.1371/journal.pbio.3000341>.

- [91] Chad J. Miller and Benjamin E. Turk. "Homing in: Mechanisms of Substrate Targeting by Protein Kinases." In: *Trends in Biochemical Sciences* 43.5 (2018), pp. 380–394. DOI: 10.1016/j.tibs.2018.02.009. URL: <https://doi.org/10.1016/j.tibs.2018.02.009>.
- [92] *Recombinant human cAMP-dependent protein kinase: PKA, C alpha, 50 µg*. URL: <https://www.proteinkinase.biz/camp-dependent-protein-kinase-pka/1094-camp-dependent-protein-kinase-pka-c-alpha-human-50-microg.html>. (accessed: 17-02-2022).
- [93] Robert Roskoski. "[1] Assays of protein kinase." In: *Methods in Enzymology*. Elsevier, 1983, pp. 3–6. DOI: 10.1016/0076-6879(83)99034-1. URL: [https://doi.org/10.1016/0076-6879\(83\)99034-1](https://doi.org/10.1016/0076-6879(83)99034-1).
- [94] Donal A. Walsh, David B. Glass, and Ryan D. Mitchell. "Substrate diversity of the cAMP-dependent protein kinase: regulation based upon multiple binding interactions." In: *Current Opinion in Cell Biology* 4.2 (1992), pp. 241–251. DOI: 10.1016/0955-0674(92)90039-f. URL: [https://doi.org/10.1016/0955-0674\(92\)90039-f](https://doi.org/10.1016/0955-0674(92)90039-f).
- [95] Thilani M. Anthony et al. "ATP Analogs in Protein Kinase Research." In: *Kinomics*. Wiley-VCH Verlag GmbH & Co. KGaA, 2015, pp. 137–168. DOI: 10.1002/9783527683031.ch6. URL: <https://doi.org/10.1002/9783527683031.ch6>.
- [96] Jessica Colombo et al. "A functional family of fluorescent nucleotide analogues to investigate actin dynamics and energetics." In: *Nature Communications* 12.1 (2021). DOI: 10.1038/s41467-020-20827-4. URL: <https://doi.org/10.1038/s41467-020-20827-4>.
- [97] Lucy M. Elphick et al. "Using Chemical Genetics and ATP Analogues To Dissect Protein Kinase Function." In: *ACS Chemical Biology* 2.5 (2007), pp. 299–314. DOI: 10.1021/cb700027u. URL: <https://doi.org/10.1021/cb700027u>.
- [98] Sujit Suwal et al. "Structural Analysis of ATP Analogues Compatible with Kinase-Catalyzed Labeling." In: *Bioconjugate Chemistry* 23.12 (2012), pp. 2386–2391. DOI: 10.1021/bc300404s. URL: <https://doi.org/10.1021/bc300404s>.
- [99] Sujit Suwal and Mary Kay H. Pflum. "Phosphorylation-Dependent Kinase-Substrate Cross-Linking." In: *Angewandte Chemie International Edition* 49.9 (2010), pp. 1627–1630. DOI: 10.1002/anie.200905244. URL: <https://doi.org/10.1002/anie.200905244>.

- [100] Keith D. Green and Mary Kay H. Pflum. "Kinase-Catalyzed Biotinylation for Phosphoprotein Detection." In: *Journal of the American Chemical Society* 129.1 (2006), pp. 10–11. DOI: 10.1021/ja066828o. URL: <https://doi.org/10.1021/ja066828o>.
- [101] Keith D. Green and Mary Kay H. Pflum. "Exploring Kinase Cosubstrate Promiscuity: Monitoring Kinase Activity through Dansylation." In: *ChemBioChem* 10.2 (2009), pp. 234–237. DOI: 10.1002/cbic.200800393. URL: <https://doi.org/10.1002/cbic.200800393>.
- [102] S. Serdjukow et al. "Synthesis of  $\gamma$ -labeled nucleoside 5'-triphosphates using click chemistry." In: *Chem. Commun.* 50.15 (2014), pp. 1861–1863. DOI: 10.1039/c3cc48937j. URL: <https://doi.org/10.1039/c3cc48937j>.
- [103] Susanne Ermert et al. "Different Enzymatic Processing of  $\gamma$ -Phosphoramidate and  $\gamma$ -Phosphoester-Modified ATP Analogues." In: *ChemBioChem* 18.4 (2017), pp. 378–381. DOI: 10.1002/cbic.201600590. URL: <https://doi.org/10.1002/cbic.201600590>.
- [104] Adeline Espinasse et al. "Mechanistic Studies of Bioorthogonal ATP Analogues for Assessment of Histidine Kinase Autophosphorylation." In: *ACS Chemical Biology* 15.5 (2020), pp. 1252–1260. DOI: 10.1021/acscchembio.9b01024. URL: <https://doi.org/10.1021/acscchembio.9b01024>.
- [105] Norman Hardt, Stephan M. Hacker, and Andreas Marx. "Synthesis and fluorescence characteristics of ATP-based FRET probes." In: *Organic & Biomolecular Chemistry* 11.48 (2013), p. 8298. DOI: 10.1039/c3ob41751d. URL: <https://doi.org/10.1039/c3ob41751d>.
- [106] Sarah E. Lee et al. "The Chemoselective One-Step Alkylation and Isolation of Thiophosphorylated Cdk2 Substrates in the Presence of Native Cysteine." In: *ChemBioChem* 12.4 (Feb. 2011), pp. 633–640. DOI: 10.1002/cbic.201000528. URL: <https://doi.org/10.1002/cbic.201000528>.
- [107] Sung Won Kwon et al. "Selective Enrichment of Thiophosphorylated Polypeptides as a Tool for the Analysis of Protein Phosphorylation." In: *Molecular & Cellular Proteomics* 2.4 (2003), pp. 242–247. DOI: 10.1074/mcp.m300039-mcp200. URL: <https://doi.org/10.1074/mcp.m300039-mcp200>.
- [108] Stephan M. Hacker, Martin Mex, and Andreas Marx. "Synthesis and Stability of Phosphate Modified ATP Analogues." In: *The Journal of Organic Chemistry* 77.22 (2012), pp. 10450–10454. DOI: 10.1021/jo301923p. URL: <https://doi.org/10.1021/jo301923p>.

- [109] Ahmed Eid Fouda. "Development Of Gamma-Modified ATP Analogs To Study Kinase-Catalyzed Phosphorylations." PhD thesis. Wayne State University, 2016. URL: [https://digitalcommons.wayne.edu/oa\\_dissertations/1531](https://digitalcommons.wayne.edu/oa_dissertations/1531).
- [110] Łukasz Janczewski et al. "Microwave-assisted synthesis of dialkyl  $\omega$ -azidoalkylphosphonates." In: *Synthetic Communications* 46.19 (2016), pp. 1625–1633. DOI: 10.1080/00397911.2016.1221114. URL: <https://doi.org/10.1080/00397911.2016.1221114>.
- [111] Sung Hyun Yang, Dong Jun Lee, and Margaret A. Brimble. "Synthesis of an NDPK Phosphocarrier Domain Peptide Containing a Novel Triazolylalanine Analogue of Phosphohistidine Using Click Chemistry." In: *Organic Letters* 13.20 (2011), pp. 5604–5607. DOI: 10.1021/o1202333u. URL: <https://doi.org/10.1021/o1202333u>.
- [112] Marek R. Baranowski et al. "Synthesis of Fluorophosphate Nucleotide Analogues and Their Characterization as Tools for  $^{19}\text{F}$  NMR Studies." In: *The Journal of Organic Chemistry* 80.8 (2015), pp. 3982–3997. DOI: 10.1021/acs.joc.5b00337. URL: <https://doi.org/10.1021/acs.joc.5b00337>.
- [113]  $\gamma$ -(2-Azidoethyl)-ATP sodium salt solution. URL: <https://www.sigmaaldrich.com/DK/en/product/aldrich/808539>. (accessed: 17-02-2022).
- [114]  $\gamma$ -(2-Azidoethyl)-ATP. URL: <https://www.jenabioscience.com/click-chemistry/click-reagents-by-chemistry/azide-reagents/nucleotides/adenosines/nu-1701-gamma-2-azidoethyl-atp>. (accessed: 17-02-2022).
- [115] Sarah E. Lee et al. "Synthesis and reactivity of novel  $\gamma$ -phosphate modified ATP analogues." In: *Bioorganic & Medicinal Chemistry Letters* 19.14 (2009), pp. 3804–3807. DOI: 10.1016/j.bmcl.2009.04.028. URL: <https://doi.org/10.1016/j.bmcl.2009.04.028>.
- [116] Alan M. Marmelstein et al. "Chemical Pyrophosphorylation of Functionally Diverse Peptides." In: *Journal of the American Chemical Society* 136.1 (2013), pp. 108–111. DOI: 10.1021/ja411737c. URL: <https://doi.org/10.1021/ja411737c>.
- [117] Dorothea Fiedler, Lisa Yates, and Alan Marmelstein. "Synthetic Pyrophosphorylation Methods and Their Use in Chemical Biology." In: *Synlett* 25.16 (2014), pp. 2239–2245. DOI: 10.1055/s-0034-1378520. URL: <https://doi.org/10.1055/s-0034-1378520>.
- [118] Alan M. Marmelstein et al. "Pyrophosphorylation via selective phosphoprotein derivatization." In: *Chemical Science* 9.27 (2018), pp. 5929–5936. DOI: 10.1039/c8sc01233d. URL: <https://doi.org/10.1039/c8sc01233d>.



- [119] Alan M. Marmelstein, Javier Moreno, and Dorothea Fiedler. “Chemical Approaches to Studying Labile Amino Acid Phosphorylation.” In: *Topics in Current Chemistry* 375.2 (2017). DOI: 10.1007/s41061-017-0111-1. URL: <https://doi.org/10.1007/s41061-017-0111-1>.
- [120] Amira Khaled et al. “Exploring specificity of glycosyltransferases: synthesis of new sugar nucleotide related molecules as putative donor substrates.” In: *Carbohydrate Research* 343.2 (2008), pp. 167–178. DOI: 10.1016/j.carres.2007.11.009. URL: <https://doi.org/10.1016/j.carres.2007.11.009>.
- [121] Lisa M. Yates and Dorothea Fiedler. “A Stable Pyrophosphoserine Analog for Incorporation into Peptides and Proteins.” In: *ACS Chemical Biology* 11.4 (2016), pp. 1066–1073. DOI: 10.1021/acscchembio.5b00972. URL: <https://doi.org/10.1021/acscchembio.5b00972>.
- [122] Lisa M. Yates and Dorothea Fiedler. “Establishing the Stability and Reversibility of Protein Pyrophosphorylation with Synthetic Peptides.” In: *ChemBioChem* 16.3 (2015), pp. 415–423. DOI: 10.1002/cbic.201402589. URL: <https://doi.org/10.1002/cbic.201402589>.
- [123] Ernesto Brunet et al. “Click-chemistry-based bis-triazolylpyridine diphosphonate ligand for the sensitized luminescence of lanthanides in the solid state within the layers of  $\gamma$ -zirconium phosphate.” In: *Tetrahedron Letters* 50.38 (Sept. 2009), pp. 5361–5363. DOI: 10.1016/j.tetlet.2009.07.027. URL: <https://doi.org/10.1016/j.tetlet.2009.07.027>.
- [124] S. Schwan et al. “Substituent Pattern Effects on the Redox Potentials of Quinone-Based Active Materials for Aqueous Redox Flow Batteries.” In: *ChemSusChem* 13.20 (2020), pp. 5480–5488. DOI: 10.1002/cssc.202000454. URL: <https://doi.org/10.1002/cssc.202000454>.
- [125] Süleyman Er et al. “Computational design of molecules for an all-quinone redox flow battery.” In: *Chemical Science* 6.2 (2015), pp. 885–893. DOI: 10.1039/c4sc03030c. URL: <https://doi.org/10.1039/c4sc03030c>.
- [126] Kristina Wedege et al. “Organic Redox Species in Aqueous Flow Batteries: Redox Potentials, Chemical Stability and Solubility.” In: *Scientific Reports* 6.1 (2016). DOI: 10.1038/srep39101. URL: <https://doi.org/10.1038/srep39101>.
- [127] Amanda L. Eckermann et al. “Electrochemistry of redox-active self-assembled monolayers.” In: *Coordination Chemistry Reviews* 254.15-16 (2010), pp. 1769–1802. DOI: 10.1016/j.ccr.2009.12.023. URL: <https://doi.org/10.1016/j.ccr.2009.12.023>.

- [128] Fanfan Gao et al. “Electrocatalytic Activity of Modified Graphite Felt in Five Anthraquinone Derivative Solutions for Redox Flow Batteries.” In: *ACS Omega* 4.9 (2019), pp. 13721–13732. DOI: 10.1021/acsomega.9b01103. URL: <https://doi.org/10.1021/acsomega.9b01103>.
- [129] Sri R. Narayan et al. “Next-generation aqueous flow battery chemistries.” In: *Current Opinion in Electrochemistry* 18 (2019), pp. 72–80. DOI: 10.1016/j.coelec.2019.10.010. URL: <https://doi.org/10.1016/j.coelec.2019.10.010>.
- [130] Xinxin Xiao et al. “A symmetric supercapacitor/biofuel cell hybrid device based on enzyme-modified nanoporous gold: An autonomous pulse generator.” In: *Biosensors and Bioelectronics* 90 (2017), pp. 96–102. DOI: 10.1016/j.bios.2016.11.012. URL: <https://doi.org/10.1016/j.bios.2016.11.012>.
- [131] Serge Cosnier, Michael Holzinger, and Alan Le Goff. “Recent Advances in Carbon Nanotube-Based Enzymatic Fuel Cells.” In: *Frontiers in Bioengineering and Biotechnology* 2 (2014). DOI: 10.3389/fbioe.2014.00045. URL: <https://doi.org/10.3389/fbioe.2014.00045>.
- [132] Bo Hu et al. “A pH-Neutral, Metal-Free Aqueous Organic Redox Flow Battery Employing an Ammonium Anthraquinone Anolyte.” In: *Angewandte Chemie International Edition* 58.46 (2019), pp. 16629–16636. DOI: 10.1002/anie.201907934. URL: <https://doi.org/10.1002/anie.201907934>.
- [133] Yang Song and Garry R. Buettner. “Thermodynamic and kinetic considerations for the reaction of semiquinone radicals to form superoxide and hydrogen peroxide.” In: *Free Radical Biology and Medicine* 49.6 (2010), pp. 919–962. DOI: 10.1016/j.freeradbiomed.2010.05.009. URL: <https://doi.org/10.1016/j.freeradbiomed.2010.05.009>.
- [134] Christopher Batchelor-McAuley et al. “Voltammetric Characterization of DNA Intercalators across the Full pH Range: Anthraquinone-2, 6-disulfonate and Anthraquinone-2-sulfonate.” In: *The Journal of Physical Chemistry B* 114.11 (2010), pp. 4094–4100. DOI: 10.1021/jp1008187. URL: <https://doi.org/10.1021/jp1008187>.
- [135] Brian Huskinson et al. “A metal-free organic–inorganic aqueous flow battery.” In: *Nature* 505.7482 (2014), pp. 195–198. DOI: 10.1038/nature12909. URL: <https://doi.org/10.1038/nature12909>.
- [136] Jonathan Clayden, Nick Greeves, and Stuart Warren. *Organic Chemistry*. 2nd ed. MTM, 2017.

- [137] P.W.G. SMITH and A.R. TATCHELL. "AROMATIC NITRATION—NITRO COMPOUNDS." In: *Aromatic Chemistry*. Elsevier, 1969, pp. 21–45. DOI: 10.1016/b978-0-08-012948-8.50005-x. URL: <https://doi.org/10.1016/b978-0-08-012948-8.50005-x>.
- [138] Alain G. Giuglio-Tonolo et al. "A Survey of Synthetic Routes and Antitumor Activities for Benzo[g]quinoxaline-5, 10-diones." In: *Molecules* 25.24 (2020), p. 5922. DOI: 10.3390/molecules25245922. URL: <https://doi.org/10.3390/molecules25245922>.
- [139] Yanyan Zheng et al. "Synthesis, SAR and pharmacological characterization of novel anthraquinone cation compounds as potential anticancer agents." In: *European Journal of Medicinal Chemistry* 125 (2017), pp. 902–913. DOI: 10.1016/j.ejmech.2016.10.012. URL: <https://doi.org/10.1016/j.ejmech.2016.10.012>.
- [140] Yunyan Hou and Peter Wan. "Formal intramolecular photoredox chemistry of anthraquinones in aqueous solution: photodeprotection for alcohols, aldehydes and ketones." In: *Photochemical & Photobiological Sciences* 7.5 (2008), p. 588. DOI: 10.1039/b718970b. URL: <https://doi.org/10.1039/b718970b>.
- [141] Yan Guo et al. "Unraveling the Photodeprotection Mechanism of Anthraquinon-2-yl-methoxycarbonyl-Caged Alcohols Using Time-Resolved Spectroscopy." In: *The Journal of Organic Chemistry* 83.21 (2018), pp. 13454–13462. DOI: 10.1021/acs.joc.8b02252. URL: <https://doi.org/10.1021/acs.joc.8b02252>.
- [142] *Types of Molecular Bonds*. [Online; accessed 2022-02-14]. 2020. URL: <https://phys.libretexts.org/@go/page/4541>.
- [143] Elena Sperotto et al. "The mechanism of the modified Ullmann reaction." In: *Dalton Transactions* 39.43 (2010), p. 10338. DOI: 10.1039/c0dt00674b. URL: <https://doi.org/10.1039/c0dt00674b>.
- [144] Andrea Francesca Quivelli et al. "Reshaping Ullmann Amine Synthesis in Deep Eutectic Solvents: A Mild Approach for Cu-Catalyzed C–N Coupling Reactions With No Additional Ligands." In: *Frontiers in Chemistry* 7 (2019). DOI: 10.3389/fchem.2019.00723. URL: <https://doi.org/10.3389/fchem.2019.00723>.
- [145] Faysal Benaskar et al. "Copper(0) in the Ullmann heterocycle-aryl ether synthesis of 4-phenoxy pyridine using multimode microwave heating." In: *Tetrahedron Letters* 51.2 (2010), pp. 248–251. DOI: 10.1016/j.tetlet.2009.10.126. URL: <https://doi.org/10.1016/j.tetlet.2009.10.126>.

- [146] Younis Baqi and Christa E. Müller. “Rapid and Efficient Microwave-Assisted Copper(0)-Catalyzed Ullmann Coupling Reaction: General Access to Anilinoanthraquinone Derivatives.” In: *Organic Letters* 9.7 (2007), pp. 1271–1274. DOI: 10.1021/o1070102v. URL: <https://doi.org/10.1021/o1070102v>.
- [147] Gwilherm Evano and Nicolas Blanchard, eds. *Copper-Mediated Cross-Coupling Reactions*. John Wiley & Sons, Inc., 2013. DOI: 10.1002/9781118690659. URL: <https://doi.org/10.1002/9781118690659>.
- [148] Carlo Sambigao et al. “Copper catalysed Ullmann type chemistry: from mechanistic aspects to modern development.” In: *Chem. Soc. Rev.* 43.10 (2014), pp. 3525–3550. DOI: 10.1039/c3cs60289c. URL: <https://doi.org/10.1039/c3cs60289c>.
- [149] Xavi Ribas and Imma Güell. “Cu(I)/Cu(III) catalytic cycle involved in Ullmann-type cross-coupling reactions.” In: *Pure and Applied Chemistry* 86.3 (2014), pp. 345–360. DOI: 10.1515/pac-2013-1104. URL: <https://doi.org/10.1515/pac-2013-1104>.
- [150] Shovan Mondal. “Recent advancement of Ullmann-type coupling reactions in the formation of C–C bond.” In: *ChemTexts* 2.4 (2016). DOI: 10.1007/s40828-016-0036-2. URL: <https://doi.org/10.1007/s40828-016-0036-2>.
- [151] Donald Bethell, Iwan L. Jenkins, and Peter M. Quan. “Kinetic and product studies on Ullmann amination of 1-halogenoanthraquinones catalysed by copper(I) salts in acetonitrile solution.” In: *Journal of the Chemical Society, Perkin Transactions 2* 11 (1985), p. 1789. DOI: 10.1039/p29850001789. URL: <https://doi.org/10.1039/p29850001789>.
- [152] Sadao Arai, Mitsuhiro Hida, and Takamichi Yamagishi. “The Ullmann Condensation Reaction of Haloanthraquinone Derivatives with Amines in Aprotic Solvents. III. The Formation and Role of Copper(II) Species in the Condensation with 2-Aminoethanol by Copper(I) Catalyst.” In: *Bulletin of the Chemical Society of Japan* 51.1 (1978), pp. 277–282. DOI: 10.1246/bcsj.51.277. URL: <https://doi.org/10.1246/bcsj.51.277>.
- [153] Enas M. Malik et al. “Ullmann reactions of 1-amino-4-bromoanthraquinones bearing various 2-substituents furnishing novel dyes.” In: *Dyes and Pigments* 131 (2016), pp. 33–40. DOI: 10.1016/j.dyepig.2016.03.023. URL: <https://doi.org/10.1016/j.dyepig.2016.03.023>.
- [154] Mounir Mansour et al. “Activation of aryl halides by Cu<sup>0</sup>/1, 10-phenanthroline: Cu<sup>0</sup> as precursor of CuI catalyst in cross-coupling reactions.” In: *Chemical Communications* 45 (2008), p. 6051. DOI: 10.1039/b814364a. URL: <https://doi.org/10.1039/b814364a>.

- [155] Jiao Jiao et al. "A Facile and Practical Copper Powder-Catalyzed, Organic Solvent- and Ligand-Free Ullmann Amination of Aryl Halides." In: *The Journal of Organic Chemistry* 76.4 (2011), pp. 1180–1183. DOI: 10.1021/jo102169t. URL: <https://doi.org/10.1021/jo102169t>.
- [156] Raed M. Al-Zoubi et al. "Copper(I)-catalyzed regioselective Ullmann-type coupling of primary carbamates and 5-substituted-1, 2, 3-triiodobenzenes: facile synthesis of 2, 3-diiodinated N-aryl carbamates." In: *New Journal of Chemistry* 45.19 (2021), pp. 8432–8439. DOI: 10.1039/d1nj01332g. URL: <https://doi.org/10.1039/d1nj01332g>.
- [157] Lauren M. Huffman et al. "Observation and Mechanistic Study of Facile C O Bond Formation between a Well-Defined Aryl–Copper(III) Complex and Oxygen Nucleophiles." In: *Chemistry – A European Journal* 17.38 (2011), pp. 10643–10650. DOI: 10.1002/chem.201100608. URL: <https://doi.org/10.1002/chem.201100608>.
- [158] Hai-Zhu Yu et al. "Alternative Mechanistic Explanation for Ligand-Dependent Selectivities in Copper-Catalyzed N- and O-Arylation Reactions." In: *Journal of the American Chemical Society* 132.51 (2010), pp. 18078–18091. DOI: 10.1021/ja104264v. URL: <https://doi.org/10.1021/ja104264v>.
- [159] Theodore Cohen, John Wood, and Albert G. Dietz. "Organocopper intermediates in the exchange reaction of aryl halides with salts of copper(I). The possible role of copper(III)." In: *Tetrahedron Letters* 15.40 (1974), pp. 3555–3558. DOI: 10.1016/s0040-4039(01)91965-3. URL: [https://doi.org/10.1016/s0040-4039\(01\)91965-3](https://doi.org/10.1016/s0040-4039(01)91965-3).
- [160] Younis Baqi and Christa E Müller. "Synthesis of alkyl- and aryl-amino-substituted anthraquinone derivatives by microwave-assisted copper(0)-catalyzed Ullmann coupling reactions." In: *Nature Protocols* 5.5 (2010), pp. 945–953. DOI: 10.1038/nprot.2010.63. URL: <https://doi.org/10.1038/nprot.2010.63>.
- [161] Tran Dinh Tuong and Mitsuhiro Hida. "Mechanism of the Ullmann Condensation. I. Kinetic and Thermodynamic Studies." In: *Bulletin of the Chemical Society of Japan* 43.6 (1970), pp. 1763–1768. DOI: 10.1246/bcsj.43.1763. URL: <https://doi.org/10.1246/bcsj.43.1763>.
- [162] Tran Dinh Tuong and Mitsuhiro Hida. "Mechanism of The Ullmann Condensation Reaction. II. Effects of the Medium, the Additives and the Substituents." In: *Bulletin of the Chemical Society of Japan* 44.3 (1971), pp. 765–771. DOI: 10.1246/bcsj.44.765. URL: <https://doi.org/10.1246/bcsj.44.765>.

- [163] Noémie Elgrishi et al. “A Practical Beginner’s Guide to Cyclic Voltammetry.” In: *Journal of Chemical Education* 95.2 (2017), pp. 197–206. DOI: 10.1021/acs.jchemed.7b00361. URL: <https://doi.org/10.1021/acs.jchemed.7b00361>.
- [164] Xinxin Xiao, Pengchao Si, and Edmond Magner. “An overview of dealloyed nanoporous gold in bioelectrochemistry.” In: *Bioelectrochemistry* 109 (2016), pp. 117–126. DOI: 10.1016/j.bioelechem.2015.12.008. URL: <https://doi.org/10.1016/j.bioelechem.2015.12.008>.
- [165] Edward P. Randviir. “A cross examination of electron transfer rate constants for carbon screen-printed electrodes using Electrochemical Impedance Spectroscopy and cyclic voltammetry.” In: *Electrochimica Acta* 286 (2018), pp. 179–186. DOI: 10.1016/j.electacta.2018.08.021. URL: <https://doi.org/10.1016/j.electacta.2018.08.021>.
- [166] “Introduction.” In: *Introduction to Marcus Theory of Electron Transfer Reactions*. WORLD SCIENTIFIC, 2020, pp. 1–39. DOI: 10.1142/9789811208478\_0001. URL: [https://doi.org/10.1142/9789811208478\\_0001](https://doi.org/10.1142/9789811208478_0001).
- [167] Rudolph A. Marcus. “Reflections on electron transfer theory.” In: *The Journal of Chemical Physics* 153.21 (2020), p. 210401. DOI: 10.1063/5.0035434. URL: <https://doi.org/10.1063/5.0035434>.
- [168] R. S. Nicholson. “Theory and Application of Cyclic Voltammetry for Measurement of Electrode Reaction Kinetics.” In: *Analytical Chemistry* 37.11 (1965), pp. 1351–1355. DOI: 10.1021/ac60230a016. URL: <https://doi.org/10.1021/ac60230a016>.
- [169] Irma Lavagnini, Riccarda Antiochia, and Franco Magno. “An Extended Method for the Practical Evaluation of the Standard Rate Constant from Cyclic Voltammetric Data.” In: *Electroanalysis* 16.6 (2004), pp. 505–506. DOI: 10.1002/elan.200302851. URL: <https://doi.org/10.1002/elan.200302851>.
- [170] Achim Habekost. “Simulation and Fitting of Cyclic Voltammetry and Chronoamperometry Curves of Electrochemical Reactions with Different Mechanisms — A Didactic Perspective.” In: *World Journal of Chemical Education* 7.2 (2019), pp. 53–64. DOI: 10.12691/wjce-7-2-4. URL: <https://doi.org/10.12691/wjce-7-2-4>.
- [171] N. Aristov and A. Habekost. “Cyclic Voltammetry - A Versatile Electrochemical Method Investigating Electron Transfer Processes.” In: *World Journal of Chemical Education* 3.5 (2015), pp. 115–119. ISSN: 2375-1657. DOI: 10.12691/wjce-3-5-2. URL: <http://pubs.sciepub.com/wjce/3/5/2>.

- [172] Xiaoliang Wei et al. "A High-Current, Stable Nonaqueous Organic Redox Flow Battery." In: *ACS Energy Letters* 1.4 (2016), pp. 705–711. DOI: 10.1021/acsenenergylett.6b00255. URL: <https://doi.org/10.1021/acsenenergylett.6b00255>.
- [173] Giyun Kwon et al. "Multi-redox Molecule for High-Energy Redox Flow Batteries." In: *Joule* 2.9 (2018), pp. 1771–1782. DOI: 10.1016/j.joule.2018.05.014. URL: <https://doi.org/10.1016/j.joule.2018.05.014>.
- [174] Yichao Yan et al. "Simultaneously Enhancing the Redox Potential and Stability of Multi-Redox Organic Catholytes by Incorporating Cyclopropenium Substituents." In: *Journal of the American Chemical Society* 143.33 (2021), pp. 13450–13459. DOI: 10.1021/jacs.1c07237. URL: <https://doi.org/10.1021/jacs.1c07237>.
- [175] Xiaomei Yan et al. "Surface-confined redox-active monolayers of a multifunctional anthraquinone derivative on nanoporous and single-crystal gold electrodes." In: *Electrochemistry Communications* 124 (2021), p. 106962. DOI: 10.1016/j.elecom.2021.106962. URL: <https://doi.org/10.1016/j.elecom.2021.106962>.
- [176] Richard J. Washkuhn, Sangsom Reutrakul, and Joseph R. Robinson. "Correlation and Prediction of Rates of Alkaline Hydrolysis of Some Benzoate Esters." In: *Journal of Pharmaceutical Sciences* 59.6 (1970), pp. 779–781. DOI: 10.1002/jps.2600590611. URL: <https://doi.org/10.1002/jps.2600590611>.
- [177] Stephen W. Wright et al. "Convenient preparations of t-butyl esters and ethers from t-butanol." In: *Tetrahedron Letters* 38.42 (1997), pp. 7345–7348. DOI: 10.1016/s0040-4039(97)01792-9. URL: [https://doi.org/10.1016/s0040-4039\(97\)01792-9](https://doi.org/10.1016/s0040-4039(97)01792-9).
- [178] Daria A. Burmistrova et al. "Substituted o-Aminophenols as Redox-Mediators in the Thiol Oxidation to Unsymmetrical Disulfides." In: *Journal of The Electrochemical Society* 168.5 (2021), p. 055501. DOI: 10.1149/1945-7111/abfe43. URL: <https://doi.org/10.1149/1945-7111/abfe43>.
- [179] Erik C. B. Johnson and Stephen B. H. Kent. "Insights into the Mechanism and Catalysis of the Native Chemical Ligation Reaction." In: *Journal of the American Chemical Society* 128.20 (Apr. 2006), pp. 6640–6646. DOI: 10.1021/ja058344i. URL: <https://doi.org/10.1021/ja058344i>.
- [180] Rolf Huisgen. "1, 3-Dipolar Cycloadditions. Past and Future." In: *Angewandte Chemie International Edition in English* 2.10 (1963), pp. 565–598. DOI: 10.1002/anie.196305651. URL: <https://doi.org/10.1002/anie.196305651>.

- [181] Gavin O. Jones and K. N. Houk. "Predictions of Substituent Effects in Thermal Azide 1, 3-Dipolar Cycloadditions: Implications for Dynamic Combinatorial (Reversible) and Click (Irreversible) Chemistry." In: *The Journal of Organic Chemistry* 73.4 (2008), pp. 1333–1342. DOI: 10.1021/jo702295d. URL: <https://doi.org/10.1021/jo702295d>.
- [182] Brian Gold et al. "Selective Transition State Stabilization via Hyperconjugative and Conjugative Assistance: Stereoelectronic Concept for Copper-Free Click Chemistry." In: *The Journal of Organic Chemistry* 77.1 (2011), pp. 75–89. DOI: 10.1021/jo201434w. URL: <https://doi.org/10.1021/jo201434w>.
- [183] Martin Breugst and Hans-Ulrich Reissig. "The Huisgen Reaction: Milestones of the 1, 3-Dipolar Cycloaddition." In: *Angewandte Chemie International Edition* 59.30 (May 2020), pp. 12293–12307. DOI: 10.1002/anie.202003115. URL: <https://doi.org/10.1002/anie.202003115>.
- [184] Petra Smyslova et al. "Non-Catalyzed Click Reactions of ADIBO Derivatives with 5-Methyluridine Azides and Conformational Study of the Resulting Triazoles." In: *PLOS ONE* 10.12 (2015), pp. 1–33. DOI: 10.1371/journal.pone.0144613. URL: <https://doi.org/10.1371/journal.pone.0144613>.
- [185] Selvanathan Arumugam et al. "[18F]Azadibenzocyclooctyne ([18F]ADIBO): A biocompatible radioactive labeling synthon for peptides using catalyst free [3+2] cycloaddition." In: *Bioorganic & Medicinal Chemistry Letters* 21.23 (2011), pp. 6987–6991. DOI: 10.1016/j.bmcl.2011.09.126. URL: <https://doi.org/10.1016/j.bmcl.2011.09.126>.
- [186] Mélanie Roche et al. "[18F]FPyZIDE: A versatile prosthetic reagent for the fluorine-18 radiolabeling of biologics via copper-catalyzed or strain-promoted alkyne-azide cycloadditions." In: *Journal of Labelled Compounds and Radiopharmaceuticals* 62.2 (2019), pp. 95–108. DOI: 10.1002/jlcr.3701. URL: <https://doi.org/10.1002/jlcr.3701>.
- [187] N. S. Punekar. "Enzymatic Oxidation–Reduction Reactions." In: *ENZYMES: Catalysis, Kinetics and Mechanisms*. Springer Singapore, 2018, pp. 385–402. DOI: 10.1007/978-981-13-0785-0\_33. URL: [https://doi.org/10.1007/978-981-13-0785-0\\_33](https://doi.org/10.1007/978-981-13-0785-0_33).
- [188] Xiaomei Yan et al. "Direct electron transfer of fructose dehydrogenase immobilized on thiol-gold electrodes." In: *Electrochimica Acta* 392 (2021), p. 138946. DOI: 10.1016/j.electacta.2021.138946. URL: <https://doi.org/10.1016/j.electacta.2021.138946>.
- [189] Noémie Lalaoui et al. "Wiring Laccase on Covalently Modified Graphene: Carbon Nanotube Assemblies for the Direct Bio-electrocatalytic Reduction of Oxygen." In: *Chem-*



- istry – A European Journal* 21.8 (2014), pp. 3198–3201. DOI: 10.1002/chem.201405557. URL: <https://doi.org/10.1002/chem.201405557>.
- [190] Paolo Bollella et al. “Enhanced Direct Electron Transfer of Fructose Dehydrogenase Rationally Immobilized on a 2-Aminoanthracene Diazonium Cation Grafted Single-Walled Carbon Nanotube Based Electrode.” In: *ACS Catalysis* 8.11 (2018), pp. 10279–10289. DOI: 10.1021/acscatal.8b02729. URL: <https://doi.org/10.1021/acscatal.8b02729>.
- [191] Dónal Leech, Paul Kavanagh, and Wolfgang Schuhmann. “Enzymatic fuel cells: Recent progress.” In: *Electrochimica Acta* 84 (2012), pp. 223–234. DOI: 10.1016/j.electacta.2012.02.087. URL: <https://doi.org/10.1016/j.electacta.2012.02.087>.
- [192] Ross D. Milton and Shelley D. Minteer. “Direct enzymatic bioelectrocatalysis: differentiating between myth and reality.” In: *Journal of The Royal Society Interface* 14.131 (2017), p. 20170253. DOI: 10.1098/rsif.2017.0253. URL: <https://doi.org/10.1098/rsif.2017.0253>.
- [193] Christian Cremer and Olof Wallquist. *Sulfide dyes*. WO2006136516A2. 2006. URL: <https://patents.google.com/patent/WO2006136516A2/en>.
- [194] Mingguo Peng et al. “Transformation and toxicity assessment of two UV filters using UV/H<sub>2</sub>O<sub>2</sub> process.” In: *Science of The Total Environment* 603-604 (2017), pp. 361–369. DOI: 10.1016/j.scitotenv.2017.06.059. URL: <https://doi.org/10.1016/j.scitotenv.2017.06.059>.
- [195] Takashi Takeda, Yotaro Kasahara, and Tomoyuki Akutagawa. “Color-tunable arylamino-anthraquinone dyes through hydrogen-bond-assisted charge transfer interaction.” In: *RSC Advances* 11.39 (2021), pp. 24217–24231. DOI: 10.1039/d1ra03985g. URL: <https://doi.org/10.1039/d1ra03985g>.
- [196] Mark T. Sims et al. “Molecular Design Parameters of Anthraquinone Dyes for Guest–Host Liquid-Crystal Applications: Experimental and Computational Studies of Spectroscopy, Structure, and Stability.” In: *The Journal of Physical Chemistry C* 120.20 (2016), pp. 11151–11162. DOI: 10.1021/acs.jpcc.6b03607. URL: <https://doi.org/10.1021/acs.jpcc.6b03607>.
- [197] Klaus Hunger, ed. *Industrial Dyes*. Wiley, 2002. DOI: 10.1002/3527602011. URL: <https://doi.org/10.1002/3527602011>.

- [198] Shota Kawai et al. "The electron transfer pathway in direct electrochemical communication of fructose dehydrogenase with electrodes." In: *Electrochemistry Communications* 38 (2014), pp. 28–31. DOI: 10.1016/j.elecom.2013.10.024. URL: <https://doi.org/10.1016/j.elecom.2013.10.024>.
- [199] Michal Kizling and Renata Bilewicz. "Fructose Dehydrogenase Electron Transfer Pathway in Bioelectrocatalytic Reactions." In: *ChemElectroChem* 5.1 (2017), pp. 166–174. DOI: 10.1002/celec.201700861. URL: <https://doi.org/10.1002/celec.201700861>.
- [200] Stephen M. Jones and Edward I. Solomon. "Electron transfer and reaction mechanism of laccases." In: *Cellular and Molecular Life Sciences* 72.5 (2015), pp. 869–883. DOI: 10.1007/s00018-014-1826-6. URL: <https://doi.org/10.1007/s00018-014-1826-6>.
- [201] Youxun Liu et al. "Stable ABTS Immobilized in the MIL-100(Fe) Metal-Organic Framework as an Efficient Mediator for Laccase-Catalyzed Decolorization." In: *Molecules* 22.6 (2017), p. 920. DOI: 10.3390/molecules22060920. URL: <https://doi.org/10.3390/molecules22060920>.
- [202] Ram Chandra and Pankaj Chowdhary. "Properties of bacterial laccases and their application in bioremediation of industrial wastes." In: *Environmental Science: Processes & Impacts* 17.2 (2015), pp. 326–342. DOI: 10.1039/c4em00627e. URL: <https://doi.org/10.1039/c4em00627e>.
- [203] Katriina Matilainen et al. "Performance and penetration of laccase and ABTS inks on various printing substrates." In: *Colloids and Surfaces B: Biointerfaces* 90 (2012), pp. 119–128. DOI: 10.1016/j.colsurfb.2011.10.015. URL: <https://doi.org/10.1016/j.colsurfb.2011.10.015>.
- [204] Su Ma et al. "Direct Electron-Transfer Anisotropy of a Site-Specifically Immobilized Cellobiose Dehydrogenase." In: *ACS Catalysis* 9.8 (2019), pp. 7607–7615. DOI: 10.1021/acscatal.9b02014. URL: <https://doi.org/10.1021/acscatal.9b02014>.
- [205] Tao Liu et al. "Substituent effects on the redox potentials of dihydroxybenzenes: theoretical and experimental study." In: *Tetrahedron* 70.47 (2014), pp. 9033–9040. DOI: 10.1016/j.tet.2014.10.020. URL: <https://doi.org/10.1016/j.tet.2014.10.020>.
- [206] Ting-jian Zhang et al. "Discovery and biological evaluation of some (1H-1, 2, 3-triazol-4-yl)methoxybenzaldehyde derivatives containing an anthraquinone moiety as potent xanthine oxidase inhibitors." In: *Bioorganic & Medicinal Chemistry Letters* 27.4 (Feb. 2017), pp. 729–732. DOI: 10.1016/j.bmcl.2017.01.049. URL: <https://doi.org/10.1016/j.bmcl.2017.01.049>.

- [207] Julien Lalut et al. "Novel multitarget-directed ligands targeting acetylcholinesterase and  $\sigma 1$  receptors as lead compounds for treatment of Alzheimer's disease: Synthesis, evaluation, and structural characterization of their complexes with acetylcholinesterase." In: *European Journal of Medicinal Chemistry* 162 (Jan. 2019), pp. 234–248. DOI: 10.1016/j.ejmech.2018.10.064. URL: <https://doi.org/10.1016/j.ejmech.2018.10.064>.
- [208] Younis Baqi and Christa E. Müller. "Efficient and mild deamination procedure for 1-aminoanthraquinones yielding a diverse library of novel derivatives with potential biological activity." In: *Tetrahedron Letters* 53.50 (Dec. 2012), pp. 6739–6742. DOI: 10.1016/j.tetlet.2012.09.011. URL: <https://doi.org/10.1016/j.tetlet.2012.09.011>.
- [209] Babatope Akinbobuyi et al. "Synthesis and immunostimulatory activity of substituted TLR7 agonists." In: *Bioorganic & Medicinal Chemistry Letters* 26.17 (Sept. 2016), pp. 4246–4249. DOI: 10.1016/j.bmcl.2016.07.049. URL: <https://doi.org/10.1016/j.bmcl.2016.07.049>.
- [210] Matthew M. Cerda et al. "Dithioesters: simple, tunable, cysteine-selective H<sub>2</sub>S donors." In: *Chemical Science* 10.6 (2019), pp. 1773–1779. DOI: 10.1039/c8sc04683b. URL: <https://doi.org/10.1039/c8sc04683b>.
- [211] Hugo E. Gottlieb, Vadim Kotlyar, and Abraham Nudelman. "NMR Chemical Shifts of Common Laboratory Solvents as Trace Impurities." In: *The Journal of Organic Chemistry* 62.21 (1997), pp. 7512–7515. DOI: 10.1021/jo971176v. URL: <https://doi.org/10.1021/jo971176v>.
- [212] W. Clark Still, Michael Kahn, and Abhijit Mitra. "Rapid chromatographic technique for preparative separations with moderate resolution." In: *The Journal of Organic Chemistry* 43.14 (July 1978), pp. 2923–2925. DOI: 10.1021/jo00408a041. URL: <https://doi.org/10.1021/jo00408a041>.



